Comprehensive Simulation of Single PDC Cutter Penetration using Distinct Element Modeling (DEM) Methods

by

© **Mohammad Mozaffari**
(B.Sc in Petroleum Eng, Sharif University of Technology)
Faculty of Engineering and Applied Science
Memorial University of Newfoundland
St. John's, NL, Canada

A Thesis submitted to the School of Graduate Studies
Memorial University of Newfoundland, Canada
in partial fulfillment of the requirements for the degree of
Master of Engineering (Oil and Gas Studies)

April, 2014
Memorial University of Newfoundland
St. John's, NL, Canada

Abstract

Distinct Element Method (DEM) models are a class of material models that represent the material as a domain of small elastic balls bonded by non-linear elastic springs with defined shear and tensile bond strengths. This kind of material can represent concrete which is a material composed of a Portland cement-based matrix and rock aggregate, and has similar material properties and failure behaviour as low-permeability, sedimentary rocks.

This study investigates the performance of DEM in drilling operations by developing a toolkit. The toolkit has tried to introduce the most possible aspects of a drilling operation to qualitatively replicate the available experimental studies with optimized high accuracy.

The toolkit has maturated through this study in multiple steps. Initially there was only a cutter dragging on a rock under a vertical force in presence of confining pressure. Further enhancements such as cutter cleaning were added; also, boundary effects were minimized and particle size has been optimized. In the last step an advanced contact model, i.e. Flat-Joint contact model, has been used to better study the behavior of granular media.

The gradual process helped the toolkit grow. A number of experimental studies were re-created using this toolkit and the performance of the toolkit was tested in two scenarios against experimental and published work. The results confirm the performance and accuracy of the toolkit in replicating and predicting the experimental study qualitatively. Furthermore, the results were tested against available correlations and it has been found out that they follow the correlations closely.

Acknowledgement

Completing this work was only possible with the help of a number of people. I am very grateful of their help and they are definitely worth mentioning and thanking here.

I would like to extend my greatest appreciation and thanks to:

- My family as without their help and support I would never manage to make my way to Canada and have the opportunity to study here. Special thanks to Ewa Cichewicz, my partner, who provided my with her constant emotional support as well as her professional skills in editing this document.

- My supervisor Dr. Stephen D. Butt and my co-supervisor Dr. Katna Munaswamy who shared their knowledge and ideas and assisted in the conceptualization of my work. Special Thanks to Dr. Butt with for helping me to obtain an internship with Itasca CG, the company whose software was used as a basis for the thesis.

- Tatyana Katsaga who was my supervisor during my internship at Itasca CG. She helped me with her vast amount of knowledge in numerical modeling and gave me the chance to show my abilities in working in a company.

- All members of Advanced Drilling Group for their support, and providing a friendly work environment. Special thanks to Babak Akbari as this research and this type of modeling in the group has started with him. He also gave me with valuable advice in starting my research. Thanks to Hossein Khorshidian and Farid Arvani for their friendly and professional support and special thanks to Zheng Zhang and Yusuf Babatunde Olaiya for sharing their experimental data to use as a reference for my study.

This research was conducted at the Advanced Drilling Technology Laboratory at Memorial University of Newfoundland and was funded by the Atlantic Canada Opportunities Agency (AIF Contract no. 781-2636-1920044), the Research and Development Corporation of Newfoundland and Labrador, Husky Energy, and Suncor Energy. Four month of this research was spent as an Internship with Itasca Consulting Group, Toronto and the funding for the internship was provided by Mitacs-Accelerate program, Application Ref. No. IT02726.

Table of Contents

List of Figures

List of Tables

List of Symbols, Nomenclature or Abbreviations

BHA	Bottom Hole Assembly
CCS	Confined Compressive Strength
DEM	Distinct Element Model
DOC	Depth of Cut
FEM	Finite Element Model
HVSP	High Vibration Shaker Power
LVDT	Linear Variable Displacement Transducers
LVSP	Low Vibration Shaker Power
MRR	Material Removal Rate
MSE	Mechanical Specific Energy
MVSP	Medium Vibration Shaker Power
PDC	Polycrystalline Diamond Compact
PFC2D	Particle Flow Code in 2 Dimensions
ROP	Rate of Penetration
RPM	Revolution per Minute
UCS	Unconfined Compressive Strength
WOB	Weight on Bit
M	Moment
t_T	Grip Thickness For Tension Test
U	Relative Displacements
B	Bond state of the segment
c_b	Bond Cohesion
E	Young's Modulus

E_{eff}	Effective Young's Modulus
F	Contact Forces
F_y	Vertical Load On The Cutter
G	Initial Gap
k	Stiffness
K	Bulk Modulus
L	Length
M	Mass Of The Cutter
N	Number of the Segments
n	Normal Directions
n_B	Number Of Contacts That Initially Are Bonded
n_{fj}	Total Number Of The Flat-Joint Contacts
n_G	Number Of Contacts That Initially Are Gapped
n_s	Number Of Contacts That Initially Are Slit
P^t_c	Target Confining Pressure For CCS Test
Q	Coefficient Depending On The Shape And Orientation Of The Crack
s	Shear Directions
S	Rock Strength
v_p	Platens Velocity For Loading Specimen In Compression Tests
V_x	Horizontal Speed Of The Cutter
ε	Strain
λ	First Lamé Parameter
λ	Radius multiplier
μ	Shear Modulus
μ	Friction Coefficients

ν	Poisson's Ratio
ξ	Crack Density
ρ	Density Of The Material
σ_b	Bond tensile strength
σ^t_0	Magnitude Of The Isotropic In-Situ Stress
σ^t_a	Initial Axial Stress
τ_c	Maximum Shear Stress
Φ_b	Bond Friction Angle
Φ_B	Percentage of the Bonded Contacts
Φ_G	Percentage of the Gapped Contacts
Φ_S	Percentage of the Slit Contacts

1 Introduction

1.1 General Objectives

Computer modeling has come to the aid of researchers in the past few decades. Computer models mostly have been used to prove or strengthen a hypothesis that has been already established through experiments or analysis. Computer models come to the aid of the researchers in various stages of research to elucidate discrepancies or they are used as a means for sensitivity analysis. The importance of computer modeling is their use as guidance for further study of the phenomenon of interest.

In this study, computer modeling has been used to better understand the interaction of rock and bits in oil well drilling. Drilling is a dynamic phenomena and rock is a complex, random and non-homogeneous media. The current modeling techniques are still not fully capable of capturing all the events and simulating them properly. Mostly researchers have to apply simplifications to different aspects of their model to be able to simulate the phenomena using current techniques.

The Distinct Element Method (DEM) is one of the most advanced techniques for modelling rock-like media. It is the best method for modelling events with high deformation and strain and it is capable of modeling dynamic phenomenon. Therefore, this study uses DEM to investigate its performance in drilling operations by developing a toolkit. The focus of study is on introducing the most significant aspects of a drilling operation in this toolkit to qualitatively replicate the available experimental studies with optimized high accuracy.

1.2 Outline of study

Chapter 2 is a literature review and looks at the published research in the relative fields. The research reviewed are either exprimental, computer modeling or both. The chapter reviews the work that have successfully used numerical modeling and DEM. Then it further looks at literature dealing with rock cutting simulations. Moreover, the chapter reviews the exprimental and computer modeling literature dealing with vibration in drilling. The reserch that is used as help for developing and tuning the comprehensive rock cutting toolkit are also reviewd here. Finally the Flat-Joint contact model has been reviwed.

Chapter 3 describes DEM and Bonded Particle Model (BPM) in details. The focus is placed on PFC2D as the modeling software. The chapter reviews contact model basics, material generation and testing procedures and Flat-Joint Model formulations.

Chapter 4 is a paper published in the 46th US Rock Mechanics/Geomechanics Symposium, ARMA 12-9, held in Chicago, IL on June 24-27, 2012. This chapter studies the effect of bit vertical vibration in performance of PDC bits, a single PDC cutter-rock interaction, using distinct element methodology.

Chapter 5 is a paper prepared for submission to the International Journal of Rock Mechanics and Mining Science. This chapter goes over the development process of the rock cutting toolkit and tuning/optimizing the toolkit. It also goes over two scenarios to confirm the toolkit is properly developed by comparing the results of the toolkit with the available published work.

Chapter 6 is also a paper being prepared to be submitted to the International Journal of Rock Mechanics and Mining Science. This chapter uses the Flat-Joint contact model to develop three DEM synthetic materials based on 8 measured Drillability parameters. Using these three

materials, the chapter thoroughly studies the properties specific to Flat-Joint contact model which is an advanced contact model explained in Section 3.5. Moreover, the chapter re-tests the rock cutting toolkit using these three materials.

1.3 Significance of the research

This work started as a follow up to the work of Babak Akbari [1] in his thesis and corresponding paper [2]. There is much literature and research regarding the simulation of the rock cutting (most of these works are also reviewed in this document). However, there is a gap in research as no work has paid comprehensive attention to all the aspects of the rock cutting. For example, in large number of the similar work the cutter vertical position is fixed therefore the response of rock bit interaction to the applied vertical force to the cutter cannot be studied. A wide range of aspects of drilling are incorporated in development of this toolkit. Such developments are explained in details in Chapter 5.

Finally a step forward was taken by making use of one of the latest contact models, i.e. Flat-Joint contact model, in the aforementioned toolkit. The Flat-Joint contact model is used because of its supreme performance in modeling of compact cement-like granular rock media.

The developed toolkit has successfully showed its performance and accuracy in modeling and predicting the phenomena and has been used to further study the aspects of drilling as well as modeling itself.

2 Literature Review

2.1 Introduction

The most widely used numerical modelling methods that are used to simulate the deformation of rock materials are Finite Element Method (FEM), the Finite Difference Method (FDM), and the Distinct Element Method (DEM). FEM and FDM models simulate the rock material as a continuous domain discretized into smaller elements or regions bounded by interconnected nodes. These methods are best suited for modelling small strains in large geological structures where no material failure occurs, such as in the simulation of seismic wave propagation or closure of underground mine openings or caverns. In DEM, the material is represented as a discontinuous domain of small elastic particles bonded by non-linear elastic springs with defined shear and tensile bond strengths. This discontinuous material structure enables DEM to model small-scale failure processes by breaking the bonds between the particles, a capability which has been repeatedly demonstrated to accurately model rock failure in geomechanics experiments [3]. Xia et al. [4] investigated the failure pattern of rock under uniaxial compression test and compared the experimental results with the outputs generated with DEM compression to investigate the fracture process. They showed that rock failure simulations using DEM are in an acceptable agreement with experimental data and the fracture patterns produced by modelling closely resembled the fractures seen in the laboratory test. Potyondy & Cundall [3] modeled sandstone using DEM models constructed by packing non-uniform size particles and showed that the model described the stiffness evolution in the synthetic and laboratory specimens fairly well. Finally, DEM models are able to simulate large strains through the combined use of straining or

failing particle bonds, thus eliminating the need for complex and sophisticated constitutive laws that have been developed to enable FMD and FDM models to simulate large strains, which was demonstrated by Hentz et al. [5] during the simulation of concrete structures subjected to high dynamic strain rates. Concrete is a material composed of a Portland cement-based matrix and rock aggregate and has similar material properties and failure behaviour as low-permeability sedimentary rocks. Akbari [2] has concluded in his Thesis that the utilization of implicit FEM has proved to be extremely inefficient and probably ineffective for our purposes. Overall, the reviewed literature indicated that DEM models were the most appropriate numerical simulation approach for simulating the small scale failure processes appreciate with bit cutter penetration.

Based on the above discussion, the 2-Dimensional Particle Flow Code (PFC2D) developed by Itasca Consulting Group was selected as the DEM software for this work. PFC2D has been demonstrated to accurately represent force distribution through contacts, crack distribution, high deformation and strain rates, dynamic behaviour including elastic wave and particle motion, and other rock behaviours [e.g. 4, 6, 7, 8, 9. 10]. The calculation method is also explicit rather than implicit [11, 4]. Explicit calculations are more efficient than implicit for problems involving highly non-linear behaviour (e.g. collapse), large strain and dynamic response. This enables dynamic simulations to be performed in which information propagates across the material at a speed that depends on the mass and stiffness of the particles. It means that a critical time step according to the characteristics of the system (minimum time required for stress wave to pass from one particle to the next) is determined and dynamic equations of motion are solved for each particle and then the new contact forces are updated based on the displacements.

The remainder of this literature review is focused on the specific aspects of the thesis research, including rock cutter penetration, vibration during drilling, and recent DEM innovations such as the Flat-Joint contact model.

2.2 Rock Cutting Simulation

Several drilling laboratories around the world are focused on the investigation of single cutter penetration under a range of bit operating conditions, bit vibration, Bottom-Hole Pressure (BHP), and rock material properties, for example work of Akbari et al. [2] and Ledgerwood [12]. Such works are reviewed in this section and Section 2.3.

Correspondingly, many applications of DEM to rock cutting simulation have used similar single cutter model to compare and calibrate with the experiments, with good results. For example, it has been observed that DEM models are able to demonstrate phenomena affecting penetration mechanism of a single cutter such as, transition from brittle to ductile at high pressure conditions [8], generation of ribbon shape cutting in plastic deformation at pressurized cutting condition [12] and generation of the different fractures and cutting shapes under different load on cutter functions [13].

Ledgerwood [12] performed a series PFC cutting tests on a rock specimen with all elastic bonds deleted. The same rock with bonds has a Uniaxial Compressive Strength (UCS) of 55 MPa (8,000 psi). The rock with no bonds was identical but had cohesion of zero; this material may be imagined like loose sand. He reported in his paper that during cutting under pressure, PFC

indicates fifty times more energy is dissipated in friction (the sum of ball to ball and ball to wall friction) than is stored in elastic energy (Figure 2.1). Akbari et al. [2] in simulation of a single cutter-rock interaction applied a vertical load accompanied with a horizontal force to the cutter with Bottom-Hole Pressure (BHP). Their results showed that the corresponding penetration rate decreased logarithmically with BHP, an observation in agreement with experiments and drilling practise. Richard et al. [14] used a similar model for studying the effect of bit vibrations on drilling response. Their model is considerably close to drilling scenarios which are being performed in drilling laboratories.

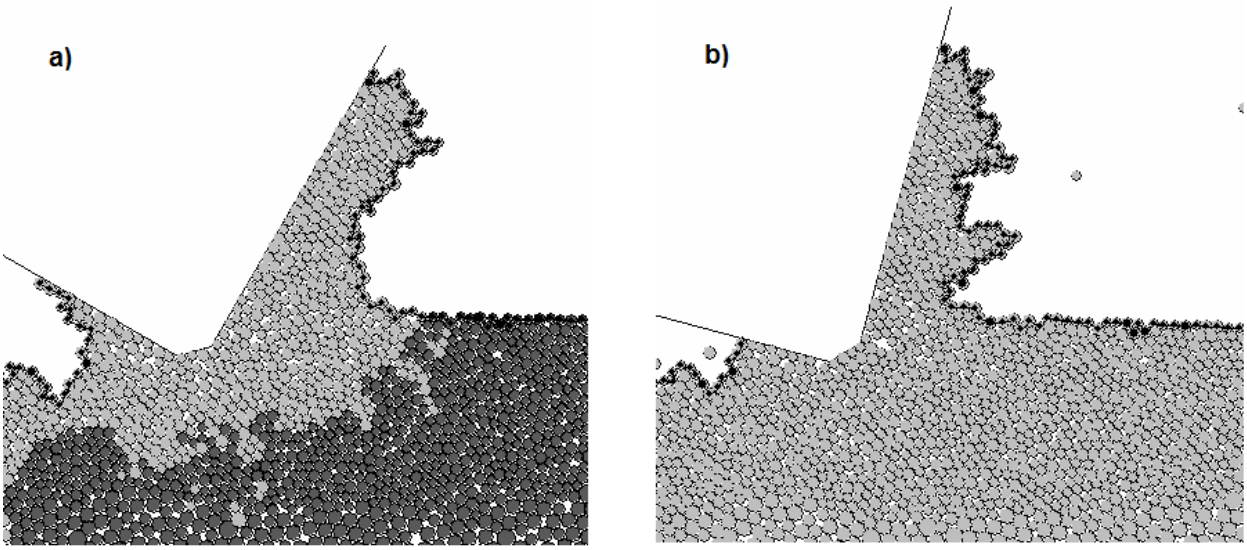

Figure 2.1 DEM cutting tests under pressure by Ledgerwood [12], a) the dark area is bonded and the grey area is unbonded crushed zone, b) the loose sand rock (grey is regions where no bond exist)

2.3 Vibration Influence on Penetration

Vertical oscillations of the bit and drill string during drilling operations, which is mainly due to forces acting on Polycrystalline Diamond Compact (PDC) bit cutters, can influence the

efficiency of penetration [15], however it is still unclear if these bit vibrations can improve or decrease the PDC bit performance [16] under field conditions. An early bit cutting model was developed [17] using PFC2D, which concluded that applied vibration shows no general relation between improvement in Material Removal Rate (MRR) and the applied vibration. However, Babatunde [18] has worked on a laboratory scale drilling rig under atmospheric conditions and got the opposite result. He used concrete specimens, created to have UCS of 50MPa to perform atmospheric drilling using a 1.25 inch diameter PDC bit under vibration. To apply the vibration, the specimens were secured on a shaking table. The vibration was applied at three different vibration powers: Low, Medium and High; all at three different frequencies: 45Hz, 55Hz and 65Hz. He also performed his test over a range of Weight on Bits (WOB). By performing his tests he concluded that the vibration can improve drilling rate, however the optimum condition is not predictable and real time monitoring of the condition is necessary to optimize vibration for the best performance. A very interesting behaviour was also observed in the trend of the results. It was observed that up to a certain WOB increase in ROP due to vibration is proportional to the amplitude of the vibration; after this certain WOB relation of ROP and Amplitude of Vibration is different for different vibration power. Similar observations were also reported by Li et al. [19].

Dunayevsky et al. [20] argued that the dynamic components of the force are primarily the result of the bit-formation interaction. Dubinsky et al. [21] suggested that dynamic forces, which are the result of bit and string interaction with rock, cause vibration in the bit. In addition it was argued that the drill string and bit vibrations are linked to the vertical stiffness of the pipe and the mass of the bottom-hole assembly. Fluctuations of forces in the direction of cut can result in bit stick-slip which in addition to an increase in the risk of Bottom-Hole Assembly (BHA) failure, yields reduction in the ROP [22]. Richard et al. [14] showed that torsional and vertical

vibrations of a PDC bit are coupled. Additionally, it has been argued that the bit oscillations could be controlled by changing the Weight on Bit (WOB) and velocity.

In other studies, improvement of bit performance has been observed when a downhole thruster is used in the Bottom Hole Assembly (BHA) [23]. Downhole thruster is a tool which converts the differential pressure of the drilling fluids between the inside of the drill string and annular space to load on bit. Therefore, by using this tool it is possible to adjust the mass of the drill collars and load on the bit independently. The result based on field data showed an improvement both in bit and drill string life.

McCray and Cole [24] reported the advantage of magnetostriction vibratory drilling. In this technology, an electromagnetic transducer produces a vibration via alternating electric current flowing through solenoids surrounding a laminated core of resonant dimensions. It was argued that by adding this tool (which produces a vibration frequency of 230 Hz) on a star type of roller cone bits can double the Rate of Penetration (ROP) at a depth of less than 100 m. No further information was provided for the performance of this vibrator at higher depths of drilling.

Pessier and Damschen [25] developed a new generation of bit which is the combination of roller cones and PDC cutters. Due to actions of inserts of rollers on rock surface, the hybrid bit can create fractures in hard rocks and enhance both the ROP and MSE.

Kolle [26] developed a hydraulic actuating tool which generates pulsation in front of the bit, and causes applying vibratory force, which was result of reduction in the pressure drop at the end of drill string. Although, laboratory tests showed the tool resulted 33% of improvement in ROP under BHP of 20 MPa, in the field tests no significant improvement in ROP has been observed.

Pixton and Hall [17] also reported the performance of a mud actuated hammer on a PDC bit which was developed at the Novatek Corporation. The PDC bit was utilized with small jets across the PDC cutters which together was called PHAST (Pulsed jet Hammer Assisted Shearing Technology) bit. The hammer assisted rotary drilling showed a promising result under atmospheric condition of the drilling, but at higher BHP condition no significant improvement was observed [27]. Akbari et al. [2] argued that applying applied vibratory forces on the cutter can create larger fractures in the rock. However the generation of these fractures was observed to be restricted at high pressures.

In another attempt for improvement in PDC bit penetration, a combination of PDC bit and roller cone bit has been developed, called a hybrid bit [25]. In this type of bit, interactions between inserts of rollers and hard rocks cause vertical movement in the bit. Improvement of ROP has been achieved in drilling of hard rocks using hybrid bits.

Overall, results of the studies reviewed in this section showed significant effects of the dynamics of bit motion on the penetration mechanism. However, the understanding of many of these interactions is not clearly understood, hence the need for the current thesis research.

2.4 Drilling Performance from DEM Results

The study of a single cutter-rock interaction model can provide detail information about effect of drilling parameters such as load on cutter, cutter mass and speed, on drilling responses e.g., cutter force components, vertical vibrations, Depth of Cut (DOC) and amount of required energy for removing the unit volume of the rock. Teal et al. [13] named the latter Mechanical Specific Energy (MSE), and a widely adopted objective in the drilling industry is achieving the higher

Rate of Penetration (ROP) with minimum MSE value. However, in the 2D DEM models, ROP is not easily calculated from the model results. Pixton and Hall [17] overcame this limitation by calculating Material Removal Rate (MRR) and in practise MRR and ROP are expected to be linearly proportional.

Prasad [28] proposed a quantitative methodology to describe rock materials in terms of their Drillability as a means of predicting ROPand wear, which are closely linked to strength and abrasivity. This methodology includes eight material properties—density, porosity, compressional and shear wave velocities, Unconfined Compressive Strength (UCS), Mohr friction angle, mineralogy and grain sizes—that can be represented on a spider plot as a Drillability curve relating all eight properties (Figure 2.2). Appendix D summarizes these eight Drillability parameters.

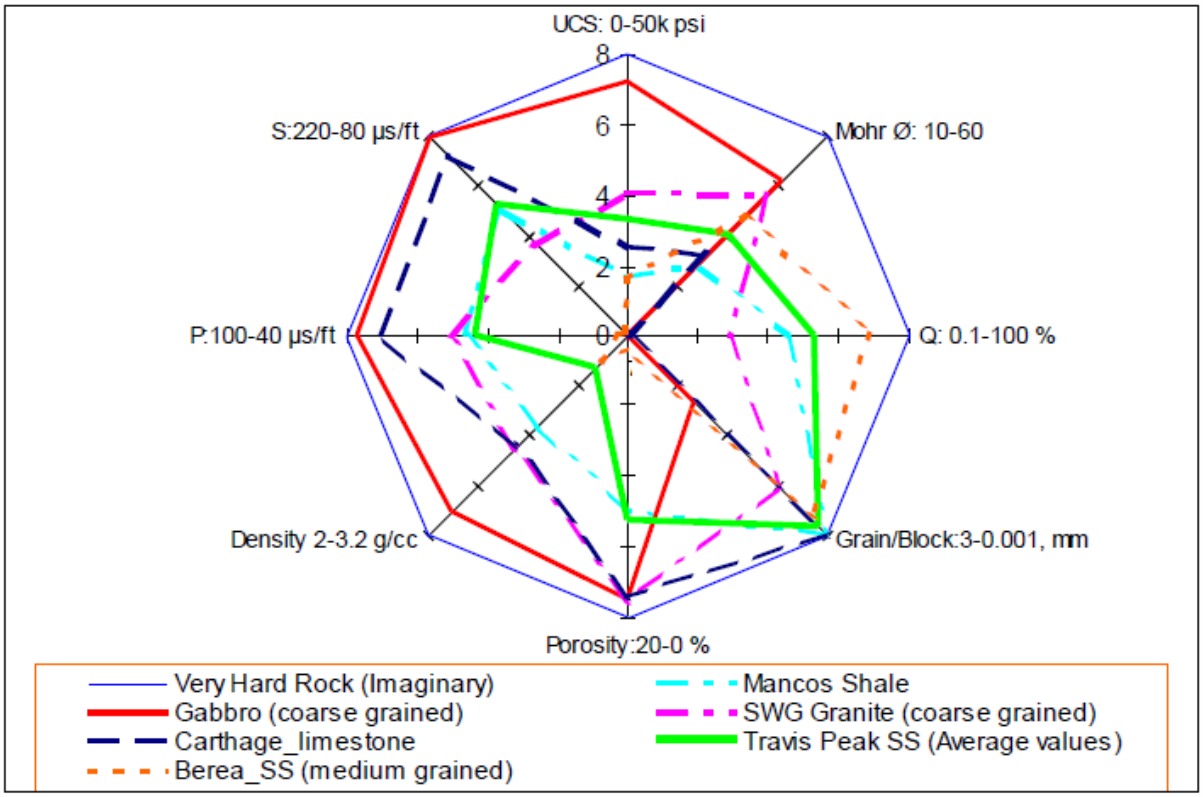

Figure 2.2, Spider plot showing drillability curves for several well-known and hypothetical rock types [28]

2.5 Recent DEM Innovations

Most DEM modelling to date has used the linear contact model. In that contact model the particles interaction is in the form of friction and exert force to one another with linear springs (contact entries) in series. The synthetic material that is simulated with this method exhibits the relevant physical behaviours of a brittle material such as rock. However, the produced assembly of the particles that create the synthetic material is a valid structure of its own and its micro-structure should not be confused with that of the actual rock [29]. If it is desired to pay attention to micro-structure of the synthetic material, user has to go with more advanced contact models such as Flat-Joint contact model. Furthermore, one major problem with linear parallel bond

model is that the UCS and tensile strength cannot be tuned separately. In the linear parallel bond model, there is no means other than bond strength to adjust the UCS of the material; therefore, the bond tensile strength should be significantly high in order for the model to represent the desired UCS. It is reported that if one matches the unconfined-compressive strength of a typical hard rock, then the direct-tension strength of the model will be too large [30]. This limitation can be overcome by using the more advanced contact model, i.e. Flat-Joint model. In this model, even after the bond is broken, the system can resist compression by interlocking the particles. This only happens because of the polygonal behaviour that the contact model causes in the particles. The polygon shape of the particles forces the particles to interlock under compression (Figure 2.3); therefore, they would resist rotation even after bond breakage [30, 31, 32].

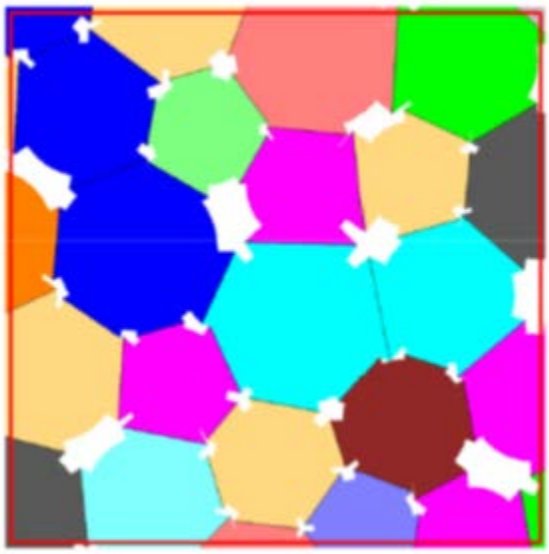

Figure 2.3, Polugon shape of particles in Flat-Joint model

3 DEM Introduction

This chapter describes DEM and Bonded Particle Model (BPM) in details. The focus here is on PFC2D as the modeling software. The chapter reviews contact model basics, material generation and testing procedures and Flat-Joint Model formulations.

3.1 Introduction to Bonded Particle Model (BPM)

One reason for the development of the numerical modeling is the need for a better assessment of the medium of the study. For example, it is really difficult to monitor the state of the stress inside a media, such as rock, using only the information measured from the boundary of the media. Therefore, numerical modeling is the most powerful means assessment, especially for the systems that are granular or assemblies of particles or spheres. Numerical models help in prediction of data regarding any point in the media during a specific test.

The term particle here differs from the normal definition of the particle in the field of mechanics, where it refers to a point of negligible size in the space. A particle in the current discussion refers to a body of finite size and mass.

A granular media is a media comprised by district particles of arbitrary shape that have interactions together at their contacts. Therefore, it is best to model such a system using Distinct Elemental Method (DEM). DEM was first developed by Cundall (1971 and 1974) for analysing problems dealing with rocks and further developed later by Potyondy and Cundall in 1979

[11,3]. Potyondy in 2004 [3] argues that rock behaves like a cemented granular material of complex-shaped grains therefore a system or a model that represents such a system can be referred to as Bonded Particle Model (BPM). A rock can be modeled in the form of a pack of grains in any arbitrary and complex shape that are cemented together at their contacts. These grains can be deformable and may even break. The breakage of the contacts is called micro-crack. Existence of the micro-cracks governs the mechanical behaviour of the rock by propagating, growth and interaction through the rock.

The micro-mechanism of formation of these micro-cracks is not understood fully yet; however, Figure 3.1 represents one of mechanisms causing brittle compression induced tensile crack. The two particles in compression are causing an axial load in the form of tension between the other two particles. If this axial load is strong enough it can break the bonds and cause tensile crack.

The assembly of these particles creates a medium. The behaviour of this medium is modeled by interaction of these particles at their contacts. The contacts are soft, meaning they have finite normal and shear stiffness. DEM equilibrium arises whenever the internal forces in the media balance each other. Contact forces propagation, displacement of particles and particle assemblies and the equilibrium is calculated by tracing the movement of the particles that cause force and moment at the contacts. The speed at which disturbances propagate through the system is a function of internal properties of the discrete media. Newtown's law of motion governs the relation between the motion and the forces causing the motion.

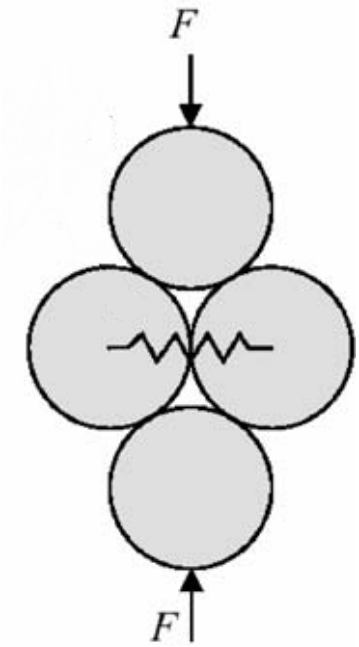

Figure 3.1, Idealized crack formation [3]

Newtown's second law provides the explanation for the motion of the particles and the force displacement law explains the resulting force in the contacts through the given motion. The DEM repeats in such a calculation in every time step. Figure 3.2 illustrates this algorithm. At the start of each time step, the position of each contact is updated according to the particle positions. Then, based on the relative position of the particles, the contact force is updated by using the force displacement law. The resulting contact force and existing body forces, such as gravity force, are applied to each particle. Next, Newtown's second law of motion is used to sum the forces on each particle to update velocity and position of the particles.

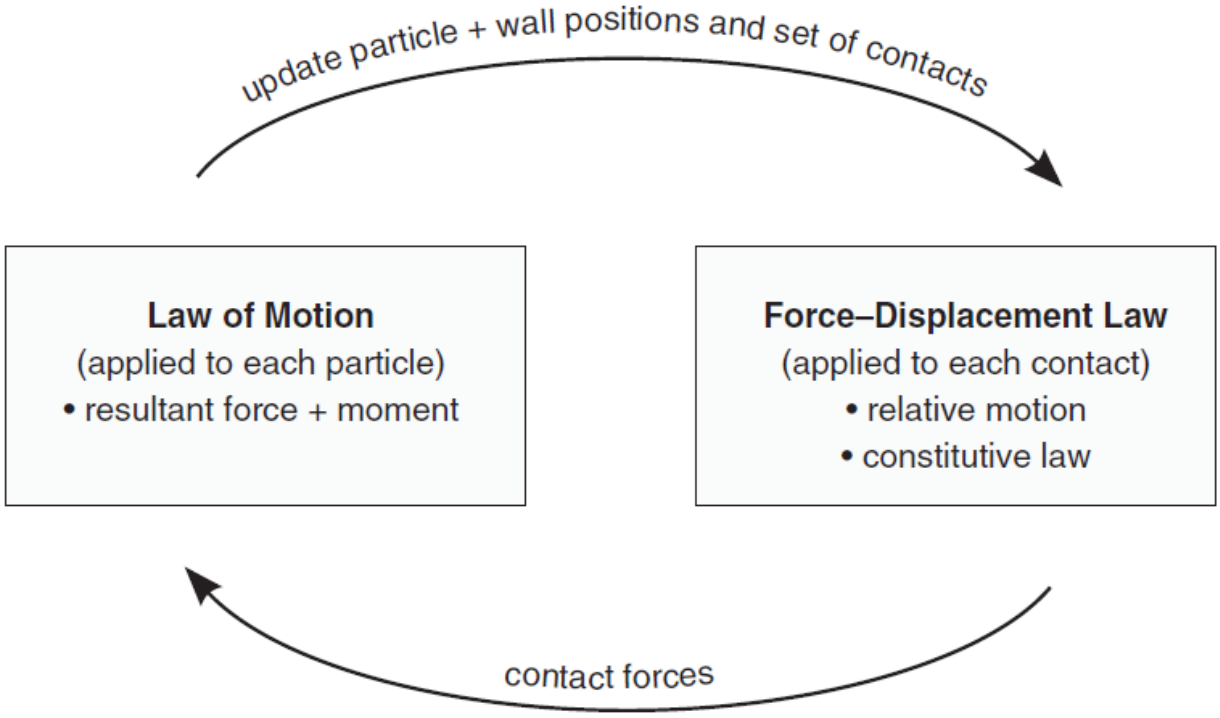

Figure 3.2, Calculation cycle in PFC2D [33]

3.2 Contact models

The behaviour of an assembly of particles is modeled by the contact model of the particles. Figure 3.3 illustrates the basics of the contact model. This section talks about the basics of contact models and general linear parallel bond model. The Interaction of the particles at their contact is replaced by a contact model in parallel with optional dashpots plus optional cement like material that act as elastic bonding agent (parallel bond). The assembly of the parts in Figure 3.3 provide an interface where particles can interact together. This interface provides stiffness, slip behaviour, damping and bonding behaviour.

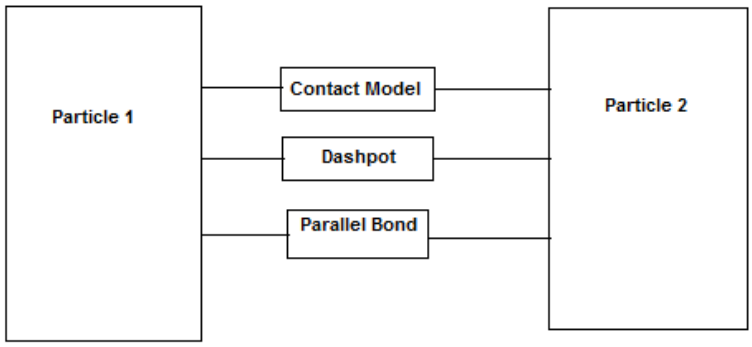

Figure 3.3, Particle Interaction and contact model [34]

3.2.1 Stiffness

Stiffness “k” relates the contact forces “F” and relative displacements “U” in the normal (n) and shear (s) directions, Equation 3.1 and 3.2. Each Contact model has its own definition of resultant contact stiffness.

$$\Delta F^n = k^n U^n \qquad 3.1$$

$$\Delta F^s = k^s U^s \qquad 3.2$$

3.2.2 Slip behaviour

Slip behaviour works closely by bonding behaviour. In the absence of bonding behaviour or after bond breakage, slip behaviour can be included and two contacting entities may slip relative to one another. Slip behaviour works by enforcing a relation between the normal and shear force. The relationship is expressed by equation 3.3.

$$F^s_{max} = \mu |F^n| \qquad 3.3$$

μ is the minimum of the friction coefficients of the two contact entries of the two particles. Therefore, slip occurs by setting the maximum shear contact force to the limit of F^{s}_{max}. If shear force exceeds in a time step, it resets to this value and the two contacting particles will slip on each other. Figures 3.4 and 3.5 illustrate this behaviour in more details.

3.2.3 Bonding behaviour

Particles can be bonded to another. The bonding of the particles provides finite tensile strength at the contacts. There are two bonding behaviours, contact bond and parallel bond. By default, particles are not bonded together and the bonding behaviour is not a prescribed behaviour. Particles may only be bonded together after they have come into contact with each other and if the contact force exceeds the bond strength then bond will be deleted.

3.2.3.1 Contact bond

Contact Bond can be envisioned as a pair of elastic springs with constant normal and shear stiffness acting at the contact point. A contact bond does not transfer moment and has a vanishingly small size that act at the contact point; therefore, it precludes the possibility of the slip. Figures 3.4 and 3.5 illustrate the behaviour of this bonding behaviour. If the contact is in tension (Figure 3.4, negative overlap) then the bond will resist tension up to a critical force. This critical force is the bond strength after which the bond breaks and would be deleted. If the bond breaks in this manner, the normal and shear forces are set to zero. In the shear direction (Figure 3.5) the bond resists the force up to a critical shear force that is the bond shear strength. If the bond breaks in this manner, provided that normal force is in compression, shear contact force will follow the rules of the slip behaviour and normal force will remain unaltered. Only after bond breakage in shear the slip can occur.

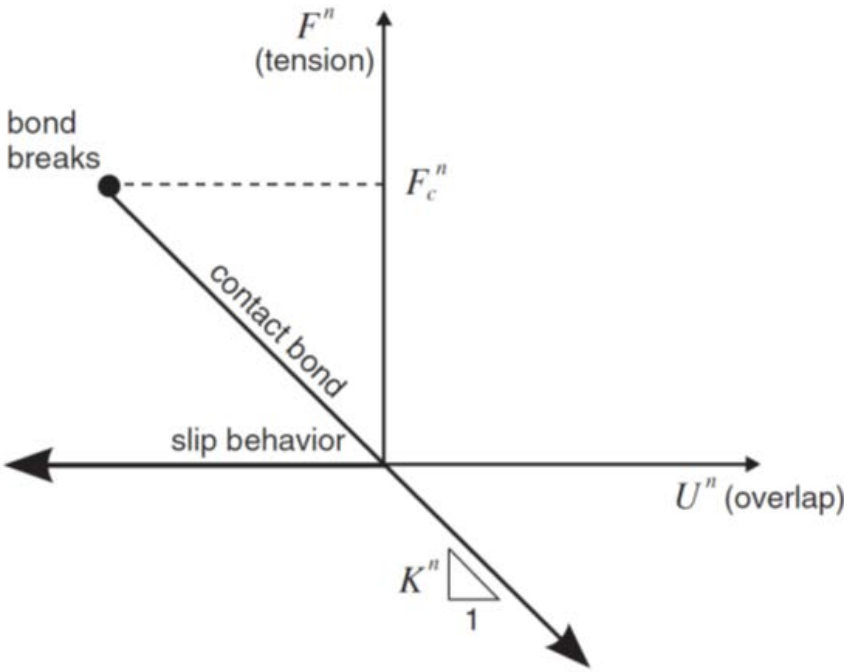

Figure 3.4, Normal Component [34]

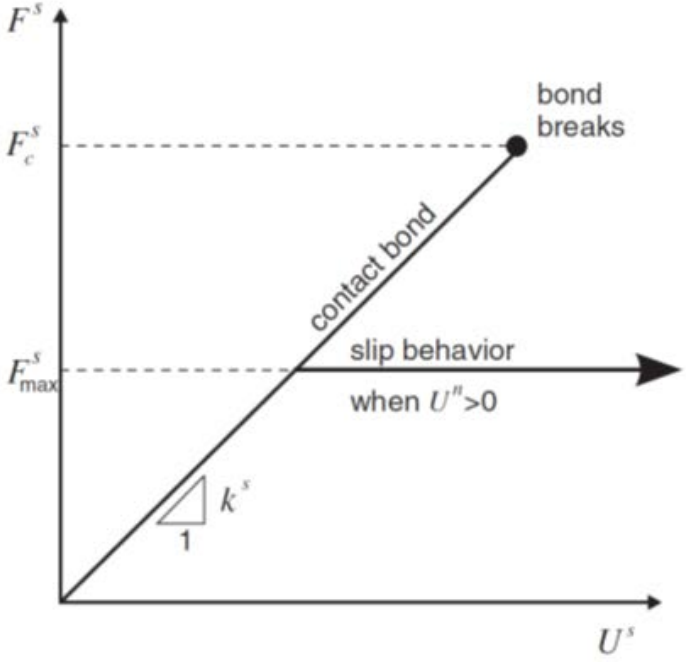

Figure 3.5, Shear Component [34]

3.2.3.2 Parallel bond

Parallel bond can be envisioned as cement like material at the contact of two particles. It acts as a finite size spring in parallel to contact model. Its existence provides strength to the contact and since it acts in parallel to contact model it does not preclude the slip behaviour. It is also capable of transmitting moment as well as force. Figure 3.6 illustrates a parallel bond. It can be envisioned as a finite thickness plate in 2D or a cylinder in 3D.

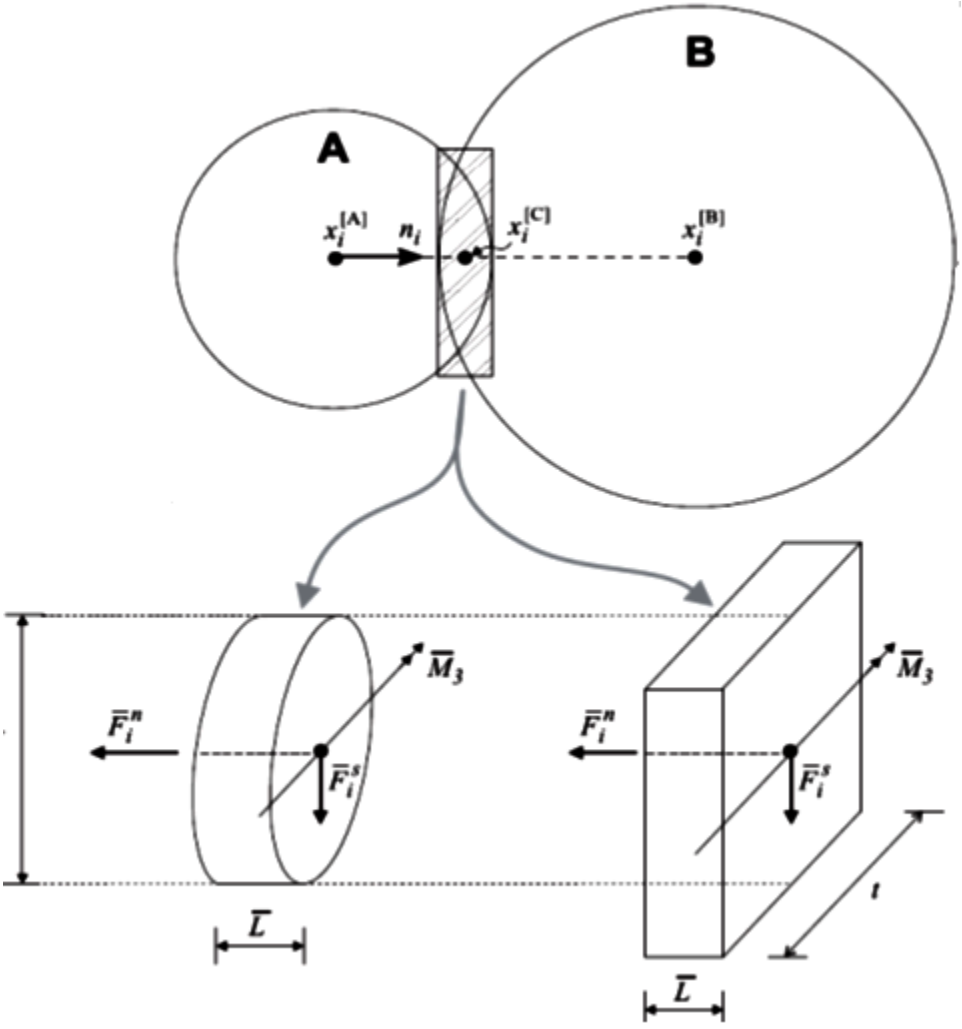

Figure 3.6, a parallel bond between two particles [38]

As stated before, a linear parallel bonded model is the basic general model. It provides constant linear stiffness and the slip behaviour exists. The contact bond is optional and parallel bond adds flexible strength to the contact. As stated, the stiffness is a constant linear value. It means that the contact stiffness between two particles [A] and [B] is calculated by assuming the two contact entities are acting in series and the resulting stiffness is computed as two springs in series (Equation 3.4 and 3.5).

$$k^n = \frac{k_n^{[A]} k_n^{[B]}}{k_n^{[A]} + k_n^{[B]}} \qquad 3.4$$

$$k^s = \frac{k_s^{[A]} k_s^{[B]}}{k_s^{[A]} + k_s^{[B]}} \qquad 3.5$$

3.3 Material generation

The PFC supporting code library, or “Fishtank”, consists of prepared codes for wide range of applications. A part of this library is designed to help researchers by the generation of materials in the form of a packed assembly of particles. This set of codes provide complete set of functionality; they create a packed assembly and they help in calibrating micro properties by subjecting the material to simulated laboratory tests which will be explained in more details in Section 3.4. Furthermore they apply the desired boundary and internal stresses and visualize the damage formation in the material. The codes are primary designed for modeling hard, crystalline rocks such as granite.

The challenge in creating a new material is obtaining the desired macro-properties and behaviour of the material. In an FEM model the material properties can be calculated and measured directly

from the laboratory test performed on the sample. However, the micro properties of a DEM model are not directly related to macro properties of the synthetic material. For this case, a calibration process should be followed. The calibration process is explained in details in Section 3.4.

The process in which Fishtank generates a well-connected material in a Material Vessel subjected under specified confining pressure is explained here. The future sections will go over the standard tests that are used in this study and a recommended calibration process.

A Material Vessel is a box that contains the material. The particles are generated within this box. The material vessel can be assumed as the domain for the generation process because all the generation process happens inside this vessel. First the vessel is filled with a dense packing of frictionless, round particle. To ensure the assembly is dense and the process is completed successfully, the number of particles is controlled so that it always ends up with 8% porosity in 2D and 35% porosity in 3D. The particles are of a specified size distribution. The size distribution is commonly specified by minimum particle size. Depending on the type of the distribution, the ratio of the maximum to the minimum particle size can be set as well. If necessary, the shape of the particles can be of any optional designed shape by replacing the round particles by the clumps of the optional shape. A clump is a particle of its own created by arbitrary placing of the basic particles. A clump will not break and the relative positions of the particles creating it are always fixed.

Initially the particles are created in half of their final size to ensure there is no overlap between them. Then the sizes are increased to the final size in a frictionless state, ensuring the system reaches equilibrium and the internal forces of the system are uniform. After this step, the

magnitude of the isotropic in-situ stress is adjusted to a value of σ^t_0. This is the average of the three direct stresses in the specimen. The isotropic in-situ stress is adjusted by adjusting the average radius of the specimen. It has been reported [29] that small changes in the average radius have great impact on the isotropic in-situ stress. Therefore, the change in the particle size specified initially will be negligible. It is also recommended [29] to adjust the σ^t_0 to less than one percent of the UCS of the sample. This is to reduce the amount of locked in forces inside the sample after bond installation and unloading in the future steps.

Next step is called floater elimination. Floater is any particle that has less than three contacts and thereby can be assume to be floating freely inside the rock matrix. They create inhomogeneity inside a solid rock after bond installation and it is better to remove them before the bond installation. The process consists of multiple cycles of fixing every particle in the system except the floaters, adjusting their radius to maximize their contacts and letting them to reach equilibrium.

Next and final step is assigning bond properties. A bond can be a contact bond, a parallel bond or both. Only after this step the friction is assigned to the particles and sample is removed from the vessel.

3.4 Calibration process

As stated previously there is no direct relation between the micro-properties of a DEM material and its macro-properties. The relationship is found by subjecting the material to a series of simulated standard laboratory tests and monitoring the behaviour of the material. The tests studied here are Direct Tension test and Compression test at confining different pressures. It is

worth to mention again that a material modeled with DEM is a valid structure of its own and its micro-structure should not be confused with the micro-structure of the physical rock. Only the macro-behaviour of the synthetic material compared to behaviour of the physical material is of importance here. If representing the micro-structure of the rock is of interest then one might consider more complicated contact models. The success of the DEM modeling at reproducing the behaviour of hard rock can be attributed directly to its ability to generate compression-induced tensile cracks [29].

The laboratory measured properties that are commonly used for characterizing rocks are elastic Young's Modulus (E), Poisson's Ratio (ν) and strength which usually is expressed as UCS. The following steps briefly summarize the recommended procedure for the basic contact models.

1) Matching Young's Modulus and Poisson's Ratio at relatively high bond strength and performing compression test at atmospheric conditions (UCS test). The reason for high strength is to delay bond breakage and obtaining a long straight line in the stress-strain curve. The Young's Modulus and Poisson's Ratio can be adjusted by adjusting the contact stiffness, k_n and k_s.

2) Once the elastic properties are matched the bond strength can be calibrated to match UCS and tensile strength of the physical sample by performing compression test at zero confinement and Direct Tension test. However, as will be discussed in more details later, the basic contact models can't match both UCS and tensile strength separately as they end up with one of the macro-properties not calibrated.

3) If the post peak behaviour is of interests the friction coefficients can be adjusted.

4) Now the failure envelope can be built by performing compression test at different confinement pressure.

3.4.1 Standard tests

3.4.1.1 Stress and Strain Measurement Schemes

Stress and strains are measured by three methods:

1) Average values from three measurement circles placed randomly in the specimen

2) Forces on walls or outer boundaries of the system.

3) Gauge balls that act like Linear Variable Displacement Transducer (LVDT) sensors touching the outer surface of the sample. These gauge balls are particles of the system and their properties are samples to obtain the stress and strain. Damage and deformation can cause great error in reading of the gauge balls.

3.4.1.2 Loading rate

The loading rate chosen is slow enough to ensure quasi-static response. This means that the loading rate is slow enough that the system has enough time to respond to the loading and adjusts the force redistributions that happen after a nonlinear event, like bond breakage or slip. This is performed by setting the velocity of loading platen to zero after each nonlinear event and letting the system reach equilibrium. It has been reported [29] that as long as loading rate is remaining

under a critical velocity the response of the system will remain the same no matter what is the velocity of the platens. If the loading rete is maintained under the specific critical velocity the system is under quasi-static condition.

3.4.1.3 Compression Test

In this test the top and lower walls act as loading platens and the side walls control the confining pressure. In case of fully Unconfined Compressive Strength (UCS) test the side walls are removed.

The first step is seating the platens phase. This is performed to reach a target confining pressure P^t_c for Confined Compressive Strength (CCS) test and an initial axial stress σ^t_a [29]. Next the loading phase starts by moving the platens toward each other at a specific velocity v_p and under a quasi-static condition. The v_p is reached slowly at multiple stages to prevent sudden movement of platen and creating unrealistic large forces. During a normal test of a bonded material the value of compression load increases to a maximum value and decrease as the specimen fails and the test can be terminated. The termination criteria can be based on either specific strain value or a reaching a ratio of maximum compression load.

During the test the value of the stress and strains are recorded in tables. The procedure for obtaining elastic properties from these history tables is described in appendix A. The maximum failure load is reported directly by the software.

3.4.1.4 Direct Tension Test

During this test the material is pulled apart slowly by gripping it at its ends. The test result, which is tensile strength of the material, is found by monitoring the stress and strain of the material.

First the material is removed from the vessel and is allowed to expand and reach equilibrium under the new condition before any stress and strain monitoring starts. Then a thin layer of particles with the thickness t_T or the grip thickness is selected from both ends of the material. The velocities of the grip layers is fixed in axial and opposite direction. The axial load is the total unbalanced force acting on the grip grains. It is observed that for coarser samples this layer might not be consistent, thereby creating some error in final value of breaking point (FISH IN PFC2D [29] and section 6.4.6).

3.5 Flat-Joint Model

3.5.1 Introduction

As stated in previous sections, the main task of PFC2D or any other DEM software, is to simulate an environment by assuming that environment is created by tiny particles that are free to move and can interact with each other at their contacts. This interaction is simulated with a contact model with optional parallel bond and dashpot in parallel. The contact model that has been used so far is the linear contact model in which the particles interaction is in the form of friction as well as force with two springs (contact entries) in series. This synthetic material that is simulated with this method exhibits the relevant physical behaviours of a brittle material such as rock. However, the micro-structure of the produced assembly of the particles that create the synthetic material with this method should not be compared with micro-structure of the actual rock. If such a thing is desired, user has to go with more advanced contact models such as Flat-Joint contact model. Furthermore one major problem with linear parallel bond model is that, as discussed before, the UCS and tensile strength cannot be tuned separately. In the linear parallel bond model there is no means other than bond strength to adjust the UCS of the material;

therefore the bond strength should be significantly higher in order for the model to represent the desired UCS. It is reported that if one matches the UCSof a typical hard rock then the direct-tension strength of the model will be too large [30]. This limitation can be overcome by using the more advanced contact model, i.e. Flat-Joint model. In this model, even after the bond is broken the system can resist compression by interlocking the particles. This only happens because of the polygonal behaviour that the contact model causes in the particles which forces the particles to resist rotation even after bond breakage.

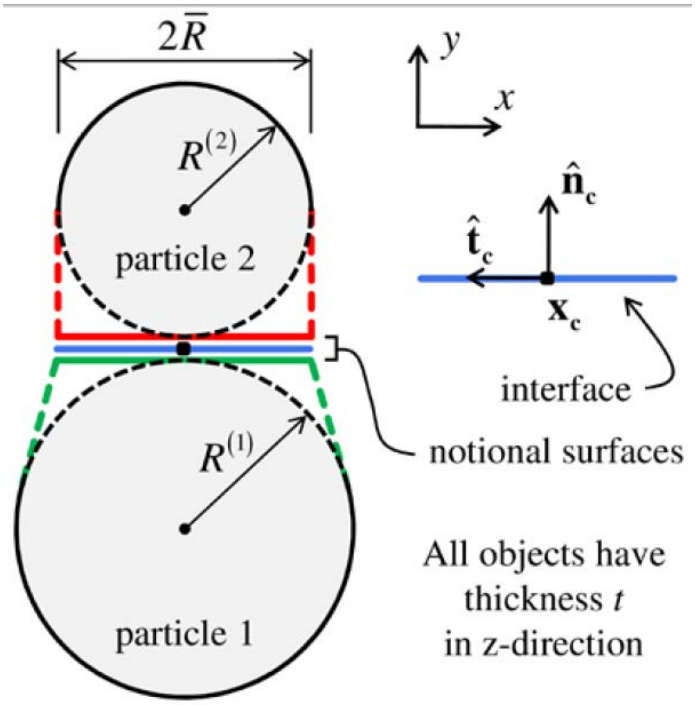

Figure 3.7, Geometry of a Flat-Joint contact [31]

Figure 3.7 illustrates a schematic of a Flat-Joint contact. The behaviour of the Flat-Joint contact is simulated by two notional surfaces. The contact between particles is no longer just a single point and the particles are not treated as round surfaces while interacting with each other. The contact point is replaced by contact interface. The contact interface is the area between to notional surfaces of the two interacting particles. Each surface is rigidly connected to its own

particle. The particles and notional surfaces are called grains and facets, respectively. The interface that exists between the two surfaces divides the facets into number of segments. Each segment can be bonded or not bonded, therefore each segment can behave linear elastic or frictional respectively. If relative displacement of the two particles exceeds the Flat-Joint diameter, the contact will be deleted and the surfaces are turned into a locally circular contact. This means if the particles come into contact after this the behaviour will be elastic and frictional (as of unbounded linear contact model), Figure 3.8.

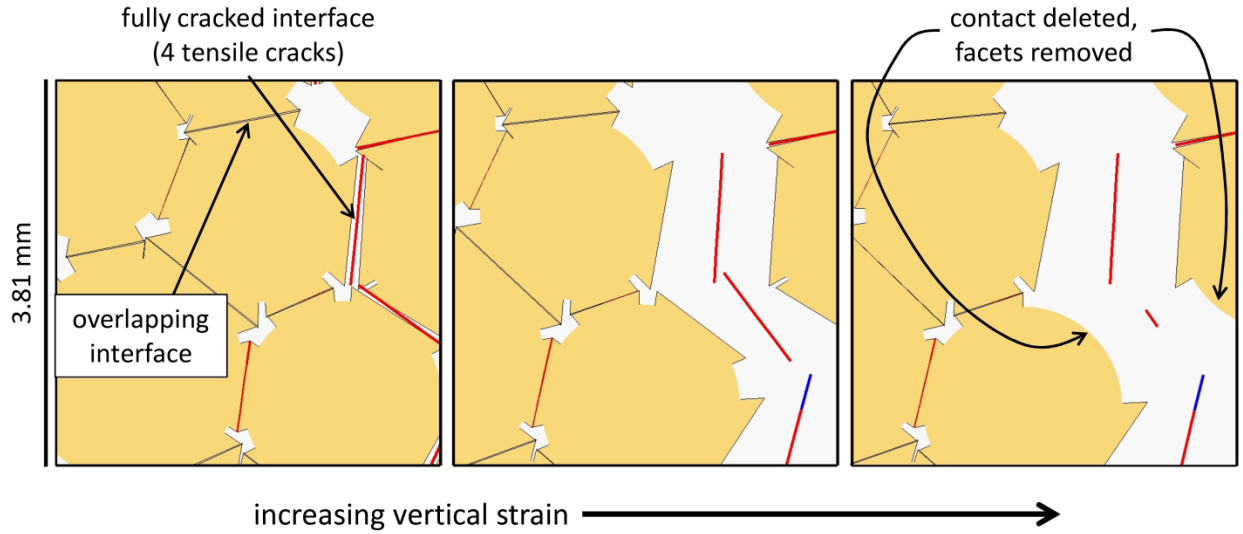

Figure 3.8, a close-up view of a Flat-Joint assembly under the load and cracking, black are the notional surfaces, red and blue are cracks [32]

3.5.2 Formulation

Table 3-1 represents the list of parameters specific to the Flat-Joint contact model. As stated before, Flat-Joint is deleted if the relative displacement of the two particles exceeds the Flat-Joint diameter and behaviour will be elastic and frictional. The parameters listed in the Table 3.1 summarize the parameters only specific to the Flat-Joint model.

Table 3-1, Flat-Joint parameters [31]

N	Number of the Segments
λ	Radius multiplier ($R = \lambda \min (R^{(1)} , R^{(2)})$)
k_n, k_s	Normal and Shear stiffness
μ	Friction coefficient
G	Initial Gap
B	Bond state of the segment
σ_b	Bond tensile strength
c_b	Bond Cohesion
Φ_b	Bond Friction Angle

The interface is divided into N segments. Each segment's behaviour is controlled by the force-displacement law. Each segment can be either bonded or unbounded; therefore, the contact can be fully bonded, partially bonded or fully unbounded.

The value of λ can be either fixed or set to a maximum. If the value is fixed the contact radius is set to the specified value, according to the Table 2.1, otherwise λ is reduced from its maximum value therefore the Flat-Joint radius is reduced to obtain a valid micro-structure. A micro-structure is called valid if the facets can be connected to the center of the particles with no overlap with the other facets. Figure 3.9 illustrates a valid and invalid micro-structure.

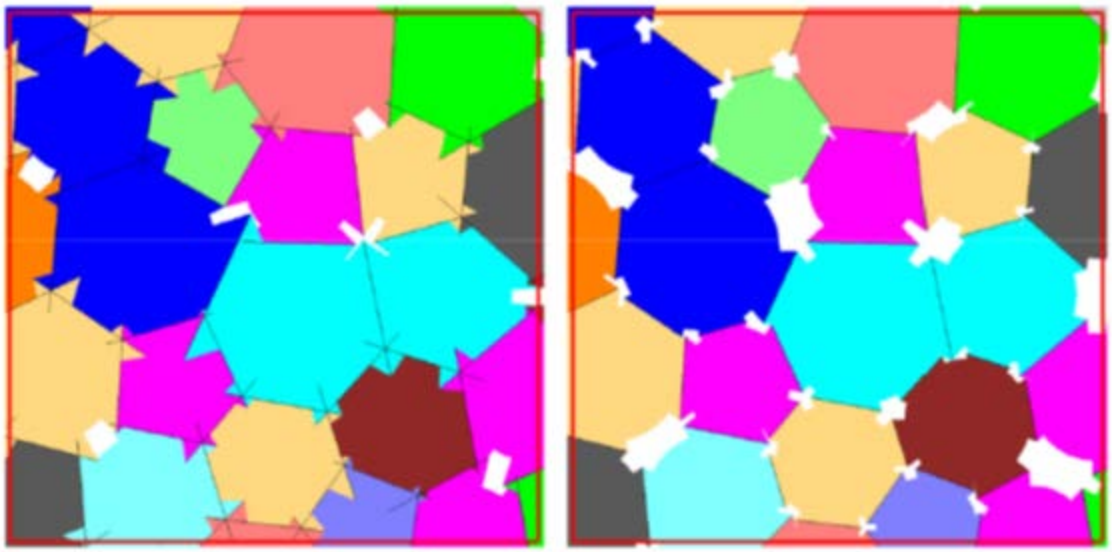

Figure 3.9, an invalid micro-structure (left) with facets overlapping. the same micro structure in the valid form (right) by reducing the Flat-Joint radiuses. [31]

The initial micro structure of the flat joint contact is either bonded (with no gap, G=0), gapped (unbounded, G>0) or slit (unbounded, G=0). These states are determined by fractions Φ_B, Φ_G, Φ_S where:

$$\Phi_B + \Phi_G + \Phi_S = 1 \qquad n_{fj} = n_B + n_G + n_s \qquad 3.6$$

$$\Phi_B = \frac{n_B}{n_{fj}} \qquad \Phi_G = \frac{n_G}{n_{fj}} \qquad \Phi_S = \frac{n_S}{n_{fj}}$$

n_{fj} is the total number of the Flat-Joint contacts and n_B, n_G, n_s are number of contacts that initially are Bonded, Gapped or slit respectively. These contacts are randomly dispersed through the Flat-Joint material.

The generalized force-displacement law updates the force and moment in each segment and may also modify the boned state of the segments. The overall procedure is described by the following three steps (The more detailed formulation is provided in [31]):

1) A normal stress is calculated for each segment based on the amount of gap on that segment at the end of previous calculation cycle. If the segment state is bonded and the normal stress is more than bond tensile strength σ_b, then bond state of the segment is turned into unbonded and the normal stress is set to equal zero.

2) A trial shear stress is calculated based on the relative displacement of the facets. Based on the bond state of the contact, next step varies.

   If segment is unbonded a maximum shear stress is calculated by:

$$\tau_c = \begin{cases} \mu\sigma & \sigma < 0 \\ 0 & \sigma \geq 0 \end{cases} \qquad \sigma = \text{normal Stress} \qquad 3.7$$

   If the trial shear stress is bigger than the maximum shear stress, the shear stress is resettled to the maximum shear stress and the segment is forced to slid; otherwise the trial shear stress is the correct shear stress of the segment

   If the segment is bonded the shear strength is calculated by:

$$\tau_c = c_b - \sigma \tan(\Phi_b) \qquad 3.8$$

   Where c_b is the bond cohesion, Φ_b is the bond friction angle and σ is the normal stress. If the trial shear stress is smaller than the shear strength, the trial shear stress is a valid stress; otherwise, the bond will break in shear and the value of the stress is set to zero.

3) The moment at the segment is calculated based on gap and bond state

3.5.3 Calibration process

The following calibration process is recommended by PFC2D Flat-Jointed Material Creation and Testing [32]. The procedure is more complicated than the previous calibration process for the linear parallel bond model.

1) Match Young's Modulus during a UCS test at high tensile strength, high bond cohesion and zero friction angle

2) Match Poissons Ratio in the same conditions of the previous step. Might need to go back and forth between 1 and 2

3) Match the bond tensile strength for tensile strength

4) Adjust bond cohesion for matching UCS.

5) Increase bond friction angle to match CCS or Mohrs friction angle

In Practice the process is not as straight-forward as the steps. Adjusting the new parameter in the next step will affect the previously adjusted parameter in the previous steps and it is required to go back to the previous steps multiple times and repeat the cycles to obtain a desired behaviour. However, this effect becomes smaller and smaller by approaching the final steps.

4 The Role of Natural Vibrations in Penetration Mechanism of a Single PDC Cutter

Co Autorship: Chapter 4 has been prepared in accordance with the regulations for a manuscript based thesis guided by Faculty of Engineering at the Memorial University of Newfoundland and has been co-authored as:

The Role of Natural Vibrations in Penetration Mechanism of a Single PDC Cutter. Hossein Khorshidian is the main author and Mohammad Mozaffari and Dr. S. D. Butt are the co-author of this paper. This paper is originally published in the 46th US Rock Mechanics/Geomechanics Symposium, ARMA 12-9, held in Chicago, IL which was held on June 24-27, 2012. Current author conducted coding, computer modeling and data extraction/analyzing. The paper is brought here with no modifications; only the Figure numbers and references are modified to match the formatting guidelines set out by Memorial University of Newfoundland compared to the submitted manuscript to the aforementioned venue.

ABSTRACT: Drilling operation with Polycrystalline Diamond Compact (PDC) bit constitutes vertical oscillations which can both negatively and positively influence the efficiency of the penetration. In order to study the effect of bit vertical vibration in performance of PDC bits, a single PDC cutter-rock interaction, using distinct element methodology, was simulated. It has been observed that the inertia of the cutter play a significant role in vertical oscillations of the cutter. In addition, it has been found that the horizontal speed of the cutter increases the mechanical specific energy of penetration. But interaction between the cutter horizontal speed

and vertical vibrations, due to imposing energized impacts on the rock-cutter interface, improves the value of MSE. However, there is an optimum level for cutter vertical vibrations to achieve an appropriate condition of penetration.

4.1 INTRODUCTION

Vertical oscillations of the bit and drill string during drilling operations, which is mainly due to forces acting on PDC bit cutters, can influence the efficiency of penetration [15]. Study of a single cutter-rock interaction model can provide detail information about effect of drilling parameters such as load on cutter, cutter mass and speed, on drilling responses e.g., cutter force components, vertical vibrations, Depth of Cut (DOC) and amount of required energy for removing the unit volume of the rock. Teal et al. [13] named the latter Mechanical Specific Energy (MSE). The objective of drilling industry is achieving the higher Rate of Penetration (ROP) with minimum MSE value. The cutting action is the result of applying a sufficient load on a cutter and moving it in the direction of the cut. Due to the discontinuous process of chips generation, the force components acting on cutter oscillate [2] and cause vibration in the cutter.

Dunayevsky et al. [20] argued that the dynamic components of the force are primarily the result of the bit-formation interaction. Also, Dubinsky et al. [21] suggested that dynamic forces, which are the result of bit and string interaction with rock, cause vibration in the bit. In addition it was argued that the drill string and bit vibrations are linked to the vertical stiffness of the pipe and the mass of the bottom-hole assembly. Fluctuations of forces in the direction of cut can result in bit stick-slip which in addition to increase in the risk of Bottom-Hole Assembly (BHA) failure, yields reduction in the ROP [22].

In another study of bit vibration, Richard et al. [14] showed that torsional and vertical vibrations of a PDC bit are coupled. Additionally, it has been argued that the bit oscillations could be controlled by changing the Weight on Bit (WOB) and velocity.

In other studies, improvement of bit performance has been observed when a downhole thruster is used in the BHA [23]. Downhole thruster is a tool which converts the differential pressure of the drilling fluids between the inside of the drill string and annular space to load on bit. Therefore, by using this tool it is possible to adjust the mass of the drill collars and load on bit independently. The result of field data also showed an improvement both in bit and drill string life.

In another attempt for improvement in PDC bit penetration, a combination of PDC bit and roller cone bit has been developed, called hybrid bit [25]. In this type of bit, interactions between inserts of rollers and hard rocks cause vertical movement in the bit. Improvement of ROP has been achieved in drilling of hard rocks using hybrid bits.

Results of the previous studies showed significant effects of the dynamics of bit motion on the penetration mechanism; however, there is still no clear insight about effects of the vibration on the penetration mechanism.

4.2 SIMULATION APPROACH

4.2.1 Introduction

In early attempts of rock-cutter simulation using distinct element model (DEM), it has been observed that DEM is able to demonstrate phenomena affecting penetration mechanism of a single cutter such as, transition from brittle to ductile at high pressure conditions [8], generation of ribbon shape cutting in plastic deformation at pressurized cutting condition [12] and generation of the different fractures and cutting shapes under different load on cutter functions [13]. Those phenomena showed an acceptable agreement with real experimental reports.

Akbari et al. [2] in simulation of a single cutter-rock interaction applied a vertical load accompanied with a horizontal force to the cutter. Richard et al. [22] also used the same model for studying the effect of bit vibrations on drilling responses. The abovementioned model is considerably close to drilling scenarios which are being performed in the drilling laboratory.

4.2.2 Generation of the simulation conditions

In order to prepare the simulation environment, steps were taken. Figure 2.1 presents a schematic view of the components and conditions of the simulation. In the first step of the simulation, a rectangular rock sample has been generated based on a DEM contact model which is supported by material genesis function in the library of PFC2D [29].

A linear contact model is chose for generation of rock sample. In the linear model particles with a specific normal and shear stiffness are joined such as two springs in series. Also, the parallel bond and dashpot can be defined along abovementioned contact model. The parallel bonds play the role of cement between particles. DEM parameters have been adjusted to match macro

properties of Carthage Limestone which was obtained from calibration with real UCS tests [29, 55]. The rock sample was generated by defining normal and shear parallel bonds with strength of 91 MN between particles. These particles constitute minimum diameter of 0.35 mm and density of 2620 Kg/m^3. In addition, the stiffness module of the particles at their contacts was adjusted to 83 GPa, which in two dimensional system it is proportional to the normal stiffness of particles. The ratio of the normal stiffness to the shear stiffness is 3.8. These parameters yield a rock sample with UCS of 115 MPa. Also, the coefficient of friction between particles was set to 0.5.

The rock sample constitutes width of 250 mm and height of 30 mm. The local damping of the rock particles is 0.5, and both the normal and shear viscose damping of the contact are adjusted to 0.2. The surface of generated rock is opened for penetration, and the other sides are confined by fixed components which are called a wall. These walls hold the specimen block from any significant motion during penetration of the cutter. The walls are 10% stiffer than the particles. Also, there is no bond and friction between the rock particles and walls.

In the second step, a PDC cutter was simulated. The cutter constitutes fine particles with a stiffness and bond strength about 100 times stronger than the rock sample with the same friction coefficient. The geometry of the cutter was designed in which the length of the cutter is 15 mm, back-rake angle is 20° and wear flat is 0.5 mm.

In the third step, the hydrostatic confining pressure and cleaning conditions were applied. The confining pressure can be applied via a force normal to the contact plane between particles which surround the rock. This pressure was fixed to 6.8 MPa (1000 Psi) for the entire test. The applied confining pressure is acting on surface and right side of the rock. Therefore, the rock will

be confined by the chain of applied pressure and the walls in the other sides. Through this method, the rock will be both pressurized and hold in its place during penetration.

Additionally, a cleaning condition was applied for removing the generated cuttings material. In the application of the cutter cleaning condition it is assumed that a fluid flow can remove the cutting material when the PDC cutter moves them up to 0.5mm above the surface of the rock. The effect of gravity was also set zero.

The cutter starts penetrating the rock by applying a vertical force in direction of “Y” axis and a horizontal velocity in direction of “X” axis (Figure 41). The particles which are used for applying the confining pressure are shown by a different color around the rock specimen. Also, the described cleaned zone is shown in front of the cutter with specified distance to the surface of the rock.

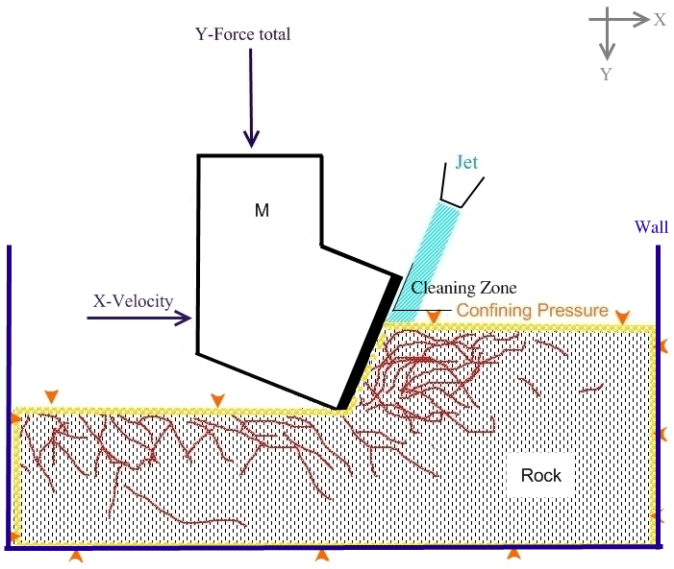

Figure 4.1 Conditions and components of the simulation

A preliminary simulation shows that the particles in the matrix of the generated rock block constitute maximum displacement of 1.25 mm by applying a vertical load of 150 KN and horizontal velocity of 1.5 m/s on a cutter with mass of 5000 kg in a penetration operation.

4.2.3 Testing parameters and data analysis

In order to study the effect of cutter oscillation on penetration responses, the mass of the cutter, vertical load on the cutter and horizontal velocity of the cuter are considered as variable parameters, which were varied over three levels. The selected levels for the mass of the cutter are 2, 11 and 20 Tonne (1000 kg), which can be defined by adjusting the density of the particles in the cutter levels for the vertical load are 100, 125 and 150 KN, and for horizontal speed (Vx) are 0.5, 1 and 1.5 m/s.

The response of the simulation are the "X" and "Y" position of the tip of the cutter, vertical and horizontal force components in the cutter vs. Time (t). In the analysis of the results it was assumed that the simulated components are extruded 1 m toward third axis which will be called the "Z" axis.

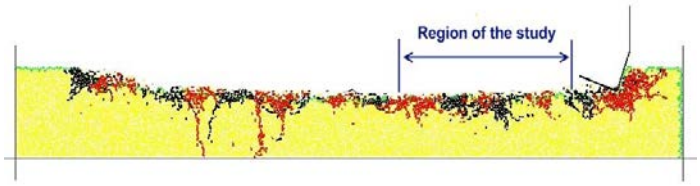

Figure 4.2 Region of study in after penetration of a single cutter

The analysis of data is performed in regions of each test the cutter stabilized its vertical position, and the DOC starts maintaining at a near constant value. The end of this region is 30 mm

away from the wall in the right side of rock. To avoid edge effect this distance is sufficient for a normal chip generation. Penetration near the rock boundary may generate a large chip with near horizontal shear plane and accompanied with upward movement of the cutter or a high horizontal force. Figure 4.2 shows a region of study in a single cutter test. It can be seen that DOC of the cutter began to increase from the start of penetration and because of equilibrium in the force components acting on cutter, reached to a stabilized condition. In order to evaluate the performance of the cutter, MSE of the penetration was computed by Eq. (4.1). The calculated MSE shows the amount of mechanical work of the horizontal force in front the cutter for removing unit volume of the rock. In this equation "F_X" is the horizontal Force in front face of the cutter, "Y" is the DOC and "ΔX" is the cutter advancement in each time step of the simulation. Also, "t_1" and "t_2" are the start and end of the time in the region of the study, and "Z" is the length of third dimension normal to the 2D plane of the simulation.

$$MSE = \frac{\sum_{t1}^{t2} F_x.\Delta X}{Z.\sum_{t1}^{t2} Y.\Delta X} \qquad (4.1)$$

4.3 RESULTS AND DISCUSSION

Table 4-1 shows results of the 27 simulation runs at specified levels of the studied factors. The first column shows the horizontal velocity of the cutter, and the second column shows the mass of the cutter at the three specified levels. The DOC and MSE of the cutter are shown in front of each specified level of vertical load.

The DOC was negatively influenced by increasing the horizontal speed of the cutter and decreasing the vertical load on the cutter. However, the mass of the cutter showed no significant influence on DOC. Also, MSE was significantly affected by all the test factors. The result of the MSE by a polynomial equation is correlated to the test factors. Eq. (4.2) shows the achieved correlation in SI units. Figure 4.3 also presents the predicted MSE vs. actual value for this correlation.

$$MSE = 2.571 + 0.147\,F_y + 4.471\,V_x - 0.00028\,M + 0.307\,(M\,.\,V_x) \qquad (4.2)$$

Where, F_y is the vertical load on the cutter, M is mass of the cutter and V_x is the horizontal speed of the cutter.

Table 4-1 Result of the test for MSE and DOC

H. Vel. (m/sec)	Mass (T)	V. Load (KN)	MSE (MPa)	DOC (mm)	V. Load (KN)	MSE (MPa)	DOC (mm)	V. Load (KN)	MSE (MPa)	DOC (mm)
0.5	2	100	22.05	7.999	125	24.06	9.437	150	26.01	10.27
0.5	11	100	17.55	7.172	125	22.25	8.455	150	23.66	9.758
0.5	20	100	18.98	8.322	125	22.32	8.534	150	24.22	9.364
1	2	100	18.18	4.478	125	23.93	7.515	150	26.63	8.461
1	11	100	27.6	7.572	125	27.11	6.827	150	29.77	8.32
1	20	100	17.46	4.357	125	20.51	8.796	150	31.84	9.385
1.5	2	100	26.08	5.822	125	26.35	6.283	150	32.65	7.739
1.5	11	100	27.95	6.407	125	28.51	6.107	150	35.17	7.916
1.5	20	100	25.1	5.712	125	32.66	6.22	150	37.34	8.811

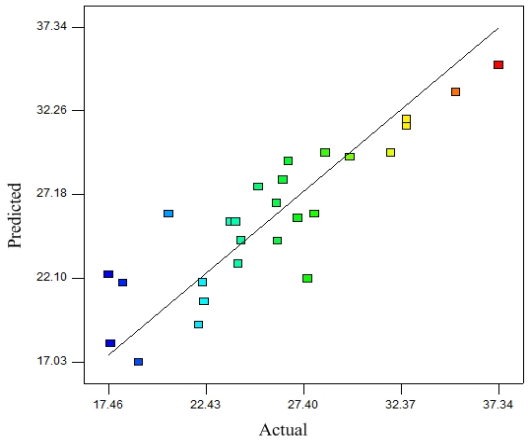

Figure 4.3 Predicted vs. actual MSE in Eq. 4.2

The correlation indicates that despite applying a cutter cleaning condition, increase in the load on cutter yields increase in the value of MSE. This can be related to an insufficient applied cleaning condition and containment of the plastic flow of generated chips resulting from a sub vertical force component under specific the back- rake angle of the cutter [35] and friction between cutter and rock particles.

Additionally, the horizontal velocity showed a positive effect on MSE, i.e. an MSE decrease, and the mass of the cutter showed a negative effect on the MSE. But the interaction between the horizontal velocity and mass of the cutter shows a positive influence on MSE. Fig. 4.4a presents the MSE vs. horizontal velocity and mass of the cutter in a 3D plot at load of 125 KN, and Fig. 4b shows the contour plot of the MSE vs. the abovementioned factors. The trend of the model for horizontal velocity and mass of the cutter at the other levels of vertical load on cutter is the same.

Eq. (4.2)., Figure 4.4a and Figure 4.4b show that increase in the mass of cutter at low cutter horizontal velocity results in a decrease of MSE.

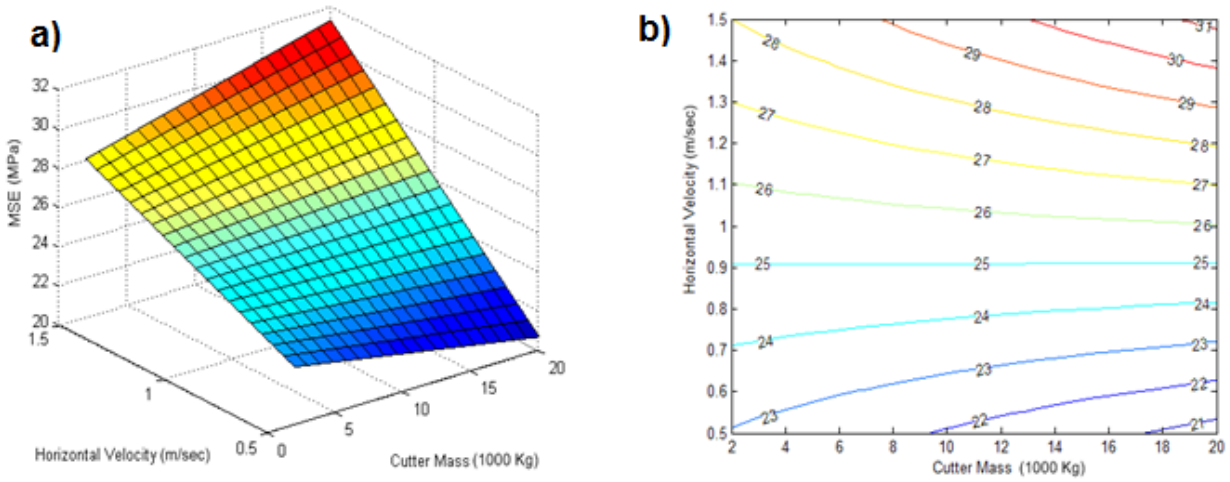

Figure 4.4 a) 3D plot of effects vs. MSE, b) Contour plot of effects vs. MSE

Additionally, at the entire cutter masses, increase in horizontal speed will increase the MSE, but at higher horizontal speeds, lowering the cutter mass decreases the MSE value. The horizontal motion of the cutter during cutting actions is accompanied with vertical oscillations. The oscillations can be observed in the vertical position, vertical velocity and vertical force components of the cutter. The vertical vibration of the cutter is mainly related to the accumulation of particles between the cutter and resultant ramp after crushing the shear plane. Crushing of the shear plane is continued until next chip will be generated. The abovementioned status of penetration, which is described by Tutluoglu [36], is depicted in Figure 4.5. Those generated particles, which are held down by a confining pressure, may cause the cutter to move upward, as the cutter is no longer able to generate a new chip with a small shear angle. The cutter can again move downward as another chip will be generated or when the upward force becomes less than the vertical load on cutter.

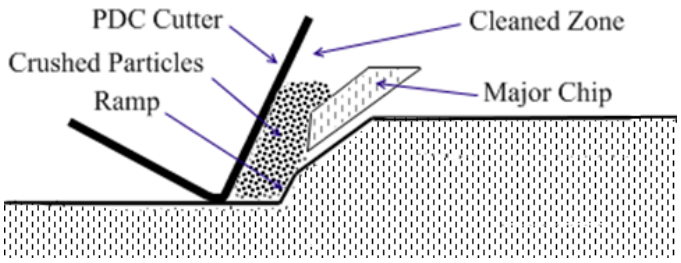

Figure 4.5 Crushed particles between cutter and generated ramp

In order to investigate the effect of the cutter mass and horizontal velocity on the above indicated oscillations, the spectrums of the cutter vertical velocity and components of force in the front face of the cutter, have been studied. The results of the spectral analysis are shown for all levels of the cutter mass, high and low levels of the cutter horizontal velocity and vertical load of 125 KN. The selected levels properly represent the significance of entire test analysis. Figures 4.6a and 4.6b show the spectral analysis for the cutter vertical velocity in the high and low horizontal speed respectively. These figures present that the vertical velocity peak amplitude is higher for low cutter mass. When the cutter constitutes a lower mass inertia, the vertical load on cutter and vertical force resulting from cutting action can excite the cutter with greater acceleration. Therefore, the velocity amplitudes in lower cutter mass conditions constitute higher peak values

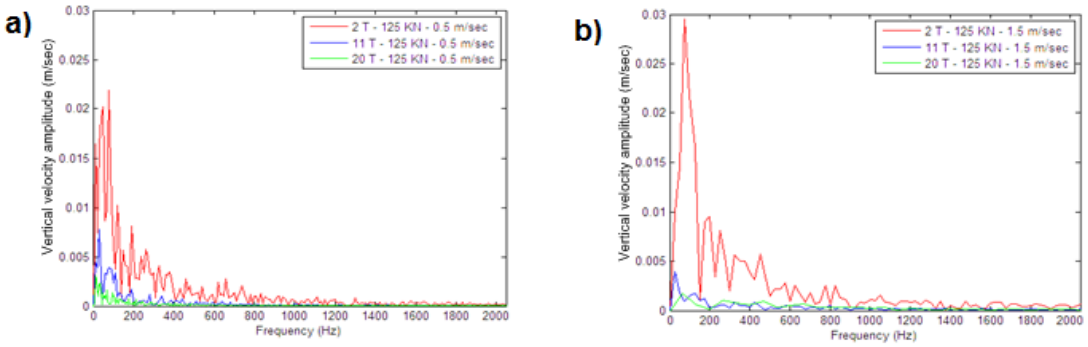

Figure 4.6, a)Spectrum of vertical velocity at horizontal speed of 0.5 m/sec and vertical load of 125 KN, b) Spectrum of vertical velocity at horizontal speed of 1.5 m/sec and vertical load of 125 KN

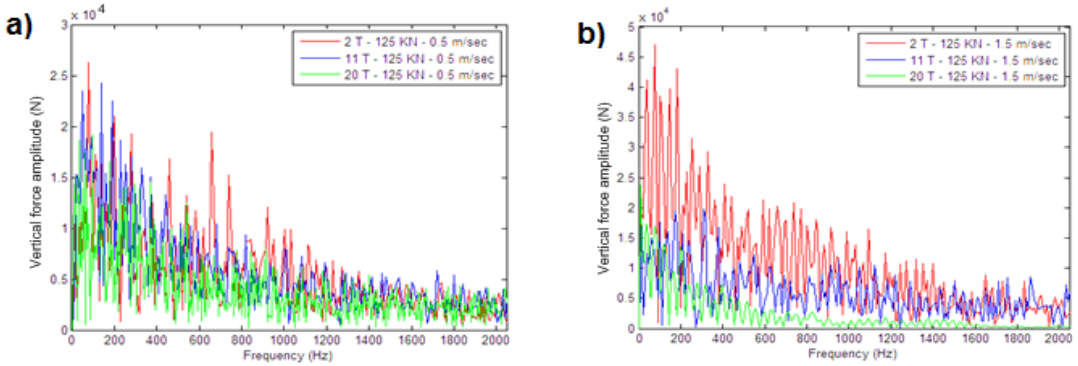

Figure 4.7 a) Spectrum of vertical force at horizontal speed of 0.5 m/sec and vertical load of 125 KN, b) Spectrum of vertical force at horizontal speed of 1.5 m/sec and vertical load of 125

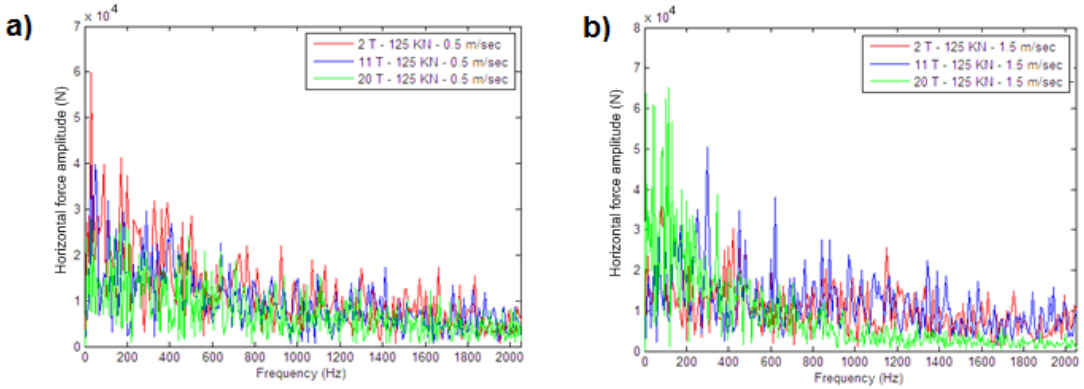

Figure 4.8, a) Spectrum of horizontal force at horizontal speed of 0.5 m/sec and vertical load of 125 KN, b) Spectrum of horizontal force at horizontal speed of 1.5 m/sec and vertical load of 125 KN

Figures 4.7a and 4.7b show the spectrum of vertical force component in the front face of the cutter. These figures imply that vertical force amplitudes of the cutter for a lower mass condition constitute greater peak values. Also, the amplitudes have higher peaks at higher horizontal velocities. Furthermore, the spectral analysis of the horizontal force in the front face of the cutter is presented in Figures 4.8a and 4.8b. The analysis shows that at low horizontal velocity, the lower cutter mass results in higher horizontal force amplitudes, but at high horizontal velocity the lower cutter mass results in lower horizontal force amplitudes.

The aforementioned results indicate that the peak amplitudes of the cutter vertical velocity are linked to the mass of the cutter. The vertical velocity peak amplitude, which is the response of tests, was applied as a factor in a new analysis. The modified polynomial correlation between MSE and peak amplitude of the cutter vertical velocity, horizontal velocity, vertical load and mass of the cutter is shown in Eq. (4.3) in SI units. It can be seen that mass of the cutter showed no significance in the modified correlation, and the role of mass is rendered to "V_y", which is the vertical velocity amplitude of the cutter. Figure 4.9 also presents the predicted MSE of the new correlation vs. actual MSE of the test. Fig. 4.9 implies that MSE shows a better correlation to vertical velocity peak amplitude than to mass of the cutter.

$$MSE = -1.923 + 0.147 \times V_y + 11.304 \times V_x + -34.793 \times V_y - 479.566 \times (V_y \times V_x) + 17894.507 \times V_v^2 \quad (4.3)$$

Figure 4.10a shows MSE vs. the cutter horizontal velocity and peak amplitude of the cutter vertical velocity in a 3D plot at the vertical load of 125 KN. Figure 4.10b also shows the contour

plot of MSE vs. aforementioned factors. The modified MSE correlation implies that improvement in cutter performance can be achieved by optimizing the cutter vertical oscillation with respect to the cutter horizontal speed.

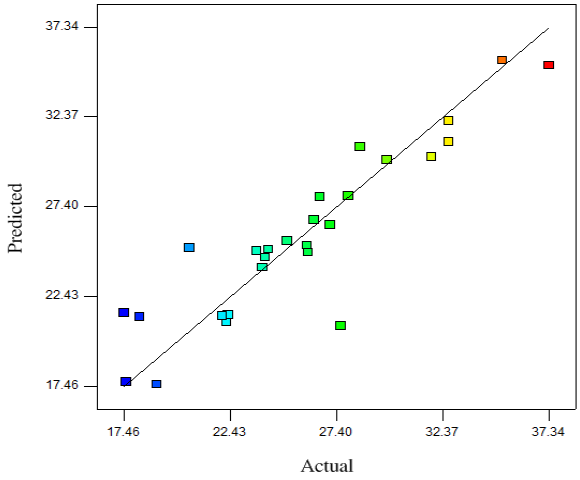

Figure 4.9 Predicted vs. actual MSE in Eq. 4.3

In drilling operations, the higher rotary speed is a potential factor for achieving higher (ROP). Although Table 4-1 shows that at a higher horizontal velocity of cutter the DOC will be decreased, in rotary drilling, due to successive cutting actions, a higher ROP may be achieved at higher rotary speeds. Moreover, an appropriate cutter vertical velocity oscillation can mitigate increase of MSE at higher rotary speeds. For example, Figure 4.10b shows that at a horizontal speed of 1.5 m/s, increase in peak amplitude of the vertical velocity via adjusting the mass of the cutter can drop the MSE from 32 MPa to 25 MPa.

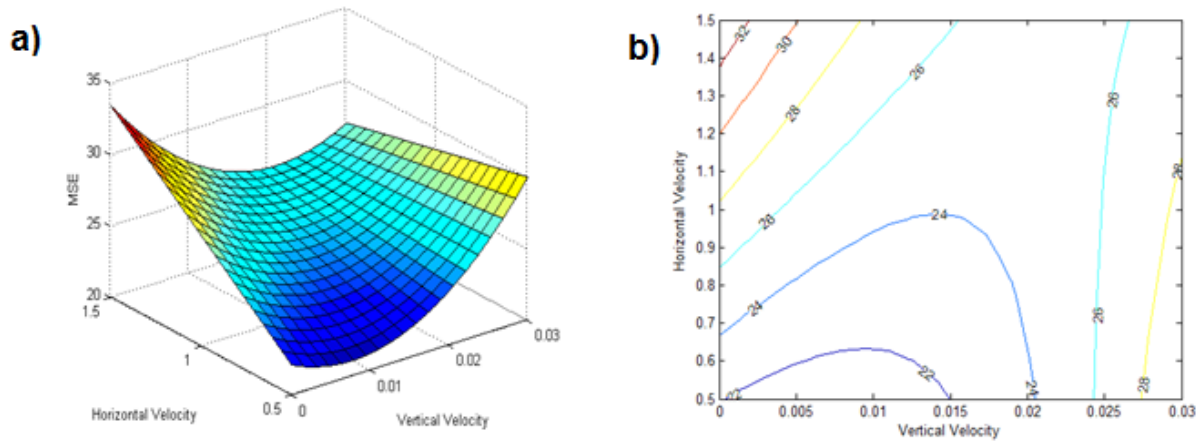

Figure 4.10, a) 3D plot of effects vs. MSE, b) Contour plot of effects vs. MSE

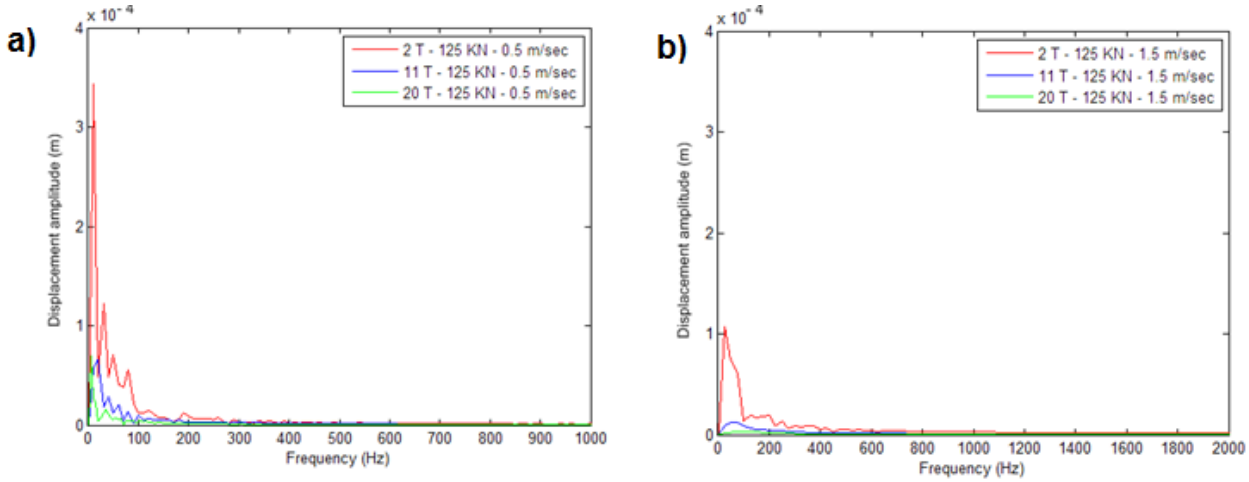

Figure 4.11, a) Spectrum of cutter axial position at horizontal speed of 1.5 m/sec and vertical load of 125 KN, b) Spectrum of cutter axial position at horizontal speed of 1.5 m/sec and vertical load of 125 KN

Spectral analysis of the cutter vertical position in the same levels of the aforementioned analysis is depicted in Figures 4.11a and 4.11b. It can be seen that the peak displacement amplitude of the cutter for a low mass condition is higher than a heavier mass. Also, this value is significantly larger at low horizontal velocity. The reason of decrease in the cutter vertical displacement amplitude in the high horizontal velocity might be due to a high horizontal inertia of the cutter. Thus, the heavier cutter tends to stay at the direction of cut with a low vertical

displacement. Consequently, in this condition the horizontal force amplitude will be larger. This increase may yield no further chip generation. Therefore, the energy of this force will be spent on crushing the rock between the shear plane and cutter. It may also be spent on vertical movement of a heavy cutter and resultant frictional forces in the rock-cutter interface. In the other hand, decreasing the cutter mass at the high speed eases its vertical movement which in addition to decreasing the horizontal force component, applies impacts on the cutter-rock interface.

Upon achieved results it is speculated that there are two signs for influence of the cutter vertical vibration on penetration mechanism. The positive effect can be significant when the cutter imposes a sufficient impact on the rock for cratering. In the other hand, the correlation shows that exceeding the optimal point of vibration will increase the MSE.

The vertical velocity amplitude and vertical displacement amplitude are linked to each other. Therefore, higher vertical velocity amplitudes results in higher displacement amplitudes. However, excessive fluctuations in vertical position of the cutter can result in no penetration in direction of the cut. In the other words, the cutter tends to slide on the ramp instead of chipping or crushing. Therefore, there is an optimal condition for vertical oscillations condition which should be controlled with respect to the other drilling parameters such as horizontal velocity and rock strength.

The main reasons of the improvement in the penetration mechanism of the PDC cutter due to vertical oscillation are both the decrease in the required horizontal force for cutter advancement and the generation of larger chips after imposing an energized impact. As the cutter vertical fluctuations exist for in all horizontal motions, a cutter with a lower inertia consumes less energy

for attaining vertical accelerations. Additionally, those impacts assist the cutter in generation of larger chips and craters. Figure 4.12a shows the generation of the cutting in front of the PDC cutter under a low vertical force oscillation condition, which represents normal chipping. Figure 4.12b shows the generation of the cutting under a high vertical force oscillation condition. The shape of the chip is similar to craters which a wedge may generate on rock surface after an impact. In Figure 4.12b the vertical crack underneath the cutter is due to applying a high energy impact to the rock. In addition to above circumstances, it is speculated that in the case of a lower inertia, the cutter applies a lower pressure on the rock. This pressure is due to accumulation of crushed particles between the rock and cutter with specific back-rake angle.

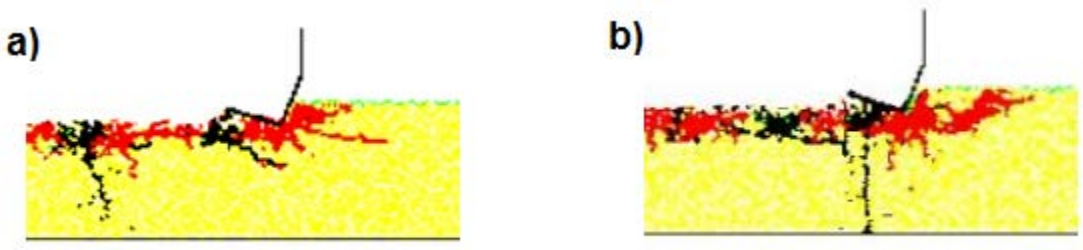

Figure 4.12, a) Generation of chip with no impact, b) Generation of chip after impact

Of course, it is important that cutter vertical vibrations would be able to generate significant cracks in the rock. Otherwise, the vibration only shows a negative effect on cutter performance, which has been observed at low horizontal speed of the cutter. The effect of cutter vertical oscillation on the penetration mechanism can be dependent on drilling conditions such as rock strength, rock elasticity, BHP, cutter geometry, DOC, bit wear and specifically, the drill string stiffness. Therefore, by considering all conditions of a drilling operation, optimizing the vertical oscillations can provide enhancements in the performance of PDC bits.

4.4 FUTURE WORK

The current work is being extended to compare with laboratory data. Those improvements can include on the simulation of the cutter cleaning condition and increasing the model size for longer bit size. It was observed that using a different amount of mass for a penetrating cutter, under same loads on cutter, causes significant changes in drilling responses. The other parameter which can impact the quality of penetration is boundary condition of the cutter e.g. as applying horizontal and vertical stiffness in appropriate locations where the horizontal velocity and vertical load are applied.

Despite many agreements of DEM with realistic penetration phenomena, e.g., properties of shear the plane, ribbon shape cuttings material and dynamic motion of the cutter, the DEM still suffers from lack of fit in amount of DOC and MSE with experimental data. Therefore, furthered improvement is required for a rock distinct element contact model which accounts for compliance at the rock-bit contact. Additionally, the current DEM model of the specimen contains particles with minimum size of 0.35 mm. Therefore, the simulation of fine particles in between the cutter and rock is limited.

4.5 CONCLUSIONS

Following points can be concluded from analysis of the cutter dynamic motion and force components in a single PDC cutter-rock interaction.

- The cutter mass in a rock penetration is a significant factor which influence the MSE of drilling.

- Decreasing the cutter mass, under the same vertical load, causes significant vertical oscillations in a horizontal penetration.

- The source of excitation is the horizontal force on the cutter which pushes the cutter up in the ramp of the rock-cutter interface. These vertical oscillations cause the cutter to impact on the rock when the cutter edge reaches the rock surface.

- The impacts of the cutter can be stronger when the cutter movement constitutes higher vertical velocity amplitudes and horizontal speeds.

- The negative effect of cutter vibrations can be due to the cutter vertical position fluctuations, and the positive effect is related to those impacts that are sufficiently powered for cratering

5 DEM Modeling of Rock and Cutter Interaction: Introduction to the Developed PFC2D Toolkit

This chapter is being prepared to be submitted to the International Journal of Rock Mechanics and Mining Science and is currently being reviewed by the co-authors. Mohammad Mozaffari is the lead author and the co-authors are S. D. Butt and K. Munaswami. Mr. Mozaffri's contribution to this paper is through:

- Writing the manuscript
- Developing the codes for the toolkit
- Performing the tests and tuning the toolkit
- Analyzing results

Dr. Butt was the main supervisor and Dr. Munaswami was the co-supervisor in this project and they provided the lead author with their feedbacks and ideas. Dr. Butt provided the technical guidelines, helping in finding the direction to develop and progress and necessary revisions to the paper. The Figure numbers and references are modified to match the formatting guidelines set out by Memorial University of Newfoundland compared to the manuscript submitted to the journal.

ABSTRACT: A two dimensional DEM rock cutting toolkit was developed. A wide range of aspects of drilling were included in this toolkit. The toolkit was set up to model drilling as realistic as possible. The position of cutter with respect to the rock is not pre-specified but is a

response of contact force between cutter and rock. The toolkit was developed to include as many as possible aspects of the phenomenon, whether simulation aspects or drilling aspects. The particle size was optimized for best performance and result accuracy. A cleaning condition was introduced to remove the crushed material and simulate effect of jet cleaning in front of cutter. A cleaning efficiency was also introduced for this cleaning condition. The toolkit was tuned through multiple steps and further adjusted based on specific needs of each test. The performance of the toolkit was tested against in two scenarios using available published works and the outputs are compared to confirm the capability of the toolkit in the predictions.

5.1 Introduction

In a drilling operation vibration of the bit is a phenomenon which influences the penetration [15] parameters. It is still unclear that if polycrystalline diamond compact (PDC) bit vibration can assist the drilling operation, or it decreases the bit performance [16].

McCray and Cole [24] reported the advantage magnetostriction vibratory drilling. In this technology, an electromagnetic transducer produces a vibration via alternating electric current flowing through solenoids surrounding a laminated core of resonant dimensions. It was argued that adding this tool which produces a vibration frequency of 230 Hz, on a star type of roller cone bits, can double the Rate of Penetration (ROP) at a depth of less than 100 m. No further information was provided for the performance of this vibrator at higher depths of drilling.

Pessier and Damschen [25] developed a new generation of bit which is the combination of roller cones and PDC cutters. Due to actions of inserts of rollers on rock surface, the hybrid bit can create fractures in hard rocks and enhance both the ROP and MSE.

In another effort, Kolle [26] developed a hydraulic actuating tool which generates pulsation in front of the bit, and causes applying vibratory force, which was result of reduction in the pressure drop at the end of drill string. Although, laboratory tests showed the tool resulted 33% of improvement in ROP under buttonhole pressure of 20 MPa, in the field tests no significant improvement in ROP has been observed.

Pixton and Hall [17] also reported the performance of a mud actuated hammer on a PDC bit which was developed at the Novatek Corporation. The PDC bit was utilized with small jets across the PDC cutters which together was called PHAST (Pulsed jet Hammer Assisted Shearing Technology) bit. The hammer assisted rotary drilling showed a promising result under atmospheric condition of the drilling, but at higher BHP conditions no significant improvement was observed [27].

In a simulation experiment of a single PDC cutter-rock interaction, Akbari et al. [2] argued that applying vibratory forces on the cutter can create larger fractures in the rock. However the generation of these fractures was observed to be restricted at high pressures.

Numerical Simulation is an approach to study and predict phenomena involving a rock-bit interaction under different conditions of drilling e.g. load on cutter, confining pressure, torque, rock strength and bottom-hole cleaning. Early studies showed that rock failure simulations using distinct element modeling (DEM), which simulates the behaviour of the system by motion of particles and their interaction, are in an acceptable agreement with experimental data [4].

Additionally, in modeling of the cutter-rock interaction, generation of ribbon shape cuttings material under pressurized condition [12], ductile behaviour of rock failure at pressurized condition [8] and generation of different pattern of chip ahead of cutter under different load on cutter functions [2], show the ability of DEM in simulation of drilling phenomena.

In the present study also DEM has been utilized to investigate the influence of PDC cutter applied vibration on ROP. An early cutting model was developed [17] using PFC2D. Using this early model, simulation of the applied vibration shows no general relation between improvement in MRR and the applied vibration, while the effect of the applied vibration is more considerable in experimental tests which have been performed in Advanced Drilling Group at Memorial University of Newfoundland. Therefore, this model may need improvement to obtain more promising results.

The 2-dimensional particle flow code (PFC2D) was selected for this work because of its capability in modeling a medium represented by DEM. It successfully represents [4, 40, 7, 8, 9. 10] events happening in such a system including force distribution through contacts, crack distribution through the medium, high deformation of the medium due to applied forces, dynamic behaviour of a medium including wave propagation and particle motion and a large number of other events.

The goal of this study is to develop a drilling toolkit that could successfully model and perform a simulation study based on some experimental works. Two works are selected to test the performance of the toolkit: Studies of the Ledgerwood [12] in 2007 and the experimental work Yusuf Babatunde [18] in his Masters.

Ledgerwood [12] performed a series PFC cutting tests on a rock specimen with all elastic bonds deleted. The same rock with bonds has a Uniaxial Compressive Strength (UCS) of 55 MPa (8,000 psi). The rock with no bonds was identical but had cohesion of zero; this material may be imagined like loose sand. He reported in his paper that during cutting under pressure, PFC indicates fifty times more energy is dissipated in friction (the sum of ball to ball and ball to wall friction) than is stored in elastic energy.

Babatunde has worked on a laboratory scale drilling rig in atmospheric condition. He used concrete specimens, created to have UCS of 50MPa to perform atmospheric drilling using a 2" Polycrystalline Diamond Compact (PDC) bit under vibration. To apply the vibration, the specimens were secured on a shaking table. The vibration was applied at three different vibration powers: Low, Medium and High; all at three different frequencies: 45Hz, 55Hz and 65Hz. He also performed his test over a range of Weight on Bits (WOB). By performing his tests, he concluded that the vibration can improve drilling rate; however, the optimum condition is not predictable and real time monitoring of the condition is necessary to optimize vibration for the best performance. A very interesting behaviour was also observed in the trend of the results. It was observed that observed that up to a certain WOB, increase in ROP due to vibration is proportional to the amplitude of the vibration; after this certain WOB, relation of ROP and Amplitude of Vibration is different for different vibration power. Such behaviour was also reported by Li et al. [19].

5.2 Toolkit aspects

The objective of this model is to simulate a two-dimensional rock/bit interaction in a single cutter bit being dragged on surface of a rock. Figure 5.1 illustrates a general idea of what is this

model going to simulate. A DEM rock specimen is surrounded by walls to hold it in place. There is a single cutter being dragged at a horizontal velocity on the surface of the rock while it is being subjected to a vertical force. The crushed materials in front of the cutter are being removed by a cleaning condition to simulate effect of jet cleaning in a drilling bit. There is the capability of applying a confining pressure to the synthetic DEM material to simulate Bottom-Hole Pressure (BHP). The interaction between rock and bit can be vibratory too. Depending on the type of the vibration, i.e. force or displacement, the vibration can be applied to the bit either by vibrating the vertical force or to the whole rock by shaking the confining walls. The rest of this section will go over various important aspects of this toolkit and will explain the development process in more details.

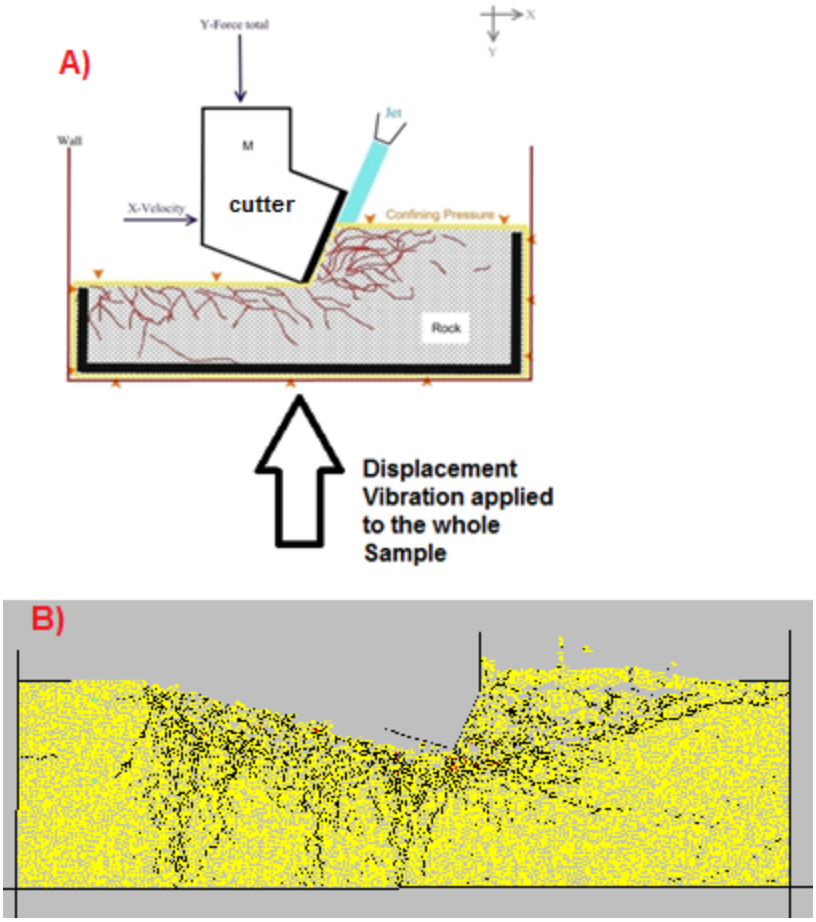

Figure 5.1, overview of the toolkit (A). Toolkit in the middle of cutting action (B)

5.2.1 Cutter and vertical force

In this model the position of the rock specimen is determined by the surrounding walls. These walls act as displacement boundaries for the rock. In order to have a more realistic model it has been decided for the cutter to be able to act on its own. This means that we want the depth of cut to be a response of the vertical force applied. This was only possible if the cutter is created by clumping a series of particles together and applying the desired vertical force to this new clumped particle. In the horizontal direction the boundary condition of the cutter is a constant horizontal velocity. This condition was selected to simulate a condition in drilling where we have

constant rotary Revolution per Minute (RPM). The resulting horizontal force on the cutter could be treated as torque on the cutter. Other boundary conditions of the cutter are no spin in X and Y direction.

5.2.2 Particle size calibration

Depending on the kind of test and required accuracy, most of the time it is required to select an optimum particle size for a DEM simulation. A series of test have also been performed to determine an optimized minimum particle size for the rock specimen. Figure 5.2 represents the results of these tests. Based on the time required to finish a single test and convergence of the amount of the output parameter, which in this case is the material removed, a minimum size of 0.35mm was determined to be the optimized value for our tests.

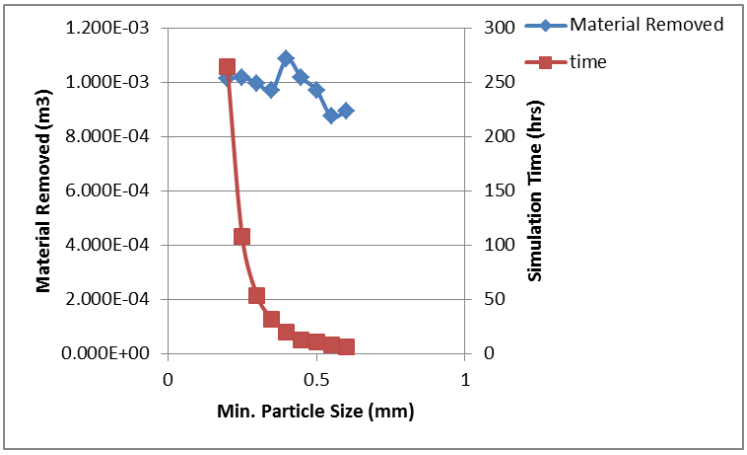

Figure 5.2, optimizing min. particle size: Material removed by drilling (left vertical axis) and total simulation time (right vertical axis)

5.2.3 Damping Layer

One of the problems in the simulation of single cutter test is the small scale of the system compared to applied vertical force on the cutter. The vertical force applied on the rock by the cutter can easily cause the rock specimen to vibrate in its place inside the walls. The rock is vibrating in its place because there is no bond between the walls and the rock. The other

problem, which mainly happens in the scenario when we have vibratory vertical force on the cutter, is the reflection of the waves from the boundary of the system or the walls. These waves could be measured by whether out of balanced force or particle displacement head moving through the rock. To mitigate the problem with vibration of the rock a layer of 10 mm in thickness of particles around the system, see Fig. 5.1, is selected and its density has been increased by 100 times. Therefore the rock specimen is going to be heavy enough so that the vertical force would not be able to move it in place. However this density contrast may cause problem with more reflection of the waves inside the system. Hence the damping coefficient in this layer has been increased to 0.95 to absorb all the waves and reduce their reflection. Figure 5.3 and Figure 5.4 show the effect of this system on the displacement over time for a particle located in the middle of the rock specimen. As it can be seen the vibrations of the particle have been significantly mitigated.

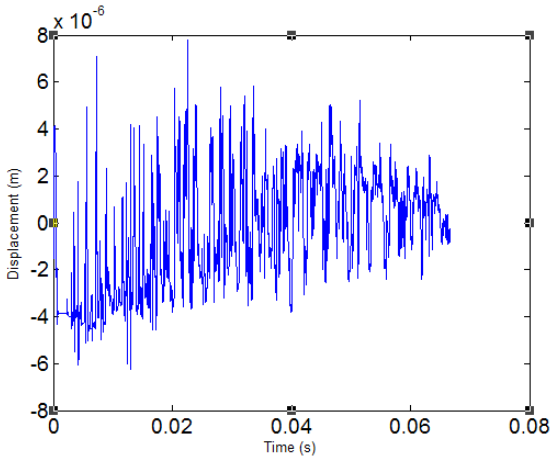

Figure 5.3, Displacement vs. Time for a specific ball in abscence of the dampening layer

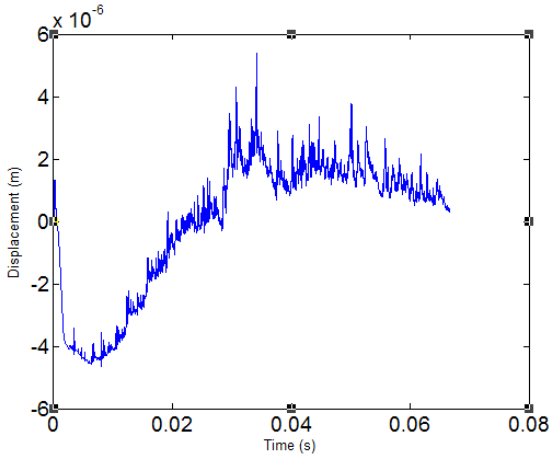

Figure 5.4, Displacement vs. Time for a specific ball in presence of the dampening layer

5.2.4 Cutter Cleaning Condition

One important part in drilling is cleaning the produced cuttings and crushed materials in front of the cutter to reduce waste of the energy by accumulation of the crushed materials in the form of friction. This condition has also been implemented in this model. In an earlier version of the model the cleaning condition was applied in which the generated cuttings were being dissipated instantly as the drilled material entered a defined region as shown in Fig. 5.1. This region is always updated so that it moves with cutter and remains 2 mm ahead of cutter and 2 mm above the surface of the rock. The dissipation process is performed via deleting the particles. A new and more restrictive method was developed to make the cleaning effect more realistic. This new method works based on how many parallel bonds an individual particle has with its surrounding particles. This number can be used to introduce cleaning efficiency in PFC2D simulations. If this number is set to higher values it means that particles with more number of bonds are being removed, which could mean that there is a more efficient and powerful cleaning present. Fig. 5.5 represents the volume removed vs. time at different efficiencies. In this figure, “0” means only a

particle with no bond remaining is cleaned, “1” means a particle with only one or fewer bonds is cleaned and so on. Furthermore, “any” represents the old cleaning method which had no restrictions and all the particles entered the defined region are removed. This figure shows that with more restriction, the volume removed is decreased. Figure 5.6 also shows the vertical position of the cutter versus time. We could see that with less volume cleaning, we have less penetration in the rock. In Figure 5.5 and 5.6 cases “2” and “any” completely overlap. This overlapping is happening due to the specific average particle size of system and with decreasing the average particle size of the rock they become separated.

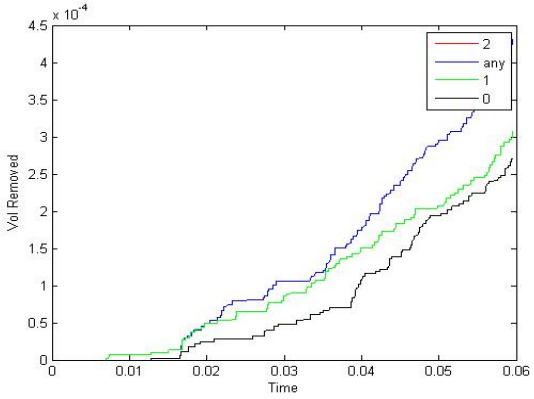

Figure 5.5, Volume cleaned at different efficiencies

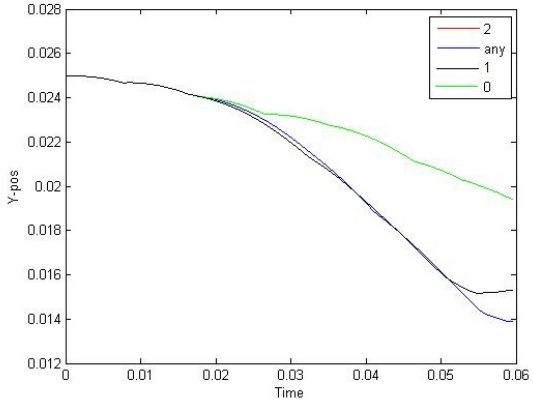

Figure 5.6, position of the tip of the cutter at different cleaning efficiencies

5.2.5 Surface Confining Pressure

One of the important parameters in the drilling of deeper oil wells is the effect of the hydrostatic pressure on the surface of the rock being drilled. This surface confining pressure exerts an extra force on the rock surface and causes a reduced Material Removal Rate (MRR). The decrease in MRR is happening by strengthening the rock plus the chip hold down phenomena. Fortunately, included in the PFC2D library, there is a series of functions with the purpose of finding a specific series of particles or "chain" based on some input parameter determined by user. This "chain" is used to apply a surface force to simulate effect of surface confining pressure. Some modifications were done on this part of library to provide a more realistic model. The most important part of these modifications is the capability for the software to recognize a clump particle as an end or start point of the chain.

The result of the MRR vs. pressure in this model indicates that increasing the confining pressure from atmospheric condition to 10 MPa decreases the MRR about 60%. The logarithmic patterns of the influence of the confining pressure on the cutter performance were also reported in many other laboratory experiments [5, 37].

5.2.6 Adjustments to perform Displacement Vibration

In scenario where displacement vibration is being applied, a few issues prevent all of the particles to vibrate properly as induced by walls. These issues have two main causes; first, there is no bond between the rock sample and the walls; secondly, there is a heavy damping layer surrounding the rock. The first issue causes the rock to slide off inside the walls. The extra weight of damping layer intensifies this effect because heavy rock cannot accelerate as fast as the surrounding walls to vibrate with it. This intensified effect damages the rock significantly (fig. 5.7). In addition, the damping layer significantly reduces the amplitude of the applied vibrations.

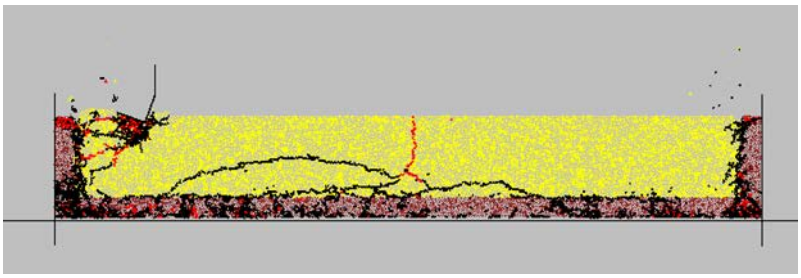

Figure 5.7, damaged rock by displacement vibration in presence of damping layer in early stage of simulation, brown layer is the damping layer

To mitigate the sliding problem two small walls are created at top corners of the rock to prevent the rock from sliding. Also, the damping layer has been removed for this scenario. As a result, the rock does not get damaged and also vibrates properly. Figures 5.8 and 5.9 compare the displacement vibration at two different points in the rock: surface and center, to the applied vibrations on the walls. In figures 5.8 and 5.9 “d2” is the case where there is no pin in presence of the damping layer (original case) while “d1” is the mitigated case. As we can see, the vibration in the “d1” is very close to the applied vibration by the walls.

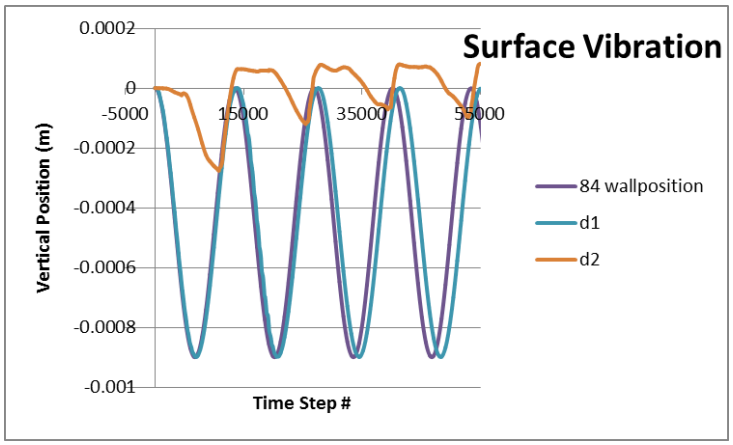

Figure 5.8, Vibration at surface (vertical position) compared to applied Vibration to the walls. d2 is the case where no adjustment has been made and d1 is the mitigated case

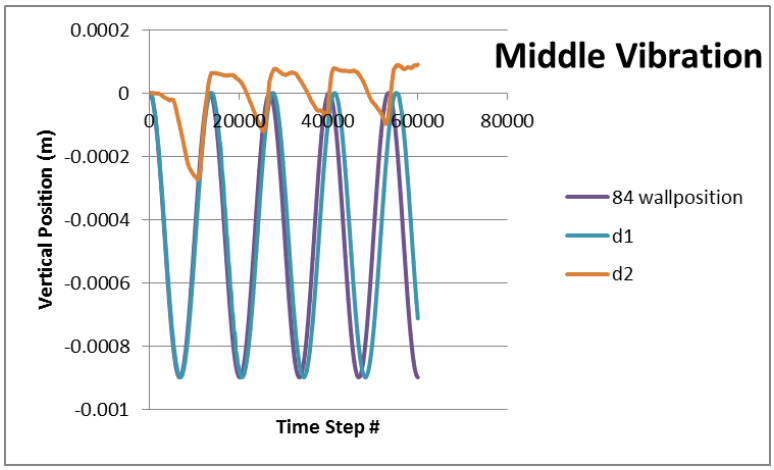

Figure 5.9, Vibration in the middle of the rock (vertical position) compared toapplied Vibration to the walls. d2 is the case where no adjustment has been made and d1 is the mitigated case

5.3 Results

5.3.1 Scenario 1: Loose Sand Model

As mentioned before, Ledgerwood [12] performed a series PFC cutting tests on a rock specimen with all elastic bonds deleted. The same rock with bonds has a Uniaxial Compressive Strength (UCS) of 55 MPa (8,000 psi). The rock with no bonds was identical but had cohesion of zero; this material may be imagined like loose sand. He reported in his paper that during cutting under pressure, PFC indicates fifty times more energy is dissipated in friction (the sum of ball to ball and ball to wall friction) than is stored in elastic energy.

In order to investigate if the same conclusion can be drawn from the new toolkit, a set of experiments were performed using data given in Table 5-1 as input parameter. The purpose of this test was to see the difference between bonded sample and loose sand sample based on the Ledgerwood‘s theory as well as effect of the cutter friction under confined pressure. The test conditions and results are provided in Table 5-1. These results include the volume removed by

cutting, Mecahnical Specific Energy (MSE) with respect to the forces on X direction and MSE with respect to the total forces.

Table 5-1 Test conditions and results

run#	clump friction	Particles	Confining Pressure	WOB	Volume Removed	MSE_X	MSE_T
1	0.5	cemented	3000psi	1.50E+05	0.000616	3.050E+07	3.073E+07
2	0.5	loose sand	3000psi	1.50E+05	0.000803	2.926E+07	3.016E+07
3	0.1	cemented	3000psi	1.50E+05	0.000667	3.030E+07	3.057E+07
4	0.1	loose sand	3000psi	1.50E+05	0.000897	2.879E+07	2.982E+07

By looking at these results it can be concluded that MSE for the loose sand case is very close to the MSE for the bonded sample. This means that in the process of cutting under the pressure most of the energy is dissipated by friction between the particles rather than bond strength. This result confirms the results of Ledgerwood. Furthermore, it can be deducted from the results that decreasing the cutter friction increases the amount of volume of the rock removed by cutting.

5.3.1.1 Scenario 1: Challenge

There is a big challenge in preparing the loose sand sample. Figure 5.10a shows the specimen before deleting bonds between the particles. The black lines indicate the contact forces. Figure 5.10b shows the same sample moments after deleting the bonds. It appears that, since there is big amount of forces between the bonded particles, by deleting the bonds the part that stabilizes these forces is removed, causing the rock sample to explode. This force that is between the bonded particles is the isotropic stress which is set in the material generation steps.

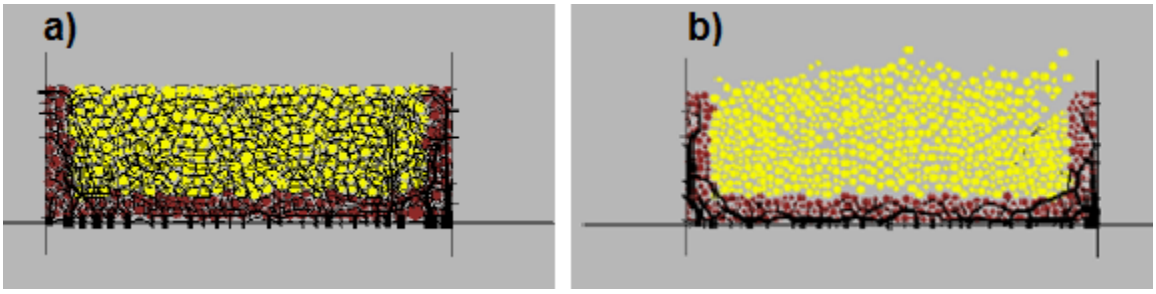

Figure 5.10 Deleting the bonds between the particles creates an explosion effect

To overcome this problem, a “Stepwise Stabilization” method for stabilizing the rock has been developed. This method is comprised of three steps. (Figure 5.11)

Step 1: After generating the material the top confining wall is not deleted. At this time we could remove the bonds between the particles without any explosion because the confining walls will keep the material pressurized.

Step 2: A confining pressure much higher than the final required confining pressure is added to the system to keep the material pressurized; now the top wall can be deleted.

Step 3: Slowly reducing the confining pressure to the desired target pressure.

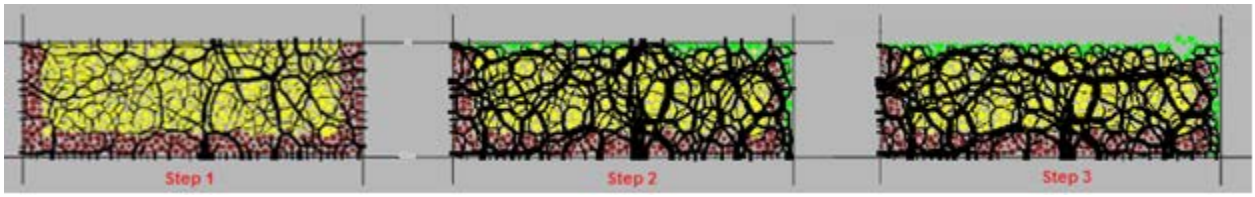

Figure 5.11 Stabilizing the rock specimen when the bonds are deleted

5.3.2 Scenario 2: Displacement Vibration

The purpose for developing this capability into the PFC2D toolkit is to perform a simulation study to replicate Babatunde's work and test the behaviour toolkit against his results. He performed his tests by applying vertical displacement vibration to the rock/bit system. His tests were performed at different Weight On Bits (WOB) by placing the rock specimens on a shaking table and varying vibration frequencies and powers. He called the three different vibration power modes Low Vibration Shaker Power (LVSP), Medium Vibration Shaker Power (MVSP) and High Vibration Shaker Power (HVSP). He later reported the vibration characteristics for each test in the form of displacement amplitude. In order to repeat his work, the toolkit needs to develop the capability to apply a displacement vibration at the contact between rock and the cutter. The system has a constant WOB applied on the cutter; therefore, the cutter cannot accept the applied displacement as second boundary condition in the vertical direction. Instead, the rock should be vibrated to create the same effect of vibration at contact between rock and the cutter (Figure 5.1). A few issues with this scenario prevent all of particles to vibrate properly as induced by walls; these issues and the solution to them are reviewed previously in Section 5.2.6.

Table 5-2 represents an overview for the domain of several parameters in the Babatunde's work. Babatunde as well as Li et al. [19] have observed that up to a certain WOB, increase in ROP due to vibration is proportional to the amplitude of the vibration; after this certain WOB, relation of ROP and amplitude of vibration is different for different vibration powers. In order to show this behaviour he represented his results in form of normalized-ROP which is ROP divided by amplitude of vibration in that specific test. Figures 5.12 to 5.14 represent experimental results of Babatunde at different frequencies.

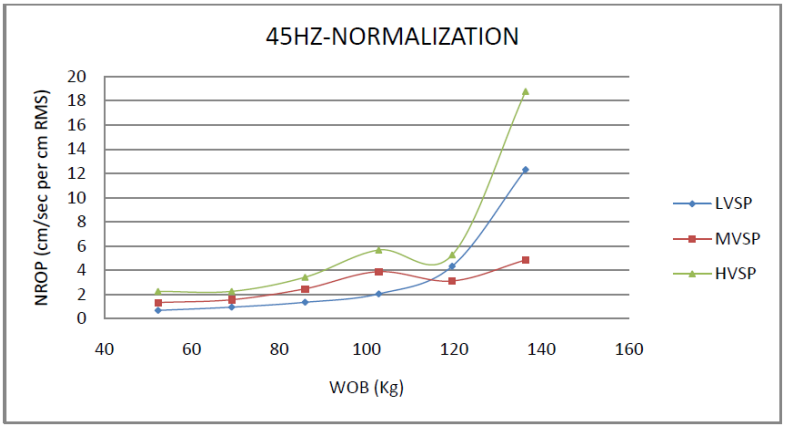

Figure 5.12 Experimental results of Babatunde at 45 Hz [18]

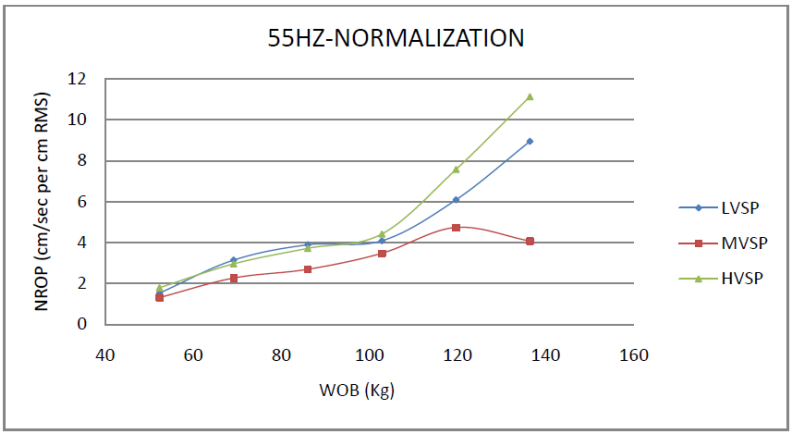

Figure 5.13 Experimental results of Babatunde at 55 Hz [18]

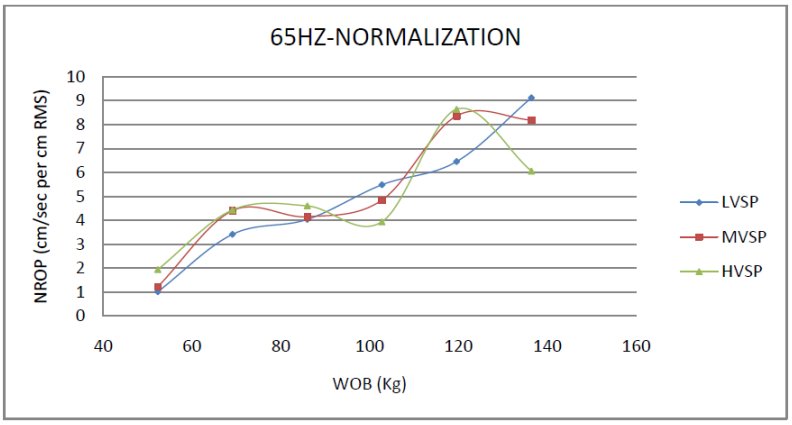

Figure 5.14 Experimental results of Babatunde at 65 Hz [18]

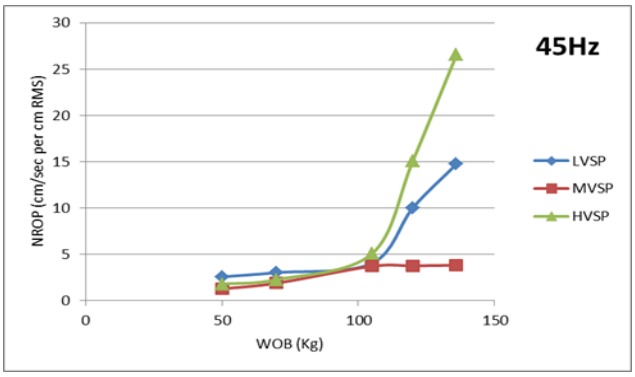

Figure 5.15 Simulation results 45 Hz

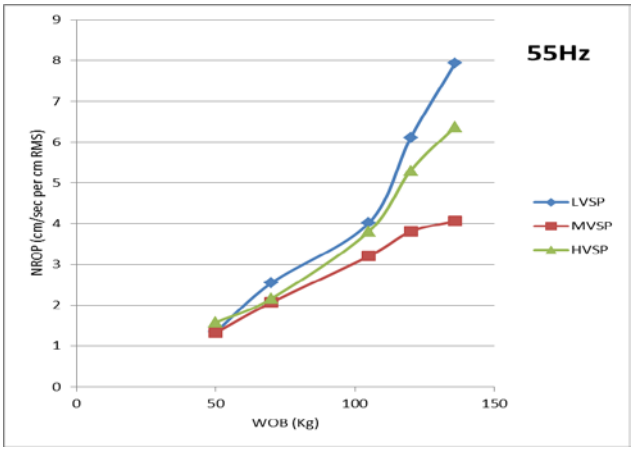

Figure 5.16 Simulation results 55 Hz

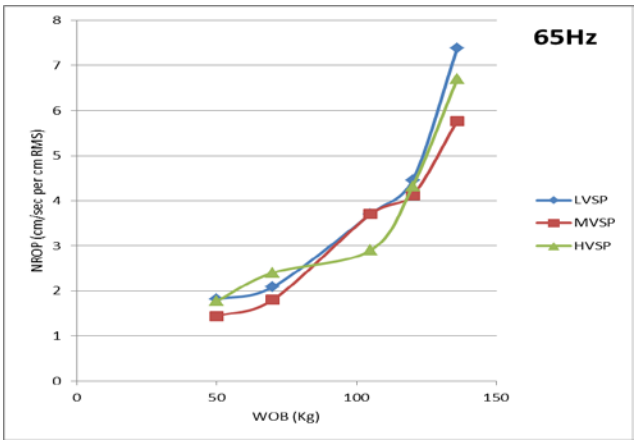

Figure 5.17 Simulation results 65 Hz

Table 5-2 Test conditions of Babatunde[18]

Parameter	Values		
WOB(kg)	45 - 129		
Frequency(Hz)	45	55	65
Shaking Power	Low	Medium	high
Bottom Hole Pressure	Atmospheric		
Bit RPM	300		

Figures 5.15, 5.16 and 5.17 represent the simulation result of the Normalized Volume Removed WOB at different frequencies for different vibration powers based on test conditions of Table 5-2. Appendix C explains the method used to calculate ROP in two dimensions. The simulation results predict that this model is showing the same behaviour mentioned above by Babatunde and Li and the model it is capable of showing the same trend. This means that the toolkit is very well capable of predicting and reproducing the phenomena qualitatively. These results are valid only for qualitative comparisons because the toolkit is in two dimensions.

5.4 Conclusion

A two dimensional DEM rock cutting toolkit was developed including a wide range of aspects of drilling. The toolkit was set up to model drilling as realistic as possible. The position of cutter with respect to the ruck is not pre-specified but is a response of contact force between cutter and rock. The toolkit was developed to include as many as possible aspects of the phenomenon, both for the simulation aspects or drilling aspects. The particle size was optimized for best

performance and result accuracy. A cleaning condition was introduced to remove the crushed material and simulate effect of jet cleaning in front of cutter. A cleaning efficiency was also introduced for this cleaning condition.

The test results indicate this toolkit is successful in replicating the experimental test results available. The confining pressure has a negative effect on Material Removal Rate and its effect becomes smaller as the pressure increases. Effect of particle friction on required energy for drilling was successfully observed. The toolkit could successfully represent that in drilling under pressure most of energy is dissipated through the particle friction rather than for breaking the rock and overcoming the bond forces.

In displacement vibration, the model successfully replicated the experimental results. The results of normalized rate of penetration vs. weight on bit follow the same qualitative pattern as the reported experimental result.

Considering all the successful replications and included aspects, this toolkit can be assumed as a very reliable candidate for further studying events dealing with drilling or investigating simulation aspects such as investigating new contact models.

6 DEM Investigation of the Drillability Parameter

This chapter is being prepared to be submitted to the International Journal of Rock Mechanics and Mining Science and is currently being reviewed by the co-authors. The lead author is Mohammad Mozaffari and the co-authors are Tatyana Katsaga and S. D. Butt. Mr. Mozaffri has performed the required research for this paper through his internship with Itasca Consulting Group, Toronto funded through Mitacs-Accelerate program and Mr. Mozaffri's contribution to this paper is through:

- Writing the manuscript
- Calibrating the synthetic material and performing the tests
- Analyzing results

Tatyana Katsaga was the supervisor of the lead author at Itasca Consulting Group. Both Butt and Katsaga provided the lead author with their feedback and ideas, technical guidelines, guidelines, the necessary revisions to the paper and helping in finding direction in order to develop and progress in this project. The figure numbers and references are modified to match the formatting guidelines identified by Memorial University of Newfoundland compared to the submitted manuscript to the journal.

ABSTRACT: The Flat-Joint contact model was used to calibrate different DEM synthetic materials. The materials were tuned based on available experimental data which are Drillability parameters for different concrete specimens. These synthetic materials were tested under normal material tests to further study the specific parameters of the Flat-Joint model and their effects.

Furthermore, the materials are used in a previously developed and tuned [38] drilling toolkit to study behaviour of different materials with this advanced contact model in drilling operation. In addition, the Drillability parameters were challenge in their capability to characterize rocks for drilling operation. The result of the new contact model was compared to the old linear parallel-bond contact model and development in replicating experimental data was observed. Furthermore, the results were tested against available correlations and it has been found out that they follow the correlations closely.

6.1 Introduction

Distinct Element Method (DEM) models [3] are a class of material models that represent the material as a domain of small elastic balls bonded by non-linear elastic springs with defined shear and tensile bond strengths. These models have the ability to model small-scale failure processes in rock-like materials. The failure of bonds between stronger grains has been repeatedly demonstrated to accurately model failure in geomechanic experiments [4, 3]. No other major form of material models (e.g. Finite Element Method, Finite Difference Method) has the ability to model these small scale failure processes in rock-like materials. Calibration of the modeled material with the real materials is performed by adjusting of ball and bond properties until properties of the simulated material can calibrate the bulk or macroscopic failure properties of real materials [3]. This kind of material can represent concrete which is a material composed of a Portland cement-based matrix and rock aggregate, and has similar material properties and failure behaviour as low-permeability, sedimentary rocks.

Baker-Hughes [28] has proposed a quantitative methodology to describe rock materials in terms of their drillability as a means of predicting rates of penetration and wear, which are closely linked to strength and abrasivity. This methodology includes eight material properties—density, porosity, compressional and shear wave velocities, Unconfined Compressive Strength (UCS), Mohr friction angle, mineralogy and grain sizes—that can be represented on a spider plot as a drillability curve relating all eight properties. Appendix D summarizes these eight Drillability parameters.

Xia et al. (2009) [4] investigated the failure patter of rock under uniaxial compression test and compared the experimental results with the outputs generated with DEM compression to investigate the fracture process. They showed that rock failure simulations using DEM are in an acceptable agreement with experimental data and the fracture patterns produced by modelling closely resembled the fractures seen in the laboratory test.

A larger number of researchers confirmed that results of the simulation test shows agreements of DEM with realistic penetration phenomena, e.g., properties of shear the plane, ribbon shape cuttings material and dynamic motion of the cutter. [39, 2, 12]

Being successful in representing the rock, flexibility in modeling of systems under high deformation which is the greatest advantage here over FEM and the successful works published in the literature [4, 40, 7, 8, 9. 10], the final conclusion was drawn that utilization of DEM would be the method of choice for this study.

The 2-dimensional particle flow code (PFC2D) was selected for this work because of its capability in modeling a medium represented by DEM. It successfully represents events happening in such a system including force distribution through contacts, crack distribution

through the medium, high deformation of the medium due to applied forces, dynamic behaviour of a medium including wave propagation and particle motion and a large number of other events. [4, 40, 7, 8, 9. 10]

The main task of PFC2D, or any other DEM software, is to simulate an environment by assuming that environment is created by tiny particles that are free to move and can interact with each other at their contacts. This interacting is simulated with a contact model, with optional parallel bond and dashpot in parallel.

The contact model that has been used in the previous study [38] is the linear contact model. In that contact model the particles interaction is in the form of friction and exert force to one another with linear springs (contact entries) in series. The synthetic material that is simulated with this method exhibits the relevant physical behaviours of a brittle material such as rock. However, the produced assembly of the particles that create the synthetic material is a valid structure of its own and its micro-structure should not be confused with that of the actual rock [29]. If it is desired to pay attention to micro-structure of the synthetic material, user has to go with more advanced contact models such as Flat-Joint contact model. Furthermore, one major problem with linear parallel bond model is that the UCS and tensile strength cannot be tuned separately. In the linear parallel bond model, there is no means other than bond strength to adjust the UCS of the material; therefore, the bond tensile strength should be significantly high in order for the model to represent the desired UCS. It is reported that if one matches the unconfined-compressive strength of a typical hard rock, then the direct-tension strength of the model will be too large [30]. This limitation can be overcome by using the more advanced contact model, i.e. Flat-Joint model. In this model, even after the bond is broken, the system can resist compression by interlocking the particles. This only happens because of the polygonal behaviour that the

contact model causes in the particles. The polygon shape of the particles forces the particles to interlock under compression; therefore, they would resist rotation even after bond breakage. [30, 31, 32]

A set of reference data were extracted using Drillability data that are experimentally measured. These set of data are used for calibrating three DEM materials. These DEM materials are to be used later in the rock cutting DEM toolkit that has been already developed and tuned by the author [38], using available experimental studies [40,12,18], to further study the behavior of different rock types in a cutting phenomenon. Table 6-1 represents these reference data. Appendix E explains the analysis of the experimental data and preparations performed for generating Table 6-1

Table 6-1, Target Properties

	UCS (MPa)	density (kg/m3)	friction angle (degree)	E (GPa)	Poisson's Ratio	T (MPa)
Low Strength Concrete	21.59	2013.9	57	27.48	0.3	2.159
Medium Strength Concrete	48.9	2291.7	59	39.14	0.25	4.89
High Strength Concrete	90	2400	62	45	0.2	9

6.2 Calibration and results

The following calibration process is recommended by PFC2D Flat-Jointed Material Creation and Testing [32]. The procedure is more complicated than the previous calibration process for the linear parallel bond model.

1) Match Young's Modulus during a UCS test at high tensile strength, high bond cohesion and zero friction angle

2) Match Poisson`s Ratio in the same conditions of the previous step. Might need to go back and forth between 1 and 2

3) Match the bond tensile strength for tensile strength

4) Adjust bond cohesion for matching UCS.

5) Increase bond friction angle to match CCS or Mohr's friction angle

In action the process is not as straight-forward as the steps. Adjusting the new parameter in the next step will affect the previously adjusted parameter in the previous steps and it is required to go back and forth multiple times between few steps. However, this effect becomes smaller and smaller by approaching the final steps. Appendix F summarizes the tests performed to tune the medium material as an example of this process. However, it is recommended to review the rest of this chapter and appendices for a better understanding of the included table in the Appendix F.

For simplicity it is assumed that the strongest material has no gapped contact, i.e. all the Flat-Joint contacts are bonded. For the medium material, an arbitrary low percentage of gapped contacts are selected. But two different weak materials are created based on two different approaches. They are to be called "Weak1" and "Weak2". The reason behind this decision was to investigate behaviour of two materials with the same target properties, but with different micro-properties. The Weak1 material has the same percentage of gapped contacts as the medium material. For the Weak2 material, a slightly different approach was followed. In this material the "slit" contacts are included for the first time. For the calibration process a minimum particle size of 0.6 mm was selected. The minimum particle size or specimen resolution was selected as it seems to be an optimum size for efficiency and accuracy. Using this size every synthetic rock specimen would end up with minimum number of particles to perform a

simulation as fast as possible and at the same time ensure the accuracy was not sacrificed. After calibration is performed the effect of minimum particle size was studied on the target properties. However the minimum particle size should be adjusted prior to each study according to the specific needs of the application. An example of this study is performed by Mozaffari et al. [38].

6.3 Analysis

For each material, a range of sensitivity analysis has been performed. The sensitivity is performed on parameters such as confining pressure, minimum particle size and specially the Flat-Joint specific contact properties, i.e. percentage and size of the gapped contacts. The rest of this section goes over the overview of this analysis.

6.3.1 Strong material

The summary of the sensitivity analysis on the strong material is provided in Table 6-2. As mentioned earlier all contacts are bonded here. The analysis is performed on the effect of minimum particle size or resolution. The compression test is also performed over a range of confining pressure from 0 Psi, which resembles UCS test, to 2000 psi. The friction angle is calculated for each stage according to appendix B. Young's Modulus and Poisson's Ratio are also calculated according to appendix A.

Table 6-2, Strong material sensitivity analysis

Rmin (mm)	Tensile Strength (Mpa)	E(Gpa) (PFC output)	v (%)(PFC output)	Strength(Mpa)(0/350/850/1200/2000 Psi)	Friction Angle (degree)
0.35	7.75	46	18	84.3	
				119.5	60.65
				141	46.36
				160	43.4
				188.5	42.5
0.6	9.5	45	19	86	
				123	61.34
				147	48.5

6.3.2 Medium material

The summary of the sensitivity analysis on the medium material is provided in Tables 6-3, 6-4 and 6-5. As mentioned earlier 5% of the contacts are gapped here and there is no slit contact. To maintain the gap size relative to the resolution the sizes of gaps are expressed with respect to the minimum particle size. Therefore, (initial gap distance/Rmin) = 0.1 for the case with Rmin=0.35mm means that the gap distance is 0.035 mm and so on for the rest of tests. The Elastic properties, i.e. Young's Modulus and Poisson's Ratio, are calculated in two methods as described in appendix A and friction angles are calculated using the method in appendix B. The analysis here is performed on both gap size and gap percentage. Once again the effect of confining pressure on the Compression test results is investigated. The entire analysis is performed on three different resolutions; min. particle sizes of 0.35mm, 0.6mm and 0.85mm.

Figure 6.1 represents the effect of gap size and percentage as well as specimen resolution for this analysis in intact specimens. As the min. particle size decreases, the number of particles in a specimen increases therefore the resolution increases. Also, increasing gapped contact percentage and its size is visible.

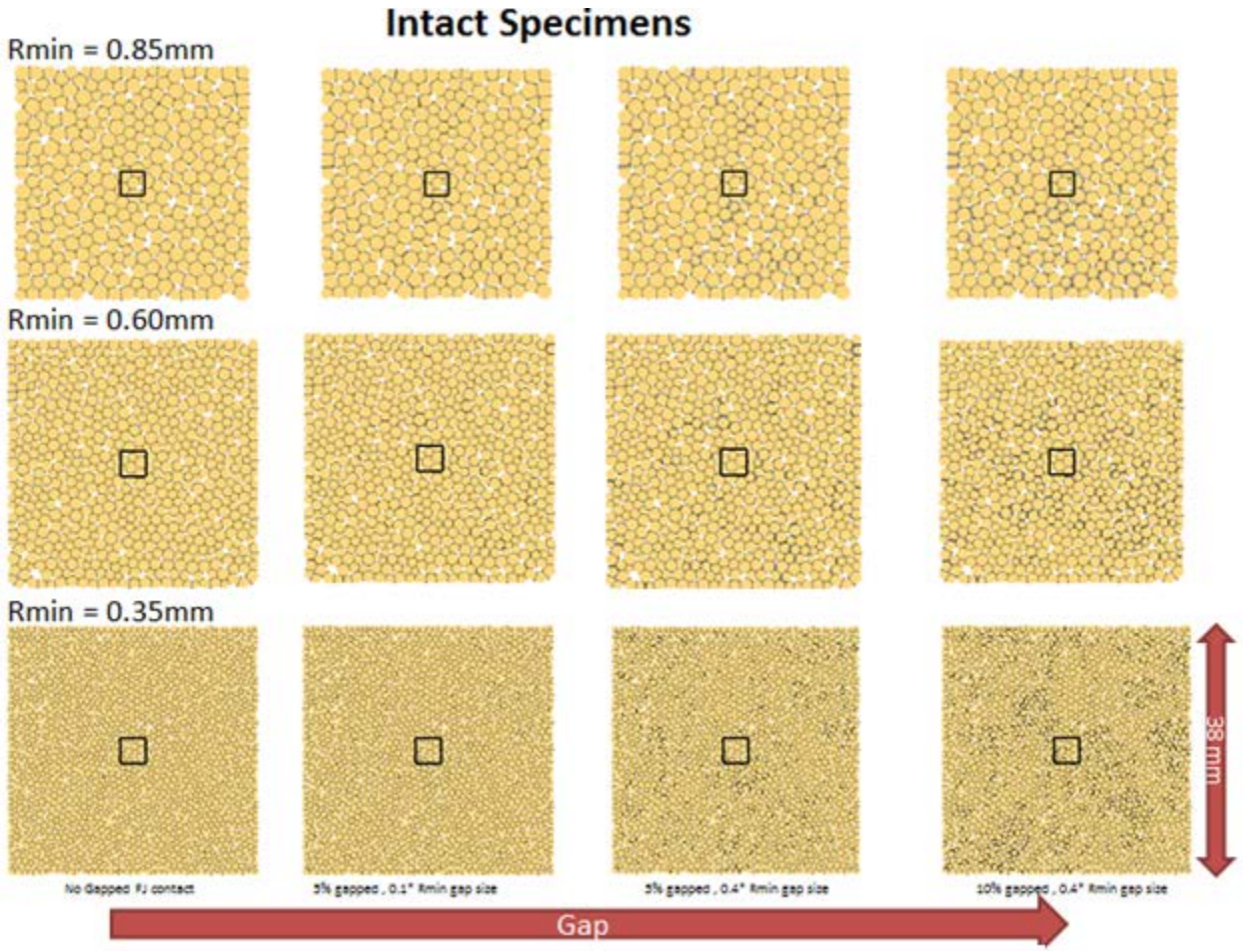

Figure 6.1, effect of gap size, gap percentage and min. particle size on medium material

Figures 6.2 and 6.3 represents the effect of gap size and percentage on UCS and CCS test results at highest resolution. They represent the decreasing strength with increasing gap. Also the failure pattern is changing from brittle with distinct shear planes to plastic with random failure and crushing. There are more shear (blue dot) micro-cracks in the CCS test in the specimen with fewer gaps. In the specimens where only gap size has changed no difference in any of the results is observed. This could be because of the relatively low gap percentage to see such an effect.

Table 6-3, Medium material sensitivity analysis, Tensile tests

		Tensile Strength (Mpa)			
gapped ratio		0.00	0.05		0.10
init. Gap dst./Rmin		0.40	0.40	0.10	0.40
Rmin (mm)	0.35	5.23	4.37	4.37	3.64
	0.6	5.40	4.86	4.86	3.93
	0.85	3.56	3.33	3.33	2.77

Table 6-4, Medium material sensitivity analysis, Elastic Properties

		Triaxial							
		E(Gpa) (PFC output/Matlab output/difference%)				v (%) (PFC output/Matlab output/difference%)			
gapped ratio		0.00	0.05		0.10	0.00	0.05		0.10
init. Gap dst./Rmin		0.40	0.10	0.40	0.40	0.40	0.10	0.40	0.40
Rmin (mm)	0.35	36.00	37.50	37.50	35.00	37.00	28.00	28.00	21.00
		46.76	42.89	42.89	37.45	25.41	26.14	26.14	25.63
		23.01	12.57	12.57	6.54	45.62	7.10	7.10	18.05
	0.6	38.00	36.80	36.90	32.00	30.50	25.70	25.80	25.00
		45.09	40.51	40.51	33.61	25.15	26.77	26.77	26.78
		15.73	9.16	8.91	4.79	21.27	4.00	3.63	6.66
	0.85	35.00	34.00	34.00	31.40	34.00	28.00	28.00	27.00
		43.91	39.28	39.28	34.32	27.59	26.76	26.76	27.82
		20.29	13.44	13.44	8.51	23.23	4.62	4.62	2.95

Table 6-5, Medium material sensitivity analysis, Compression Test

		Triaxial							
		strength(Mpa) @ (0/350/850 Psi conf.)				Friction Angle			
gapped ratio		0.00	0.05		0.10	0.00	0.05		0.10
init. Gap dst./Rmin		0.40	0.40	0.10	0.40	0.40	0.40	0.10	0.40
Rmin (mm)	0.35	68.00	44.00	44.00	28.50				
		100.70	79.70	79.70	55.00	59.60	60.85	60.85	56.40
			109.30				52.32		
	0.6	55.80	43.50	44.00	30.00				
		88.00	76.00	79.00	52.50	59.37	60.57	59.50	53.34
			100.50				48.88		
	0.85	55.50	38.00	38.00	22.50				
		84.00	57.00	57.00	40.50	57.55	50.76	50.76	49.77
			82.00				49.26		

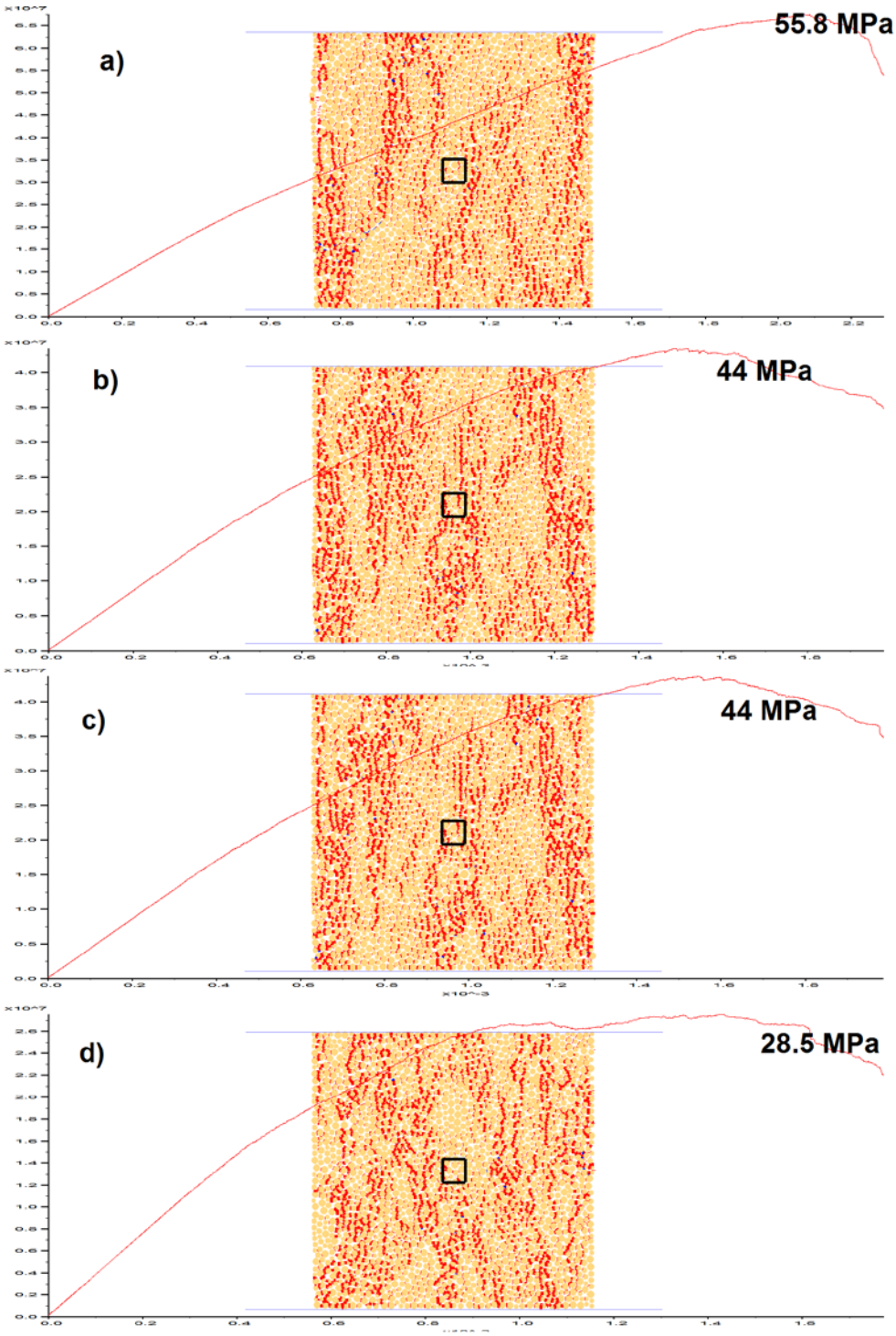

Figure 6.2, Effect of gap on UCS test for the highest resolution specimen medium material. Final state of the rock after breaking point is overlapped on Stress vs. Axia Strain curve (the CCS strength is marked on plots). Red is tensile micro-crack and blue is shear micro-crack a) No gapped FJ contact, b) 5% gapped, 0.1*Rmin Gap size, c) 5% gapped, 0.4*Rmin Gap size, d) 10% gapped, 0.4*Rmin Gap size

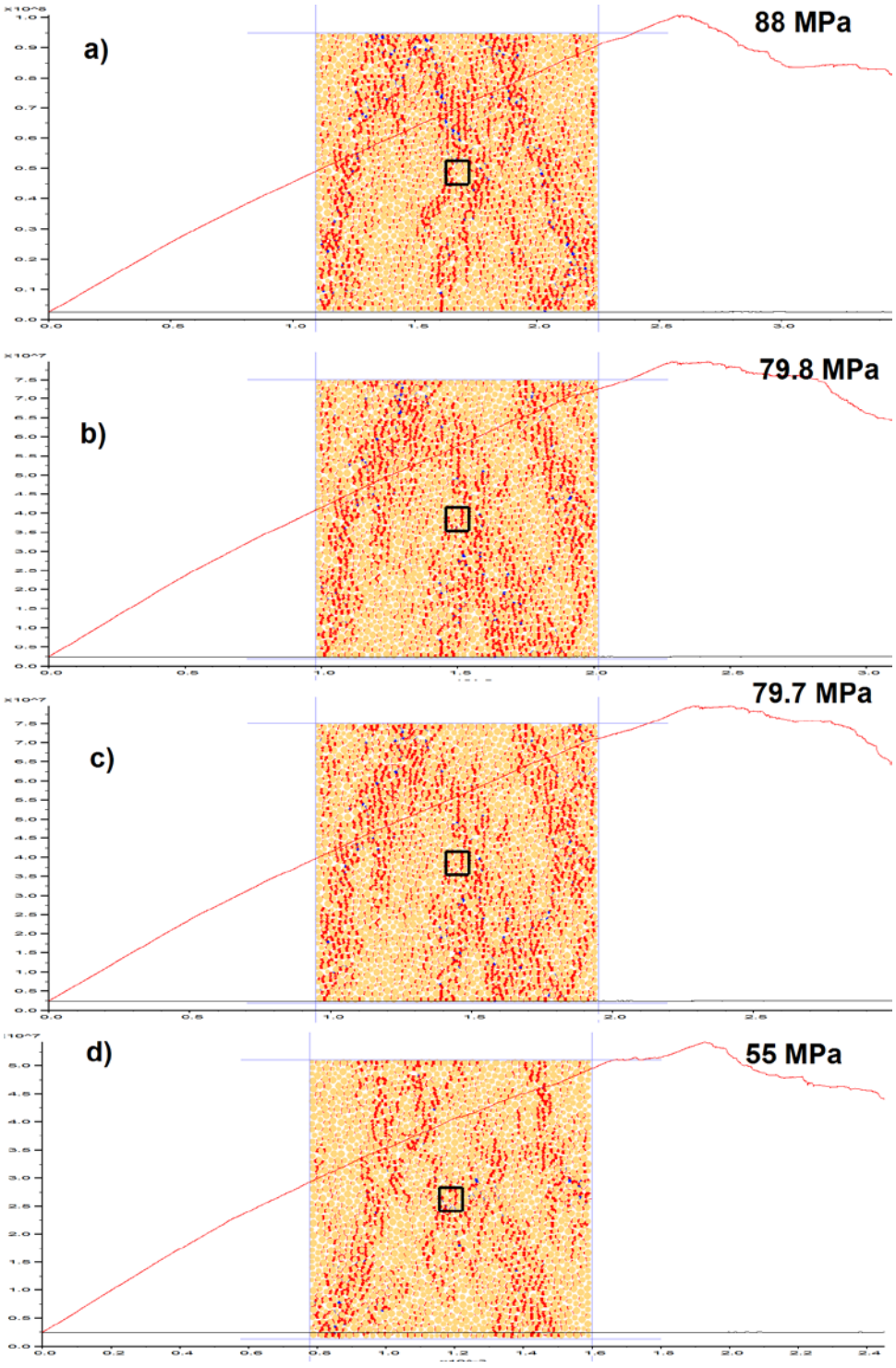

Figure 6.3, Effect of gap on CCS test for the highest resolution specimen medium material. Final state of the rock after breaking point is overlapped on Stress vs. Axia Strain curve (the CCS strength is marked on plots). Red is tensile micro-crack and blue is shear micro-crack a) No gapped FJ contact, b) 5% gapped, 0.1*Rmin Gap size, c) 5% gapped, 0.4*Rmin Gap size, d) 10% gapped, 0.4*Rmin Gap size

6.3.3 Weak1 material

The summary of the sensitivity analysis on the strong material is provided in Tables 6-6, 6-7 and 6-8. The target properties of this material are adjusted calibrate the ones of the weakest material. The gapped content for calibration is the same as the medium material. The sensitivity analysis here is concentrated on effect of gap in size and percentage over a wider range. Once again all tests are performed with no slit contact. All the tests are repeated at different resolutions as well. The Elastic properties, i.e. Young's Modulus and Poisson's Ratio, are again calculated in two methods as described in appendix A and friction angles are calculated using the method in appendix B.

Figure 6.4 represents the Stress vs. Axial and Lateral Stain for the Weak1 material at highest resolution for various gap size and percentages. It can be seen that increasing gap affects the material in behaving less brittle as well as reducing the material strength.

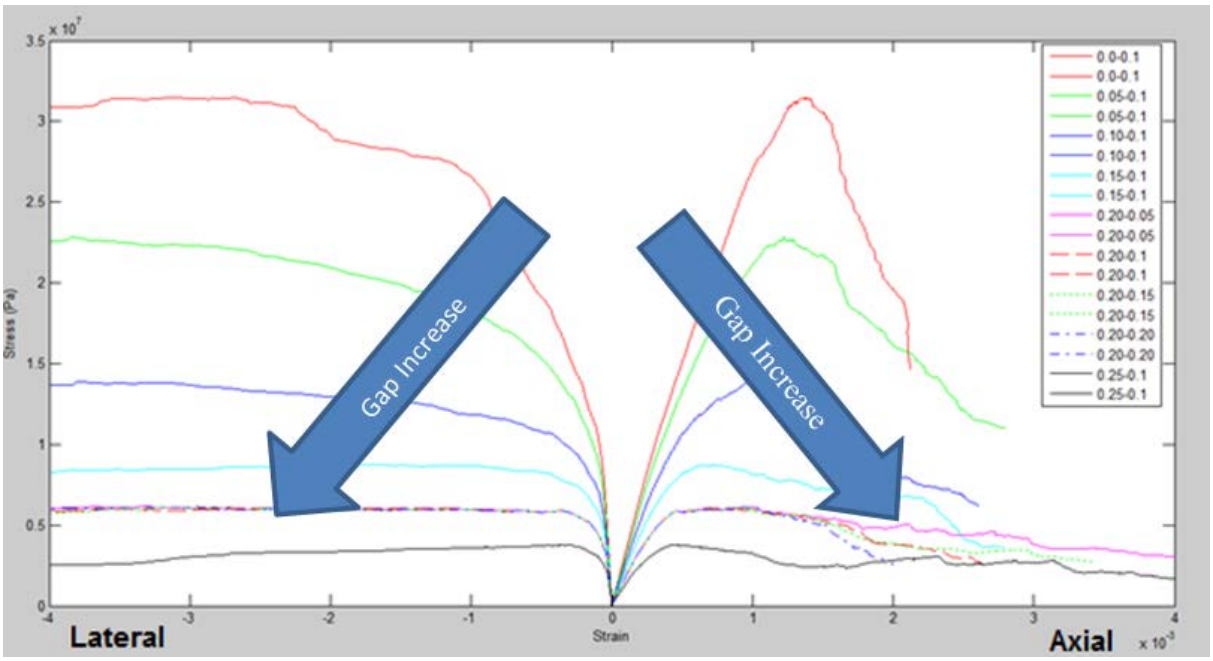

Figure 6.4, Stress vs. Axial and Lateral Stain for the Weak1 material at highest resolution for various gap size and percentages

Table 6-6, Weak1 material sensitivity analysis, Tensile tests

		Tensile Strength (Mpa)								
gapped ratio		0.00	0.05	0.10	0.15	0.20				0.25
init. Gap dst./Rmin		0.10	0.10	0.10	0.10	0.05	0.10	0.15	0.20	0.10
Rmin (mm)	0.35	2.10	2.00	1.69	1.45	1.04	1.04	1.04	1.04	0.83
	0.60	2.37	1.80	1.70	1.59	1.13	1.13	1.13	1.13	0.88
	0.85	1.89	1.65	1.43	0.95	0.87	0.87	0.87	0.87	0.71

Table 6-7, Weak1 material sensitivity analysis, Elastic Properties

		Triaxial																	
		E(Gpa) (PFC output/Matlab output/difference%)									v (%) (PFC output/Matlab output/difference%)								
gapped ratio		0.00	0.05	0.10	0.15	0.20				0.25	0.00	0.05	0.10	0.15	0.20				0.25
init. Gap dst./Rmin		0.10	0.10	0.10	0.10	0.05	0.10	0.15	0.20	0.10	0.10	0.10	0.10	0.10	0.05	0.10	0.15	0.20	0.10
Rmin (mm)	0.35	31.40	29.00	25.40	22.20	18.10	18.10	18.10	18.10	13.80	21.10	20.00	19.60	18.00	17.40	17.50	17.50	17.40	16.70
		33.02	30.03	26.04	22.18	17.73	17.73	17.73	17.73	13.01	33.02	24.91	23.95	22.12	21.00	21.00	21.00	21.00	19.87
		4.89	3.44	2.47	0.09	2.11	2.11	2.11	2.11	6.08	36.09	19.70	18.16	18.62	17.16	16.68	16.68	17.16	15.96
	0.60	32.20	29.40	26.90	24.10	17.60	17.60	17.60	17.60	13.80	20.00	20.30	19.90	18.80	20.30	20.30	20.30	20.30	19.40
		33.52	30.43	27.58	24.43	17.63	17.63	17.63	17.63	14.08	23.99	25.34	25.37	23.57	25.35	25.35	25.35	25.35	25.20
		3.94	3.37	2.48	1.36	0.19	0.19	0.19	0.19	1.99	16.62	19.88	21.56	20.25	19.92	19.92	19.92	19.92	23.02
	0.85	29.40	25.20	21.90	19.70	17.40	17.60	17.60	17.60	15.00	20.30	20.10	21.00	17.80	17.20	17.10	17.10	17.10	13.10
		30.66	26.08	22.46	19.28	16.73	16.73	16.73	16.73	13.70	24.85	26.41	27.01	23.65	23.93	23.93	23.93	23.93	17.24
		4.12	3.37	2.50	2.20	4.01	5.21	5.21	5.21	9.51	18.30	23.88	22.25	24.75	28.13	28.55	28.55	28.55	23.99

Table 6-8, Weak1 material sensitivity analysis, Compression test

		Triaxial								
		strength(Mpa) @ (0/350 Psi conf.) / Friction_angle								
gapped ratio		0.00	0.05	0.10	0.15	0.20				0.25
init. Gap dst./Rmin		0.10	0.10	0.10	0.10	0.05	0.10	0.15	0.20	0.10
Rmin (mm)	0.35	31.00	22.30	14.10	8.65	6.10	6.00	6.05	6.10	3.90
		59.00	48.50	35.20	28.50	32.60	24.40	19.07	18.80	22.10
		57.27	56.41	52.70	51.50	56.41	50.18	43.37	42.88	50.08
	0.60	28.30	24.00	17.50	11.50	7.10	7.20	7.10	7.10	4.40
		52.60	51.50	46.50	45.20	35.00	27.00	25.90	22.30	19.50
		55.22	56.99	57.54	59.81	57.22	51.50	50.57	46.54	46.41
	0.85	27.60	14.90	12.20	7.10	5.30	4.40	4.46	4.46	3.30
		58.00	46.00	45.60	34.00	37.50	13.10	12.70	11.30	13.90
		58.32	58.81	59.99	56.93	59.37	34.44	33.03	28.43	39.00

6.3.4 Weak2 material

The summary of the sensitivity analysis on the strong material is provided in Tables 6-9, 6-10 and 6-11. Once again, the target properties of this material are adjusted to calibrate the ones of the weakest material; however, this time the properties are mainly adjusted using bonded/gapped/slit state of the Flat-Joint contacts. Here all tests are performed at bonded contact percentage of 80%. The sensitivity analysis is performed on the effect of gapped/slit percentage. All the tests are repeated at different resolutions as well.

Figure 6.5 represents the Stress vs. Axial and Lateral Stain for the Weak2 material at highest resolution for various gap percentages. It can be seen that, even at constant bonded contact percentage, increasing gap decreases strength and changes the behaviour of the material into more plastic.

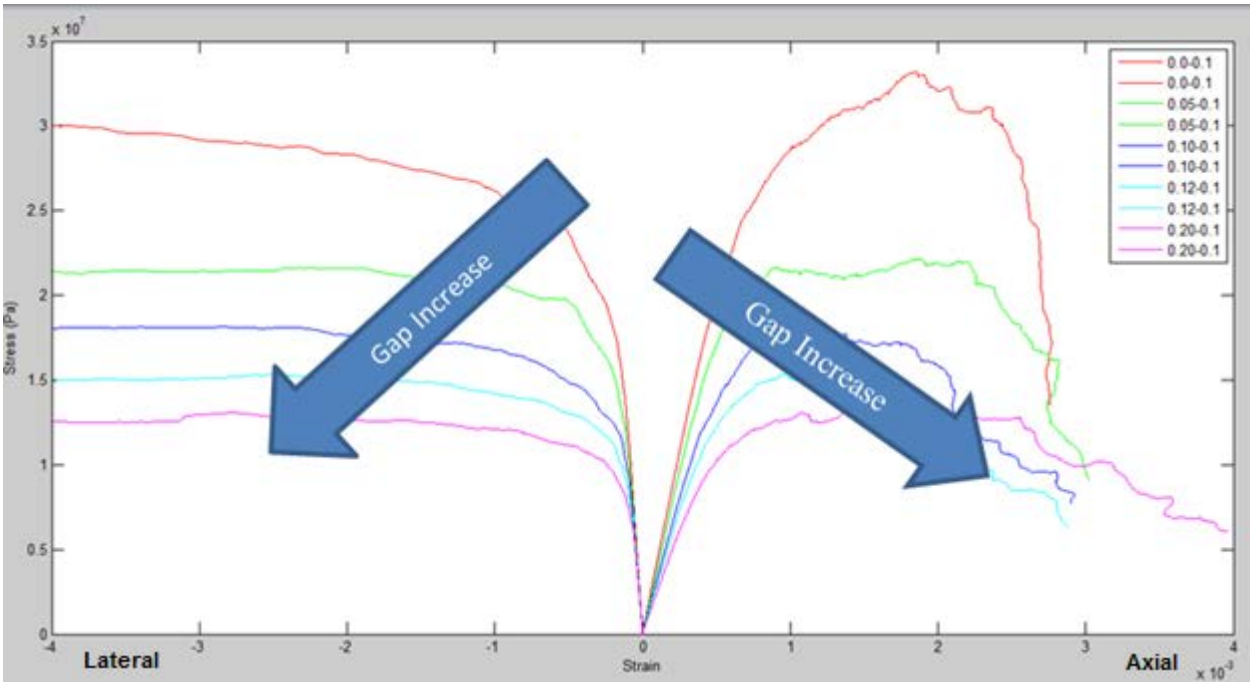

Figure 6.5, Stress vs. Axial and Lateral Stain for the Weak2 material at highest resolution for various gap percentages

Table 6-9, Weak2 material sensitivity analysis, Tensile tests

		Tensile Strength (Mpa)				
gapped ratio		0.00	0.05	0.10	0.12	0.20
Slit Ratio		0.20	0.15	0.10	0.08	0.00
Rmin (mm)	0.35	2.81	2.82	2.79	2.78	2.52
	0.60	2.35	2.37	2.35	2.33	2.27
	0.85	1.54	1.53	1.52	1.51	1.52

Table 6-10, Weak2 material sensitivity analysis, Elastic Properties

		Triaxial									
		E(Gpa) (PFC output/Matlab output/difference%)					v (%) (PFC output/Matlab output/difference%)				
gapped ratio		0.00	0.05	0.10	0.12	0.20	0.00	0.05	0.10	0.12	0.20
Slit Ratio		0.20	0.15	0.10	0.08	0.00	0.20	0.15	0.10	0.08	0.00
Rmin (mm)	0.35	40.10	36.00	30.00	28.30	23.90	25.70	25.00	25.00	21.70	19.10
		42.61	38.01	31.93	29.21	24.38	34.98	33.25	28.95	27.74	23.73
		5.88	5.30	6.05	3.11	1.95	26.52	24.80	13.64	21.77	19.49
	0.60	40.00	36.00	30.00	29.10	23.10	27.50	25.00	24.00	24.00	21.50
		43.80	38.43	32.05	30.75	23.78	37.45	35.18	32.11	31.49	27.78
		2.50	2.78	3.33	3.44	4.33	3.64	4.00	4.17	4.17	4.65
	0.85	39.90	35.60	33.70	32.00	26.20	25.50	27.50	25.80	24.70	23.40
		42.51	38.26	35.61	33.63	27.04	34.63	38.31	35.19	33.32	30.96
		6.14	6.95	5.38	4.86	3.11	26.37	28.21	26.68	25.86	24.41

Table 6-11, Weak2 material sensitivity analysis, Compression test

		Triaxial				
		strength(Mpa) @ (0/350 Psi conf.) / Friction_angle				
gapped ratio		0.00	0.05	0.10	0.12	0.20
Slit Ratio		0.20	0.15	0.10	0.08	0.00
Rmin (mm)	0.35	32.60	21.50	17.90	15.40	13.80
		98.50	69.00	52.50	50.50	37.40
		68.30	64.59	60.41	60.61	54.52
	0.60	44.50	29.40	18.00	21.70	13.00
		113.00	77.00	54.00	51.80	37.40
		68.73	64.62	60.96	58.37	54.52
	0.85	30.60	25.90	16.80	14.90	10.50
		95.30	61.00	47.00	43.50	32.00
		68.13	60.61	58.42	57.60	52.95

6.4 Discussion

6.4.1 Effect of gap on Young's Modulus

FJÆR [41] has explained the Drop in E with increasing crack according to the following formula:

$$E_{eff} = E.(1 - \xi.Q) \qquad (6.1)$$

E_{eff} effective Young's Modulus, E is Young's Modulus of the material without cracks, ξ is the crack density and is a function of the size and number of cracks, and Q is a coefficient depending on the shape and orientation of the crack. The same linear trend can be observed by looking at the Figure 6.6 which is the results of sensitivity analysis of the Weak materials.

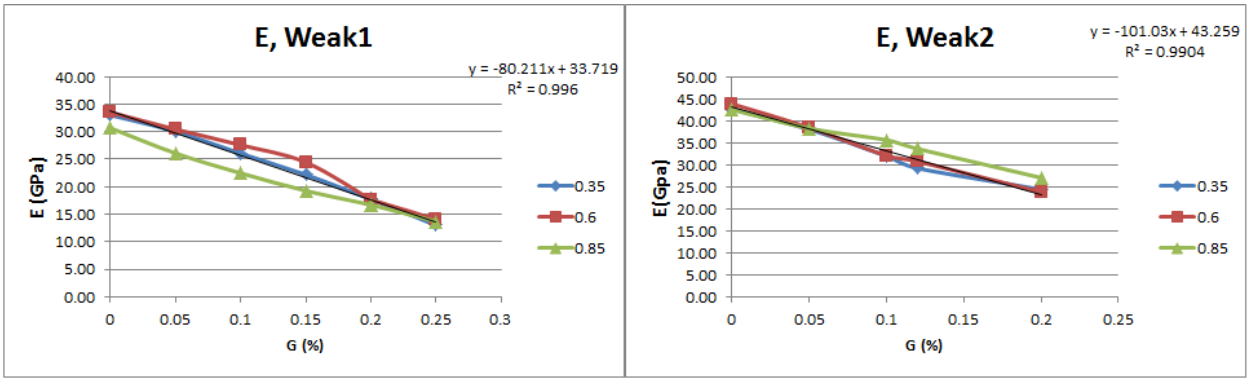

Figure 6.6, Effect of gap on Young's Modulus for Weak materials at different resolutions, data obtained using calculations on histories (Appendix A)

WALSH [42] has stated that cracks cause non-linearity at beginning of stress-strain curve then they close and the behaviour gets more linear. The very same effect is observed in the stress-strain curves of the UCS tests by increasing the gaps. At the early stage of the test, the gaps start to close and interlock and that causes non-linearity in the beginning of the tests. This phenomenon is more obvious at higher gaps. Figure 6.7 represents this phenomenon.

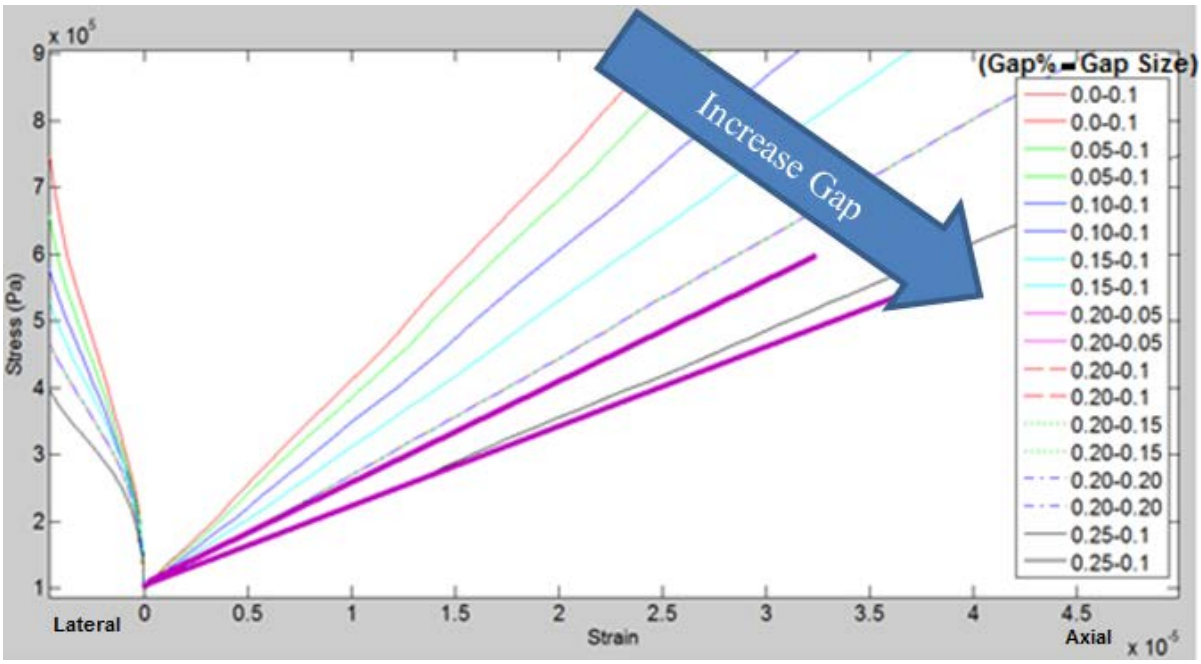

Figure 6.7, Purple line is tangent line to the in early stages of strain-stress curve of the UCS test which shows non-linearity in early stages

6.4.2 Effect of gap on Poisson's Ratio

According to Figure 6.8, the effect of gap on the Poisson's Ratio seems to be negligible on the studied range; therefore, it can't be decided if introducing gaps increases or decreases the Poisson's Ratio.

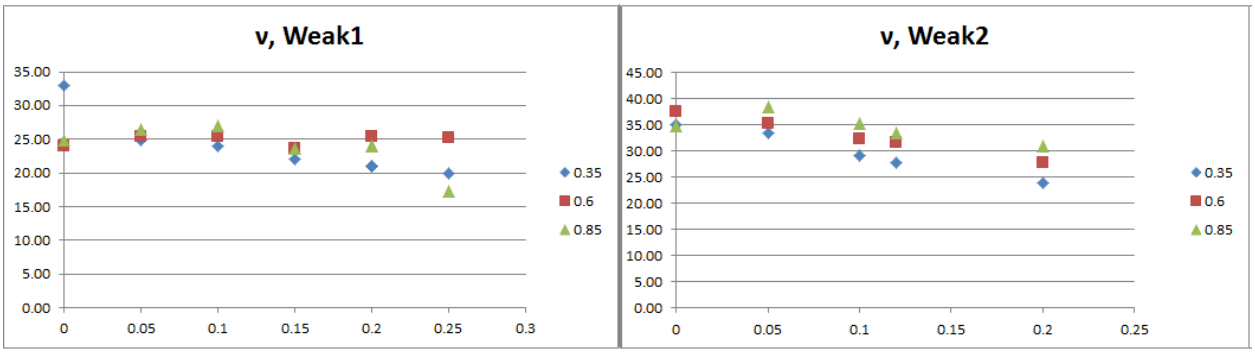

Figure 6.8, Effect of gap on Poisson's Ratio for Weak materials at different resolutions, data obtained using calculations on histories (Appendix A)

6.4.3 Effect of gap on Friction Angle and CCS

Effect of gap on friction angle can be expressed in two ways: effect of gap size and effect of gap percentage. The only parameter in the studied range that gap size has seen to be affecting is the friction angle. Figure 6.9 represents this effect. The gap size seems to reduce the friction angle. The effect of gap size itself is affected by the gap percentage: In lower percentages, the effect of gap size diminishes. That's why in the medium material CCS and friction angle do not change with gap size. It appears that this parameter does not have any effect on any parameter measured at atmospheric conditions and only affects the parameters measured under confining pressure, i.e. CCS and the friction angle.

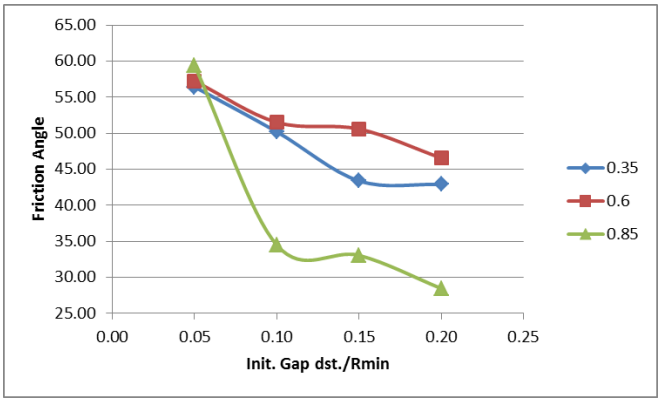

Figure 6.9, Friction angle vs. Gap size for the Weak1 at different resolutions

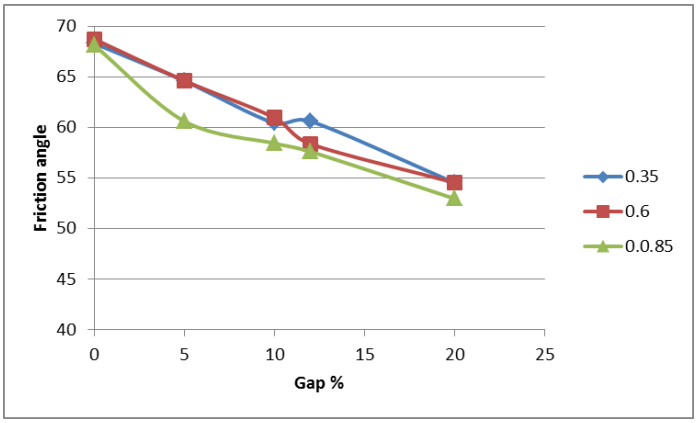

Figure 6.10, Friction angle vs. Gap percentage for the Weak2 at different resolutions

Figure 6.10 represents the effect of gap percentage on friction angle and CCS. As stated before increasing gap percentage decreases the strength of the material. In the Weak1 material, the strength reduction works by reducing bonded contacts. However in the Weak2 material the percentage of the bonded contacts is constant. It seems gaps in the Weak2 material reduce the interlocking of the particles compared to slit contacts. Reduced interlocking is the reason in the Weak2 material increasing gap and therefore decreasing the slits reduced the strength, even though bonded percentage is constant. This effect under confining pressure is visualized by reducing the friction angle and CCS.

6.4.4 Effect of gap on Failure behaviour

Figures 6.11 And 6.12 represent the state of materials after UCS test for the Weak1 and the Weak2 material that are calibrated to the target Drillability properties. Both of them having the same target properties but showing some very different behaviour. The straight line segment in the Weak2 material is shorter and the non-linear part before failure of the material is longer. The Weak2 material fails at lower strain. There are more shear micro-cracks (blue lines) in the Weak1 material. The post-failure behaviour of the Weak2 material is more plastic and the stress does not suddenly drop to a low value. These differences signify the role of micro-structure and micro-properties of a synthetic rock that are to be considered in any application.

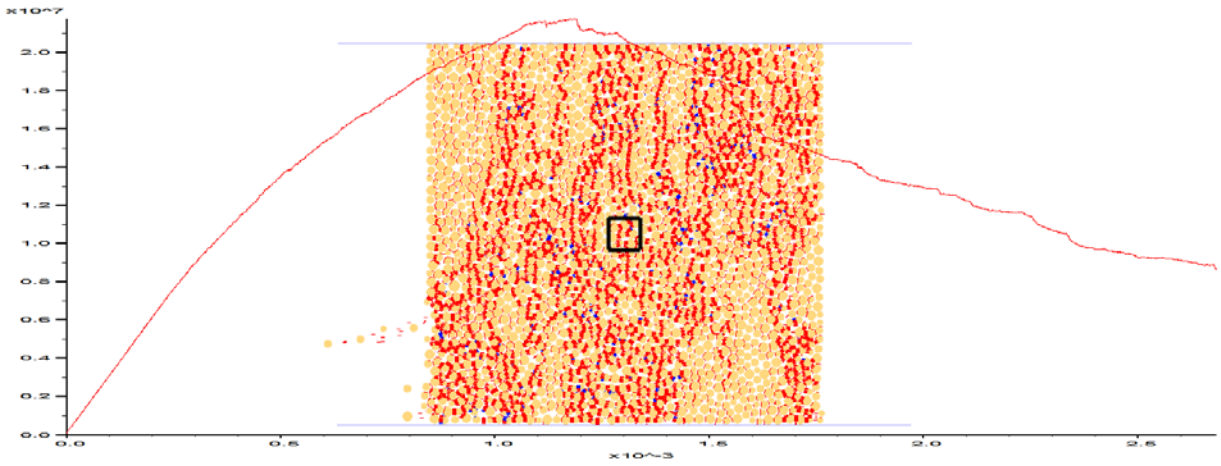

Figure 6.11, Weak1 material after UCS test

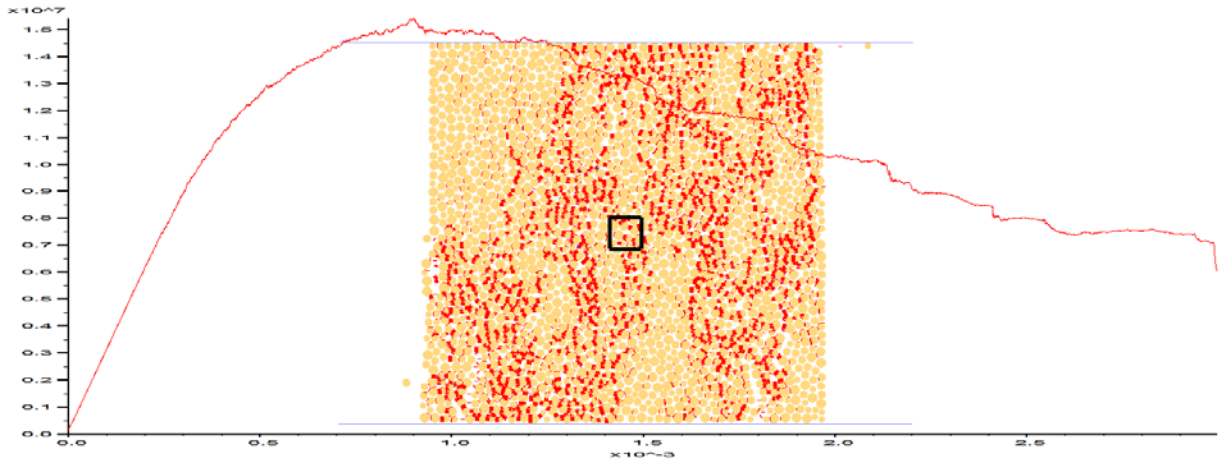

Figure 6.12, Weak2 material after UCS test

6.4.5 Effect Gap versus Slit on Tensile Strength

Tables 6-3 and 6-6 show that tensile strength for the medium and Weak1 materials are strongly affected by gap percentage. Increasing gap percentage decreases the bonds and therefore decreases the tensile strength of the material. However increasing the gap in the Weak2 material does not affect the tensile strength. By looking at the results of the tensile strength of the Weak2 material in Table 6-9, it can be seen that increasing gap does not affect the tensile strength. In the Weak2 material any increase in the gap means decrease in slit and the number of bonded contacts is unaffected. Furthermore, in the tensile strength test the interlocking of the particles

and friction between them has the minimum effect on the test results. In another words there is no difference between gap and slit regarding tensile strength test.

6.4.6 Minimum Particle size and Resolution

Tables 6-2 through 6-11 represent the summary of the sensitivity results for each material. The tests are repeated at three resolutions or min. particle size. Figure 6.1 compares the medium material at different resolutions; in a fixed specimen size, lowering the min. particle size increases the resolution. The aforementioned tables confirm that all the results at different resolutions are within acceptable small tolerance; therefore the minimum particle size of 0.6 that was selected for the calibration process was a valid resolution. However, this is only true for the current application. In any other application of the materials analysis for particle size selection should be performed again.

The only test result that varies with resolution is the tensile strength test. FISH IN PFC2D [29]explains that the tension test is performed by selecting a group of particles at two opposite side boundaries of the specimen and applying an opposite velocity to them (Figure 6.13). Therefore, the particles selected to apply this velocity and their arrangements are very important. In the lower resolutions, the selection of the particles is not performed properly. The size of the particles is bigger and the chance of having the center of particles in the specified grip thickness is smaller (Figure 6.14). This inconsistency in the layer that is imposing tension will cause error in the result of tension test with decreasing resolution.

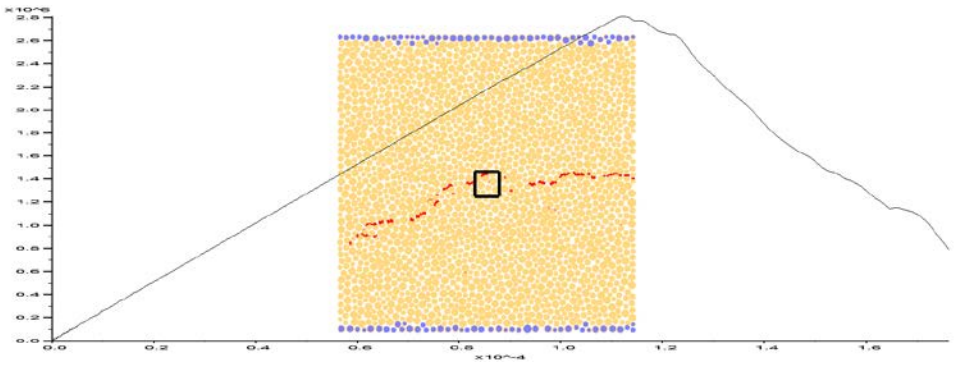

Figure 6.13, Specimen after the tension test. Blue particles are the particles selected to apply the velocity

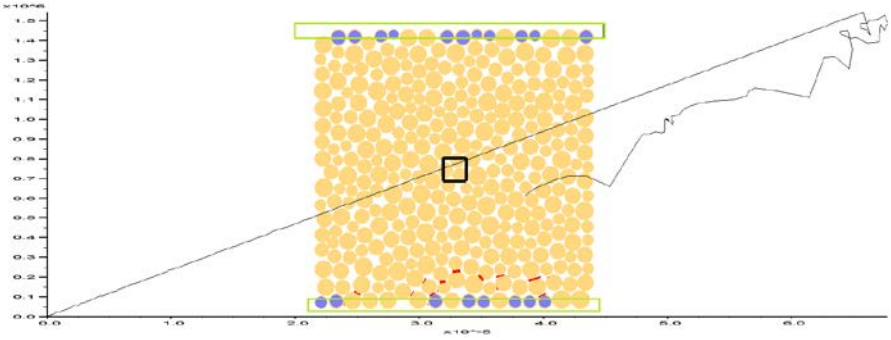

Figure 6.14, Specimen after the tension test in low resolution. Green rectangle shows the specified range for selecting boundary particles. In lower resolution, not enough particle fall in that range

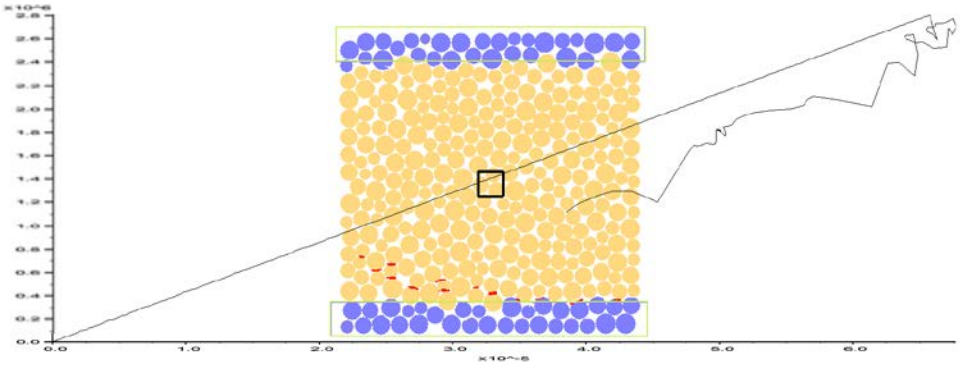

Figure 6.15, Direct Tension Test with increased the grip size

This problem has been solved by increasing the grip size t_T (Section 3.4.1.4). As can be seen in Figure 6.15, the thickness of grip layer has been increased; therefore, a continuous layer of the particles are selected to apply the desired velocity for the direct tension test.

Table 6-12, Comparing the results of the Direct Tension Test after increasing the grip size with the highest resolution sample, Medium Material

			Medium Material Tensile Strength (Mpa)			
gapped ratio			0.00	0.05		0.10
init. Gap dst./Rmin			0.40	0.40	0.10	0.40
Rmin (mm)	0.35		5.23	4.37	4.37	3.64
	0.85	before increase	3.56	3.33	3.33	2.77
		after increase	5.33	4.52	4.52	3.77

Table 6-13, Comparing the results of the Direct Tension Test after increasing the grip size with the highest resolution sample, Weak1 Material

			Weak1 Material Tensile Strength (Mpa)								
gapped ratio			0.00	0.05	0.10	0.15	0.20				0.25
init. Gap dst./Rmin			0.10	0.10	0.10	0.10	0.05	0.10	0.15	0.20	0.10
Rmin (mm)	0.35		2.10	2.00	1.69	1.45	1.04	1.04	1.04	1.04	0.83
	0.85	before increase	1.89	1.65	1.43	0.95	0.87	0.87	0.87	0.87	0.71
		after increase	2.27	2.21	1.88	1.73	1.34	1.34	1.34	1.34	0.98

Table 6-14, Comparing the results of the Direct Tension Test after increasing the grip size with the highest resolution sample, Weak2 Material

			Weak2 Material Tensile Strength (Mpa)				
gapped ratio			0.00	0.05	0.10	0.12	0.20
init. Gap dst./Rmin			0.10	0.10	0.10	0.10	0.10
Rmin (mm)	0.35		2.81	2.82	2.79	2.78	2.52
	0.85	before increase	1.54	1.53	1.52	1.51	1.52
		after increase	2.52	2.55	2.48	2.45	2.19

Table 6-12 through 6-14 summarizes the result of the Direct Tension Test for the low resolution materials before and after increasing the grip size compared with the results of the Direct Tension Test of the highest resolution material. Increasing the grip size fixes the problem where tension test results varied with resolution; therefore, it can be concluded that for material testing experiments the result of the experiments are independent of the particle size or resolution.

6.5 Cutting results

The four synthetic DEM materials are input materials to the drilling toolkit [38] to investigate the performance of the Flat-Joint contact model against the linear parallel bond contact model during cutting action. Furthermore having multiple materials with different properties is a great asset in investigating the behaviour of the toolkit against available drilling correlations.

A part of the same set of experimental data as Babatunde [18] used in the development of the toolkit are used for comparison and input to the tests. Babatunde worked on a laboratory scale drilling rig in atmospheric condition. He used fine grained concrete specimens, created to have UCS of 50MPa to perform atmospheric drilling using a 2” Polycrystalline Diamond Compact (PDC) bit under vibration. To apply the vibration, the specimens were secured on a shaking table. The vibration was applied at three different vibration powers: Low, Medium and High; all at three different frequencies: 45Hz, 55Hz and 65Hz. He also performed his test over a range of Weight on Bits (WOB). By performing his tests he concluded that the vibration can improve drilling rate; however, the optimum condition is not predictable and real time monitoring of the condition is necessary to optimize vibration for the best performance. A very interesting behaviour was also observed in the trend of the results. It was observed that up to a certain WOB, increase in ROP due to vibration is proportional to the amplitude of the vibration; after

this certain WOB, relation of ROP and Amplitude of Vibration is different for different vibration power. Such behaviour was also reported by Li et al. [19].

Figure 6.16 represents the result of normalized ROP (n-ROP) vs. WOB for the medium material. N-ROP is calculated by dividing each ROP with the amplitude of the applied vibration. The ROP in two dimensions is calculated based on procedures of Mozaffari [38]. The experimental tests were performed on a concrete specimen with UCS of about 50MPa; therefore, the medium material is the best match to the concrete specimen for comparing the results. Figure 6.16 represents the experimental results. All the results provided here are only at 45Hz. By comparing Figures 6.16 and 6.17, the great capability of the cutting toolkit in re-producing the trends in the results can be it can be observed. As was reported by Babatunde and Li [18, 19], up to a certain WOB, increase in ROP due to vibration is proportional to the amplitude of the vibration; after this certain WOB, relation of ROP and Amplitude of Vibration is different for different vibration powers. However, the magnitude of the results is different from the experimental results and results cannot be compared quantitatively with the experimental results. This has also been reported previously by Khorshidian [39]. He stated that DEM still suffers from lack of fit in amount of Depth of Cut (DOC) and Mechanical Specific Energy (MSE) with experimental data. The achieved DOC is higher and MSE is lower than experimental results [43]. This raises the question of whether ROP in two dimensional modeling should be compared with the experimental results. For the current study, it is safe to only assume the qualitative results are valid and the quantitative results are not a good reference of study.

Figure 6.18 represents the results of the same tests using a synthetic material by linear parallel bond contact model with the same UCS as medium material. A quick comparison of the Figures 6.16 through 6.18 concludes the improvement of qualitative modeling using the Flat-Joint model.

Flat-Joint model (figure 6.16) represents a better qualitative match to the experimental results compared to the linear parallel bond model.

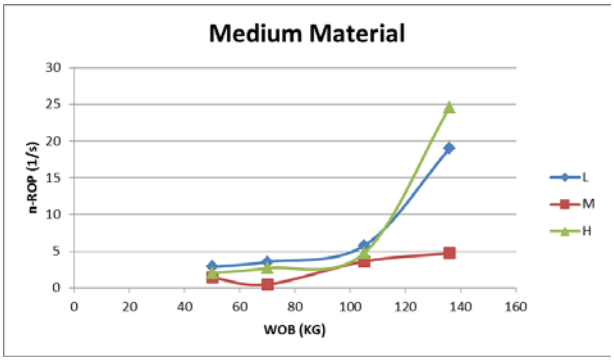

Figure 6.16, Simulation results normalized ROP vs. WOB for the medium material at different vibration powers

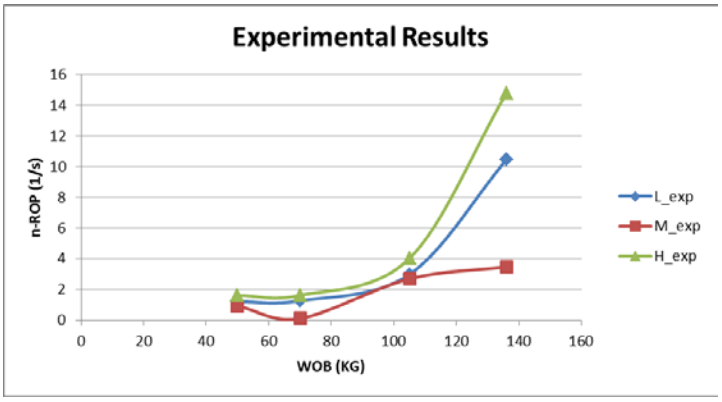

Figure 6.17, Experimental results normalized ROP vs. WOB at different vibration powers [18]

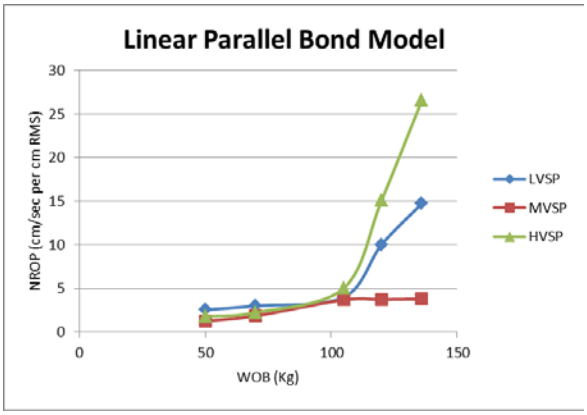

Figure 6.18 Simulation results normalized ROP vs. WOB at different vibration powers. The material generated using linear parallel bond model at UCS of 50MPa [38]

Figures 6.19 and 6.20 represent the results of the same tests for the Strong and Weak1 material. They also represent the same trend as mentioned before; after a certain WOB, relation of ROP and Amplitude of Vibration is different for different vibration powers. Therefore, it can be concluded that this behaviour is an intrinsic behaviour of drilling phenomenon and is independent of the rock type and strength of the material. However the cause of such behaviour remains unknown.

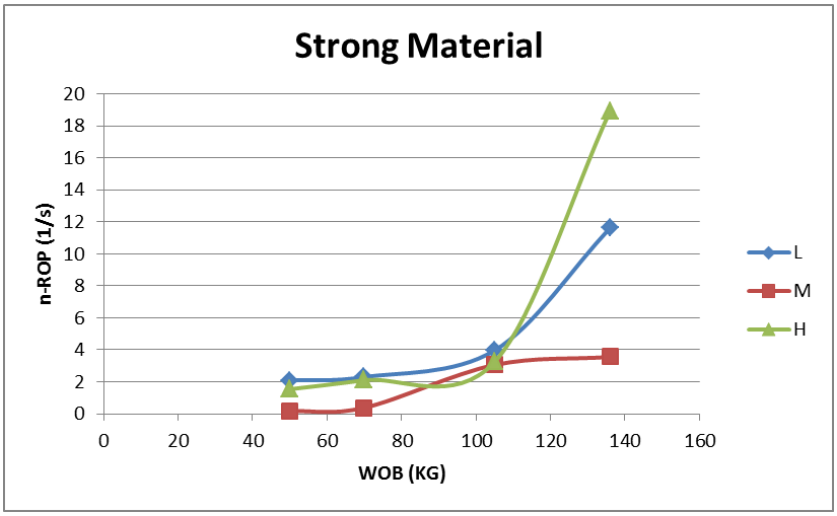

Figure 6.19, Simulation results normalized ROP vs. WOB for the Strong material at different vibration powers.

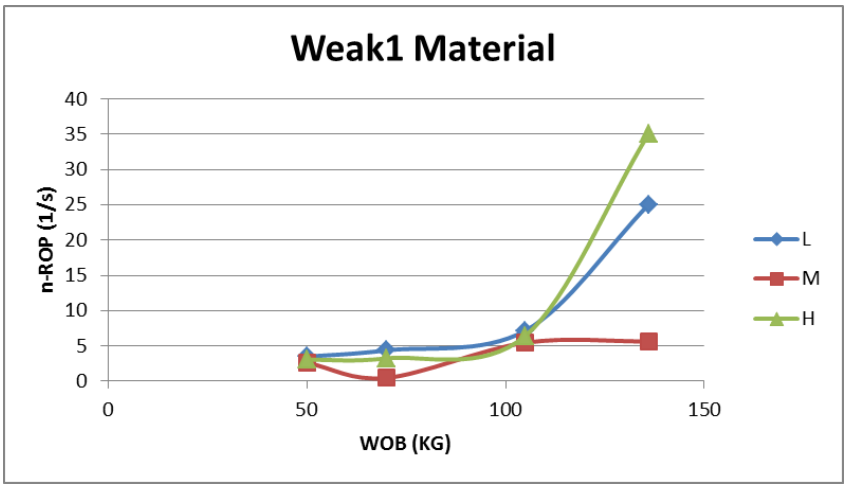

Figure 6.20, Simulation results normalized ROP vs. WOB for the Weak1 material at different vibration powers

Figure 6.21 illustrates ROP for three materials strengths vs. WOB. The results show the expected dependency of ROP on rock strength: The higher the strength, the lower ROP. Moreover, not only increasing strength decreases the ROP, but at higher strengths the effect of WOB decreases. This effect is illustrated on Figures 6.22 and 6.23.

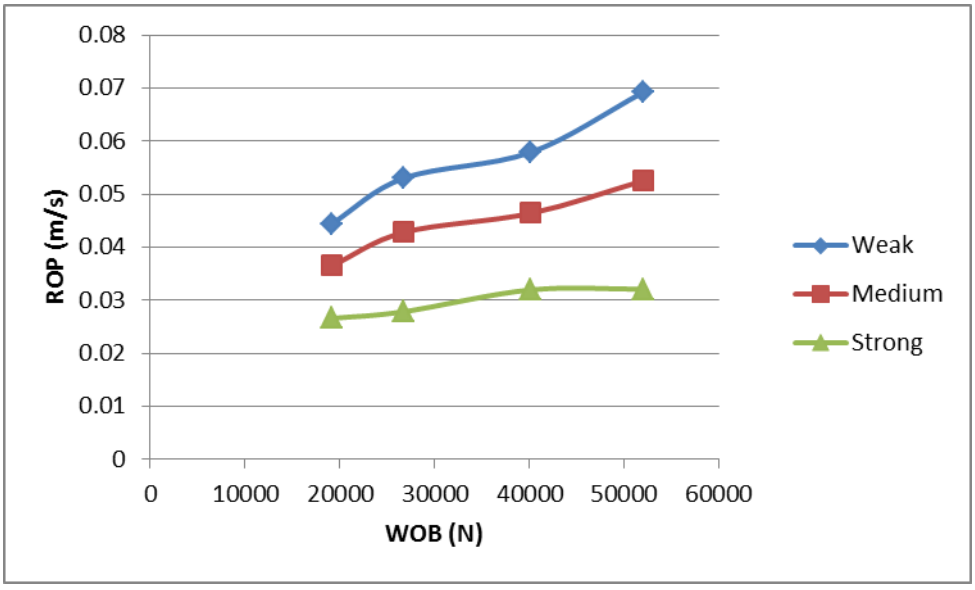

Figure 6.21, Simulation results. ROP vs. WOB for different strengths

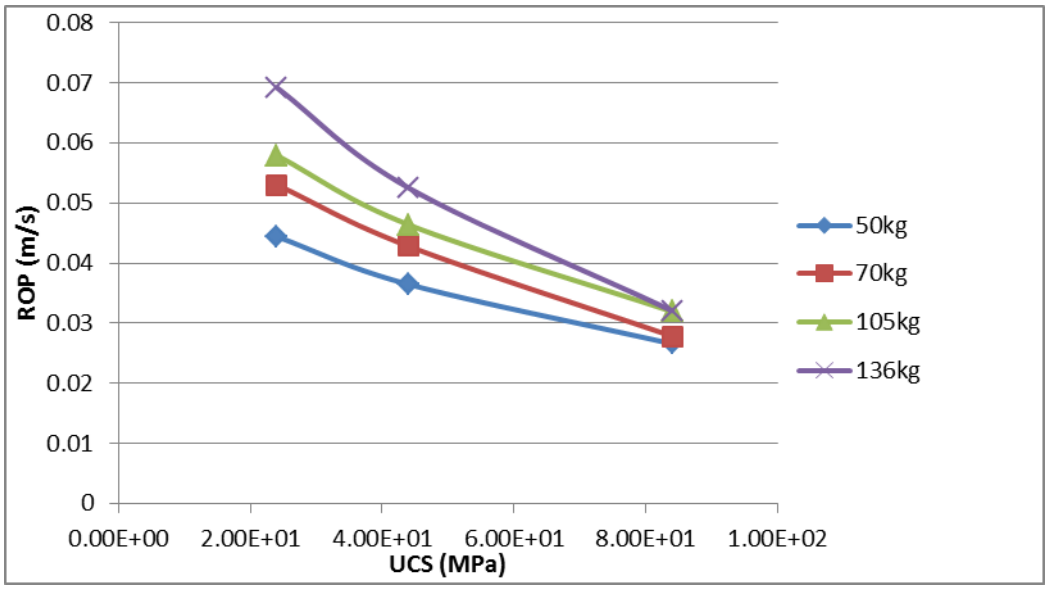

Figure 6.22, Simulation results. ROP vs. UCS at different WOB

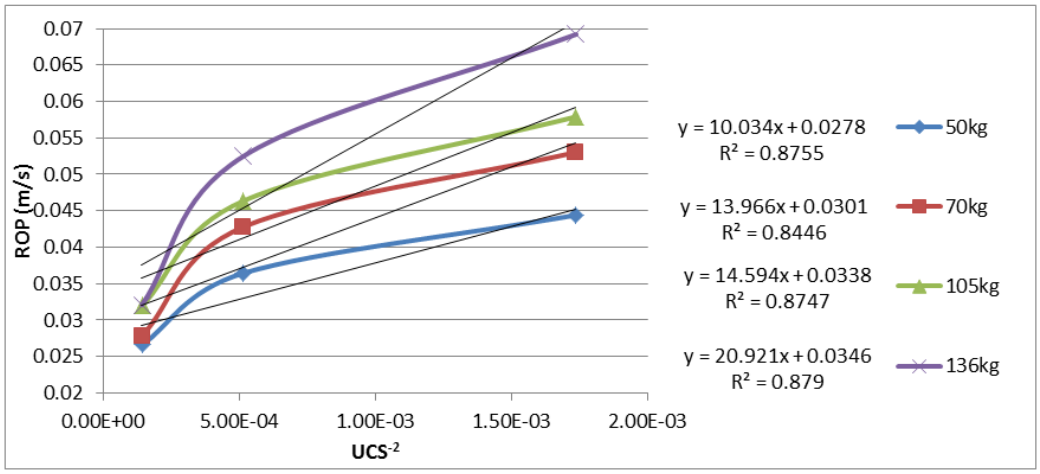

Figure 6.23, Simulation results. ROP vs. UCS^{-2} at different WOB

Figure 6.24 adds the results for ROP of Weak2. It can be seen that, despite of what was the expected result, Weak1 and Weak2 Materials are representing different results. These are two rocks with the same Drillability parameters; however, the ROP is not the same and Weak2 has lower ROP. Even at lower WOB, the ROP of Weak2 is lower than the medium material with twice the strength. This represents the importance of the micro-structure of the material for drilling studies: except Weak2 material, the rest of materials have negligible amount of gapped

contacts. This means they have relatively similar micro-structure; therefore, ROP is increasing with decreasing strength. Weak2 is not obeying this rule, which means an extra parameter is affecting the behaviour of rock under cutting. This extra parameter in this case is the rock micro structure. Baker-Hughes [28] stated that his eight Drillability parameters are enough to describe rock characteristics for drilling. However, the last part of tests revealed that even though the Weak2 material and Weak1 material have the same macro properties, i.e. calibrated to the same target properties as of Table 6-1 and having the same particle coarseness, they are behaving differently. It should be considered that these tests are not performed under normal drilling conditions where the rock is under borehole pressure; therefore, the results are not against the Baker-Hughes statement. The existence of micro-cracks, as one of parameters affecting the microstructure of the rock, can be an extra parameter to consider in the rock characterization in atmospheric condition; however, micro-cracks are mostly closed off under confinement and their existence can be neglected.

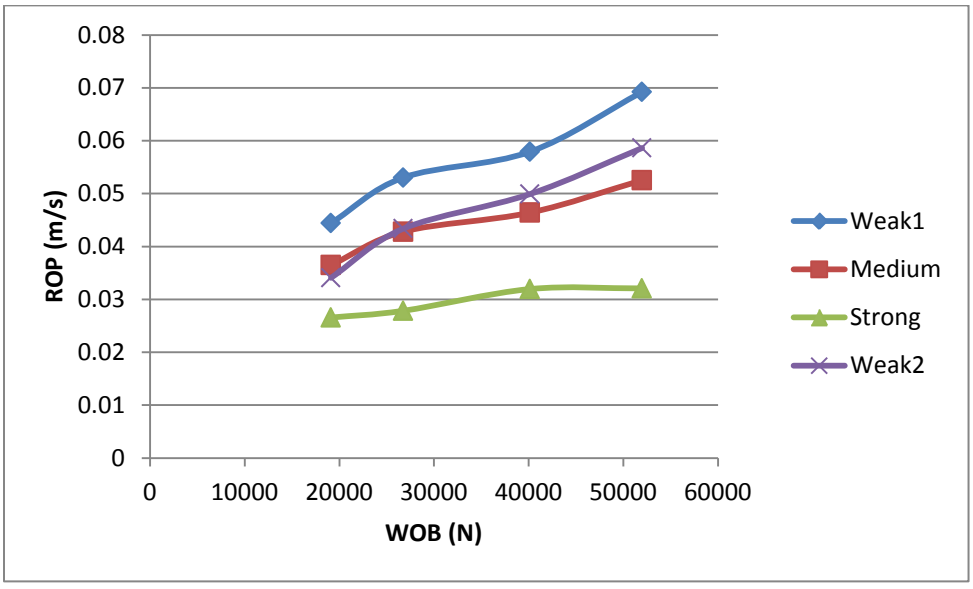

Figure 6.24, Comparing ROP of Weak1 and Weak2 vs. WOB for low vibration power

Maurer in 1966 [44] proposed a relation between ROP and rock strength and WOB. According to this relation ROP has direct linear relation with WOB squared and also direct linear relation with $1/S^2$ where S is rock strength or UCS. Figure 6.25 illustrates plot of ROP vs. WOB squared for the three materials. According to this plot, the cutting toolkit is showing this behaviour with high accuracy. Furthermore, by looking again at the Figure 6.24 the direct relation of ROP to $1/S^2$ has been also predicted by model with good accuracy.

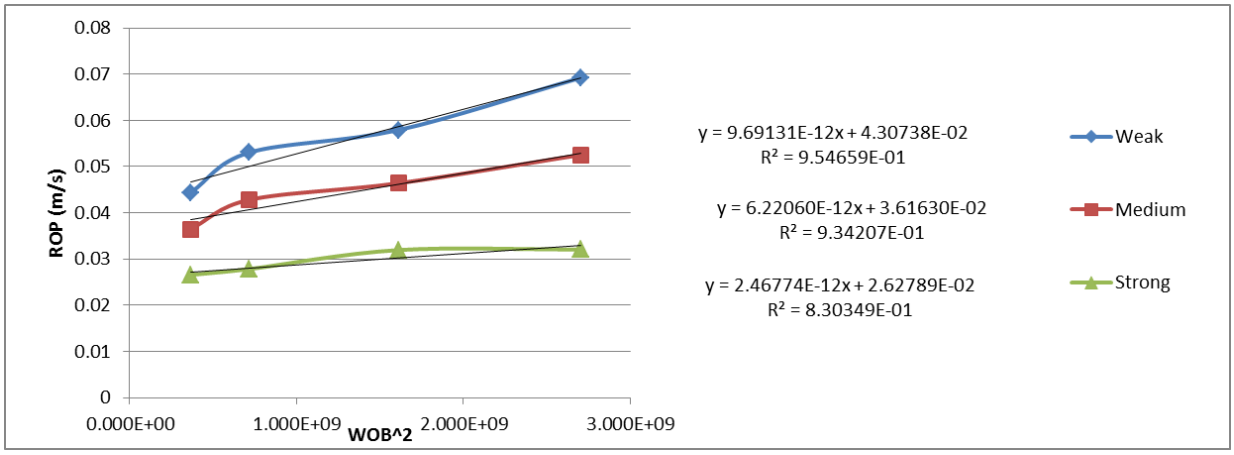

Figure 6.25 Simulation results. ROP vs. WOB^2 at different strength

6.6 Conclusion

Three synthetic materials were calibrated using available experimental data. The data were selected based on eight Drillability parameters by Baker-Hughes. These materials were subjected to a wide range of tests from standard rock tests to cutting test. The rock cutting tests were performed using a previously developed comprehensive DEM rock cutting toolkit.

The standard rock tests revealed that minimum particle size have negligible effect on behaviour of rock governed by flat joint model where the rock is subjected to either compression or tension test. Furthermore, micro-structure showed a great impact on the failure pattern of the rocks.

The cutting tests revealed that the eight Drillability parameters by Baker-Hughes are not enough parameters to characterize the rock at atmospheric conditions. Existence of micro-cracks, as one of parameters affecting the microstructure of the rock, can be an extra parameter to consider in the rock characterization in atmospheric condition; however, micro-cracks are mostly closed off under confinement and their existence can be neglected. Therefore, the eight Drillability parameters are sufficient and simple enough parameters to describe the rock with enough details for normal drilling conditions.

Additionally, the performance of the toolkit was tested once again. The results were in good accordance with the Maurer model. This proves again that this toolkit can be assumed as a very reliable candidate for further studying events dealing with drilling or investigating simulation aspects such as investigating new contact models.

7 Conclusion

A comprehensive numerical study was performed. The study covers Distinct Elemental Method (DEM) modeling from basics to advanced modeling. The study is divided in three stages and the work is published or being published through three papers.

The study started from developing a basic toolkit for assessing the rock cutting phenomena with a single PDC cutter. Following points can be concluded from analysis of the cutter dynamic motion and force components in a single PDC cutter-rock interaction.

- The cutter mass in a rock penetration is a significant factor which influences the MSE of drilling.
- Decreasing the cutter mass, under the same vertical load, causes significant vertical oscillations in a horizontal penetration.
- The source of excitation is the horizontal force on the cutter which pushes the cutter up in the ramp of the rock-cutter interface. These vertical oscillations cause the cutter to impact on the rock when the cutter edge reaches the rock surface.
- The impacts of the cutter can be stronger when the cutter movement constitutes higher vertical velocity amplitudes and horizontal speeds.
- The negative effect of cutter vibrations can be due to the cutter vertical position fluctuations, and the positive effect is related to those impacts that are sufficiently powered for cratering

In the second stage, the toolkit was developed more by adding more aspects of drilling to it. It is now possible to apply confining pressure to the rock to simulate BHP. The effect of jet cleaning was considered in the toolkit. The jet effect was simulated through cleaning condition in front of the cutter. This cleaning condition can also have its own cleaning efficiency.

In a real drilling condition, rock is almost an infinite media; however, in a DEM modelling the rock media cannot be big enough and one would end up with boundary effects. This also was overcome with introducing a layer at the boundaries to simulate the effect of infinite media by absorbing most of the incoming waves.

The efficiency and performance of the toolkit was tested using various published work. The test results indicate this toolkit is successful in replicating the experimental test results available. The confining pressure has a negative effect on MRR and its effect becomes smaller as the pressure increases. The effect of particle friction on required energy for drilling was successfully observed. The toolkit could successfully represent that in drilling under pressure most of energy is dissipated through the particle friction rather than for breaking the rock and overcoming the bond forces.

In displacement vibration, the model successfully replicated the experimental results. The results of normalized rate of penetration vs. weight on bit follow the same qualitative pattern as the reported experimental result.

Considering all the successful replications and included aspects, this toolkit can be assumed as a very reliable candidate for further studying events dealing with drilling or investigating simulation aspects such as investigating new contact models.

In the third stage, in order to simulate the dynamic events occurring in the compactly packed granular media with more accuracy a more appropriate and advanced contact model, i.e. Flat-Joint contact model, was introduced in the model. Furthermore, properties specific to the new contact model were investigated in details.

Three synthetic materials were calibrated using available experimental data. The data were selected based on eight Drillability parameters by Baker-Hughes. These materials were subjected to a wide range of tests from standard rock tests to cutting test. The rock cutting tests were performed using a previously developed comprehensive DEM rock cutting toolkit.

The standard rock tests revealed that minimum particle size have negligible effect on behaviour of rock governed by flat joint model where the rock is subjected to either compression or tension test. Furthermore, micro-structure showed a great impact on the failure pattern of the rocks.

The cutting tests revealed that the eight Drillability parameters by Baker-Hughes are not enough to characterize the rock at atmospheric conditions. Existence of micro-cracks, as one of parameters affecting the microstructure of the rock, can be an extra parameter to consider in the rock characterization in atmospheric condition; however, micro-cracks are mostly closed off under confinement and their existence can be neglected. Therefore, the eight Drillability parameters are sufficient and simple enough parameters to describe the rock with enough details for normal drilling conditions.

Additionally, the performance of the toolkit was tested once again with available drilling models. The results were in good accordance with the Maurer model. This proves again that this toolkit can be assumed as a very reliable candidate for further studying events dealing with drilling or investigating simulation aspects such as investigating new contact models.

7.1 Future Work and Recommendations

One of the aspects that DEM modeling as well as the current study is suffering from is the lack of ability to include pore pressure in the studies. The new version of the PFC2D software, i.e. PFC 5.0, has showed capability in defining multiple contact models within the same model through its contact model assignment table. It might be possible to define a new particle as with properties similar to a liquid to introduce into the simulation environment. Such capability is currently being investigated by the author and the current modeling method can greatly benefit from such addition to it.

The current work is performed in two dimensions and showed reasonable qualitative results. However, a three dimensional study can be a good next step for investigating the current field of study using the current modeling technique.

References

1. Akbar Babak, *Polycrystalline Diamond Compact Bit-Rock Interaction*, Final MEng. Thesis, Memorial University of Newfoundland, St. John's, NL, Canada. June, 2011

2. Akbari, B., Butt, S.D., Munaswamy. K., and Arvani, F. 2011. *Dynamic Single PDC Cutter Rock Drilling Modeling And Simulations Focusing On Rate Of Penetration Using Distinct Element Method*. 45th U.S. Rock Mechanics / Geomechanics Symposium. San Francisco, California: American Rock Mechanics Association

3. Potyondy, D. O., and P. A. Cundall. (2004) "*A Bonded-Particle Model For Rock,*" Int. J. Rock Mech. Min. Sci., 41, 1329-1364.

4. Xia, M., Zhou, K., & Zhao, B. (2009). *Experimental Study And PFC Modelling Of Failure Process Of Brittle Rock Under Uniaxial Compression.* 43rd U.S. Rock Mechanics Symposium & 4th U.S. – Canada Rock Mechanics Symposium. Asheville, North Carolina: American Rock Mechanics Association.

5. S. Hentz , F.V. Donze´ and L. Daudeville. "*Discrete Element Modelling Of Concrete Submitted To Dynamic Loading At High Strain Rates.*" Computers and Structures,vol. 82, pp. 2509–2524, 2004

6. H. Huang, E. Detournay and B. Bellier. "*Discrete element modeling of rock cutting*." Informatyka w Technologii Materiałów, vol. 7, no. 2, pp. 224-230, 2007

7. Q.M. Gong, J. Zhao and H.Y. Sian."*Numerical simulation of influence of joint orientation on rock fragmentation process induced by a TBM cutter*." Tunneling and Underground Space Technology, vol. 20, Issue 2, pp. 183-191, 2005

8. G. Block and H. Jin. "*Role of failure mode on rock cutting dynamics*", presented at the 2009 SPE annual technical conference and exhibition, New Orleans, LA, USA, 2009

9. J.A. Mendoza, I.K. Gamwo,W. Zhang and Lin J.S. "*Discrete element modeling of rock cutting using crushable particles*", presented at the 44th U.S. Rock mechanics symposium and 5th U.S./Canada Rock mechanics symposium, Salt Lake City, UT, USA, 2010

10. D.O. Potyondy, J.F. Hazzard *Effects Of Stress And Induced Cracking On The Static And Dynamic Moduli Of Rock* Proceedings of the First International FLAC/DEM Symposium on Numerical Modeling, Minneapolis, Minnesota, August 2008

11. P.A. Cundall, O.D.L. Strack, *A Discrete Numerical Model For Granular Assemblies*. Geotechnique, 29:47–65, 1979

12. L.W. Ledgerwood III, *PFC Modeling Of Rock Cutting Under High Pressure Conditions*, 1st Canada - U.S. Rock Mechanics Symposium, May 27 - 31, 2007 , Vancouver, Canada

13. Teale, R. 1965. *The Concept of Specific Energy in Rock Drilling.* Intl. J. Rock Mech. Mining Sci. 2: 57-53

14. Richard, T., Detournay, E., Fear, M., Miller, B., Clayton, R., & Matthews, O. 2002. *Influence of bit-rock interaction on stick-slip vibrations of PDC bits.* SPE Annual

Technical Conference and Exhibition. San Antonio, Texas: Copyright 2002, Society of Petroleum Engineers Inc

15. Aadnoy, B.S., Cooper, I., Miska, Z.S., Mitchel, R.F., and Payne, L. 2009. *Wellbore Measurement: Tools, Techniques, and Interpretation*. In Advanced Drilling and Well Technology. Texas: SPE, 544-556

16. Dupriest, F. E., & Koederitz, W. L. (2005). *Maximizing Drill Rates with Real-Time Surveillance of Mechanical Specific Energy.* SPE/IADC Drilling Conference. Amsterdam, Netherlands: SPE/IADC Drilling Conference

17. Pixton, D. and Hall, D. *A New-Generation Mud-Hammer Drilling Tool*, Annual report. Retrieved 24 Nov. 2010 from: http://www.netl.doe.gov/KMD/cds/Disk28/NG2-2.PDF

18. Babatunde Olaiya Yusuf, *The Effects Of Varying Vibration Frequency And Power On Efficiency In Vibration Assisted Rotary Drilling*, Final MEng. Thesis, Memorial University of Newfoundland, St. John's, NL, Canada. November, 2011

19. Li Heng. "*Experimental Investigation of The Rate of Penetration of Vibration Assisted Rotary Drilling* – Master's Thesis" Memorial University of Newfoundland, St. John's, NL, Canada, January 2011

20. Dunayevsky, VA., Abbasian, F., and Judzis, A. 1993. *Dynamic Stability of Drillstring Under Fluctuating Weight on Bit*. SPEDC 8 (2): 84-92. SPE-14329-PA. DOI: 10.2118/14329-PA

21. Dubinskey, V.S.H., Henneuse, H.P., and Kirkman, M.A. 1992. *Surface Monotoring of Downhole Vibrations*: Russian, European, and American Approaches. Paper SPE 24969

presented at European Petroleum Conference, Cannes, France, 16-18 November. DOI: 10.2118/24969-MS

22. Payne, M.L., Abbasian, F., and Hatch, A.J. 1995. *Drilling Dynamic Problems and Solutions for Extended-Reach Operations.* In Drilling Technology PD-volume 65, ed. J.P. Vozniak, 191-203. New York: ASME

23. Matthias, R., G, H., P., & Friedhelm, M.,. 1995. *Drilling Performance Improvements Using Downhole Thrusters*. SPE/IADC Drilling Conference. Amsterdam, Netherlands: 1995 Copyright 1995, SPE/IADC Drilling Conference

24. McCray, W. and Cole, F. W. (1959). *Oil Well Drilling Technology*. Oklahoma: University of Oklahoma Press, Norman. 352-355

25. Pessier, R., & Damschen, M. 2011. *Hybrid Bits Offer Distinct Advantages in Selected Roller-Cone and PDC-Bit Applications*. SPE Drilling & Completion, (03)

26. Kolle, J. (2004). *HydroPulse Drilling, Final Report*. Retrieved 24 Apr. 2011 from http://www.netl.doe.gov/technologies/oil-gas/publications/.../Final_34367.pdf

27. Tibbitts, G. and Judzis, A. (2001). *Optimization of Mud Hammer Drilling Performance A Program to Benchmark the Viability of Advanced Mud Hammer Drilling,* Quarterly report. Retrieved 24 Nov. 2010 from http://www.osti.gov/bridge/servlets/purl/809137-vz9VbT/native/809137.pdf

28. Prasad, U., Baker Hughes, *Drillability Of A Rock In Terms Of Its Physico-Mechanical And Micro-Structural Properties,* ARMA 09-40, 2009

29. Particle Flow Code in 2 Dimensions (PFC2D) Unpublished User Manual included with 2012 software release, *FISH IN PFC2D* - Section 3 : PFC Fishtank

30. Potyondy, D. O., *A Flat-Jointed Bonded-Particle Material for Hard Rock* ARMA 12-501., 46th US Rock Mechanics/Geomechanics Symposium, Chicago, IL, June 24-27, 2012

31. Particle Flow Code in 2 Dimensions (PFC2D) Unpublished Technical Memorandum included with 2012 software release, PFC2D Flat-Joint Contact Model

32. Particle Flow Code in 2 Dimensions (PFC2D) Unpublished Technical Memorandum included with 2012 software release, PFC2D Flat-Jointed Material Creation and Testing

33. Particle Flow Code in 2 Dimensions (PFC2D) Unpublished User Manual included with 2012 software release, Theory and Background: General Formulation

34. Particle Flow Code in 2 Dimensions (PFC2D) Unpublished User Manual included with 2012 software release, Theory and Background: Contact Models

35. Detournay, E., & Tan, C. P. 2002. *Dependence of Drilling Specific Energy on Bottom-Hole Pressure in Shales*. SPE/ISRM Rock Mechanics Conference. Irving, Texas: 2002., SPE Inc

36. Tutluoglu, Levent. 1984. *Mechanical rockcutting with and without high pressure water jets.* University Microfilms International, Ann Arbor, MI. PhD dissertation, University of California, Berkeley

37. P.A. Cundall. ―*A Computer Model For Simulating Progressive Large Scale Movements In Blocky Rock Systems*.‖ in Proceedings of the Symposium of the International Society of Rock Mechanics,Nancy, France, 1971, pp. 213-216

38. Mozaffari, M., Butt, S. D and Munaswami, K. "*DEM Modeling of Rock and Cutter Interaction: Introduction to the Developed PFC2D Toolkit*" (**Publications under development for submission to the International Journal of Rock Mechanics and Mining Sciences / Chapter 3 of the current document**)

39. Khorshiduian Hossein, *Phenomena Affecting Penetration Mechanism of Polycrystalline Diamond Compact Bit,* Final MEng. Thesis, Memorial University of Newfoundland, St. John's, NL, Canada. July, 2012

40. Khorshidian, H., Mozaffari, M. and Butt, S. D, T*he Role Of Natural Vibration In Penetration Mechanism Of A Single PDC Cutter,* ARMA 12-9, in Proc., 46th US Rock Mechanics/Geomechanics Symposium, Chicago, IL, June 24-27, 2012

41. Fjær, E., Holt, R.M., Horsrud, P., Raaen, A.M., and Risnes, R., 2008: *Petroleum Related Rock Mechanics* 2nd edition, Elsevier, Amsterdam. Page 44

42. J. B. WALSH *The Effect of Cracks in Rocks on Poisson's Ratio* JOURNALO F GEOPHYSICALR ESEARC VOL. 70, NO. 20, 1965

43. Rafatian, N., Miska, S., Ledgerwood, L. W., Ahmed, R., Yu, M. and Takach, N. (2010). *Experimental Study Of MSE Of A Single PDC Cutter Under Simulated Pressurized Conditions.* SPE Drilling and Completion, (119302), 10-18

44. W. C. Maurer, Esso Production Research Co. T*he State Of Rock Mechanics Knowledge In Drilling* The 8th U.S. Symposium on Rock Mechanics (USRMS), September 15 - 17, 1966 , Minneapolis, MN

45. Fjær, E., Holt, R.M., Horsrud, P., Raaen, A.M., and Risnes, R., 2008: *Petroleum Related Rock Mechanics* 2nd edition, Elsevier, Amsterdam. Page 22

46. Fjær, E., Holt, R.M., Horsrud, P., Raaen, A.M., and Risnes, R., 2008: P*etroleum Related Rock Mechanics* 2nd edition, Elsevier, Amsterdam. Page 175

47. Alexandre Schubnel, Philip M. Benson, Ben D. Thompson, Jim F. Hazzard, R. Paul Young , *Quantifying Damage, Saturation And Anisotropy In Cracked Rocks By Inverting Elastic Wave Velocities* Pure appl. geophys. 163 (2006) 947–973

48. Fjær, E., Holt, R.M., Horsrud, P., Raaen, A.M., and Risnes, R., 2008: *Petroleum Related Rock Mechanics* 2nd edition, Elsevier, Amsterdam. Page 192

49. Fjær, E., Holt, R.M., Horsrud, P., Raaen, A.M., and Risnes, R., 2008: *Petroleum Related Rock Mechanics* 2nd edition, Elsevier, Amsterdam. Page 60

50. Fjær, E., Holt, R.M., Horsrud, P., Raaen, A.M., and Risnes, R., 2008: *Petroleum Related Rock Mechanics* 2nd edition, Elsevier, Amsterdam. Page 9

51. Fjær, E., Holt, R.M., Horsrud, P., Raaen, A.M., and Risnes, R., 2008: *Petroleum Related Rock Mechanics* 2nd edition, Elsevier, Amsterdam. Page 62

52. Fjær, E., Holt, R.M., Horsrud, P., Raaen, A.M., and Risnes, R., 2008: *Petroleum Related Rock Mechanics* 2nd edition, Elsevier, Amsterdam. Page 63

53. Particle Flow Code in 2 Dimensions (PFC2D) Unpublished User Manual included with 2012 software release, Introduction

54. David O. Potyondy T*he Bonded-Particle Model as a Tool for Rock Mechanics Research and Application:* Current Trends and Future Directions 7th Asian Rock Mechanics Symposium 15-19 October 2012, Seoul, Korea

55. Emam, Sacha. and David Potyondy. 2010. Technical Memorandum. Internal Technical Memorandum - PFC2D Rock-Cutting Procedures.

56. Tomofumi, K., and Lanru Jing. *Effects Of Model Scale And Particle Size On Micro-Mechanical Properties And Failure Processes Of Rocks A Particle Mechanics Approach.* Engineering Analysis with Boundary Elements. 31:5,458-472, 2007

Appendix A Procedures for calculating Young's Modulus and Poisson's Ratio

Under a compression test, Young Modulus is defined as axial stress applied at any time (σ) divided by amount of axial strain (ε), therefore:

$$\varepsilon_x = \frac{1}{E}\,\sigma_x \qquad \text{A.1}$$

The definition is then generalized by the slope of the linear section of the Stress-Strain plot in compression test. Poisson's Ratio (ν) is defined by ratio of the axial strain to lateral strain:

$$\nu = -\frac{\varepsilon_y}{\varepsilon_x} \qquad \text{A.2}$$

Both these quantities are measured in the linear section of the Stress-Strain curve. This is because they are elastic properties of material and any non-linear behaviour of the material in the Stress-Strain diagram means mechanical failure which is not an elastic behaviour.

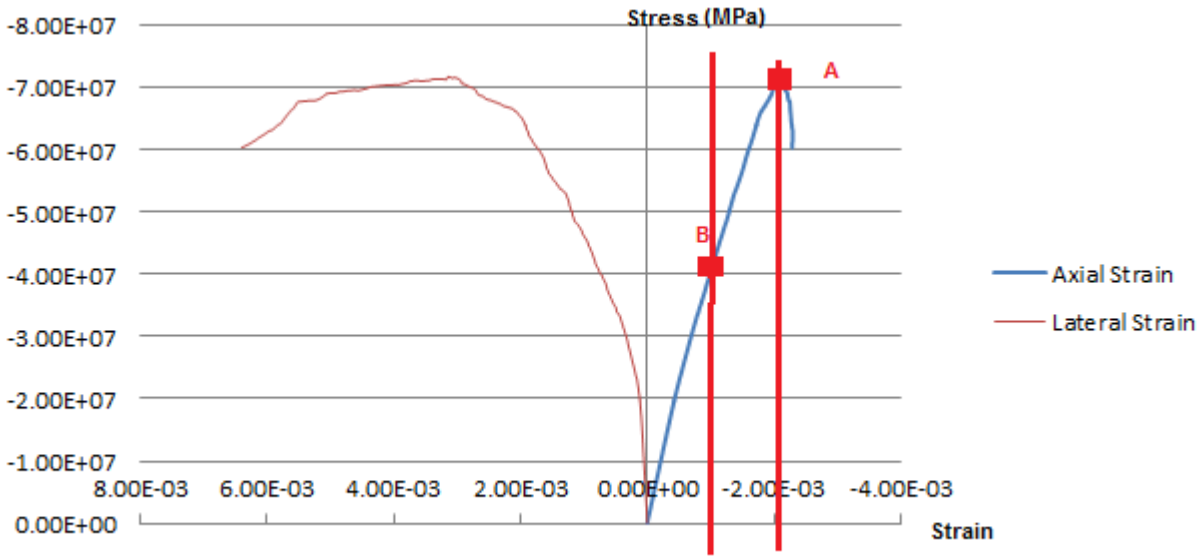

Figure A-1 A typical Stress-Strain plot

In PFC2D, the Stress-Strain is constantly being recorded and monitored for failure of the rock. Once the failure is detected, the values of the relevant parameters (Stress, Lateral Strain and Axial Strain) are selected at a point in the middle of failure (point B in Figure A-1) and they are used for calculating the elastic properties. The position of the point B is adjustable; however, the default position is exactly halfway before failure. This is a good assumption in the strong rocks, which they have a long linear section in their Stress-Strain plot. However, as illustrated in the Figures A-2 and 6.6, weaker rocks have more non-linear and plastic behaviour and selecting the exact middle point is not accurate. This point might fall in the non-linear section Figure A-2) and one point criteria is not accurate enough.

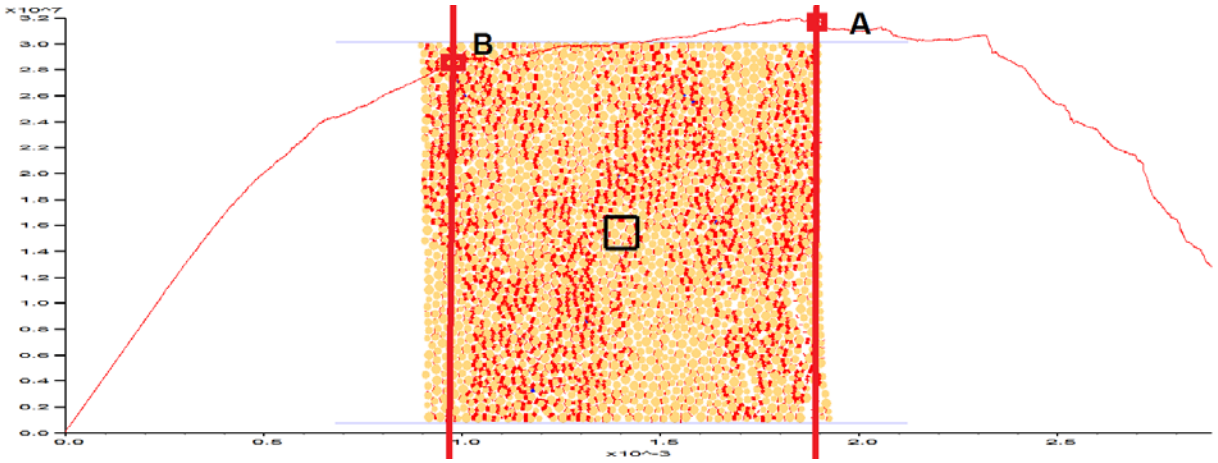

Figure A-2 Stress-Strain plot for weak and plastic material

Therefore, it is necessary to develop a secondary method. This is performed by exporting the Data points to the Matlab software and plotting them. Using visual technic, the start point and end point of strain section for each stress-strain plot was selected (Figure A-3) and the elastic properties were calculated using the following relationships:

E = Slope of line AB

$$\nu = \frac{\text{Slope of line CD}}{\text{Slope of line AB}} \qquad \text{A.3}$$

Tables 6-5 to 6-8 provide the results of these calculations.

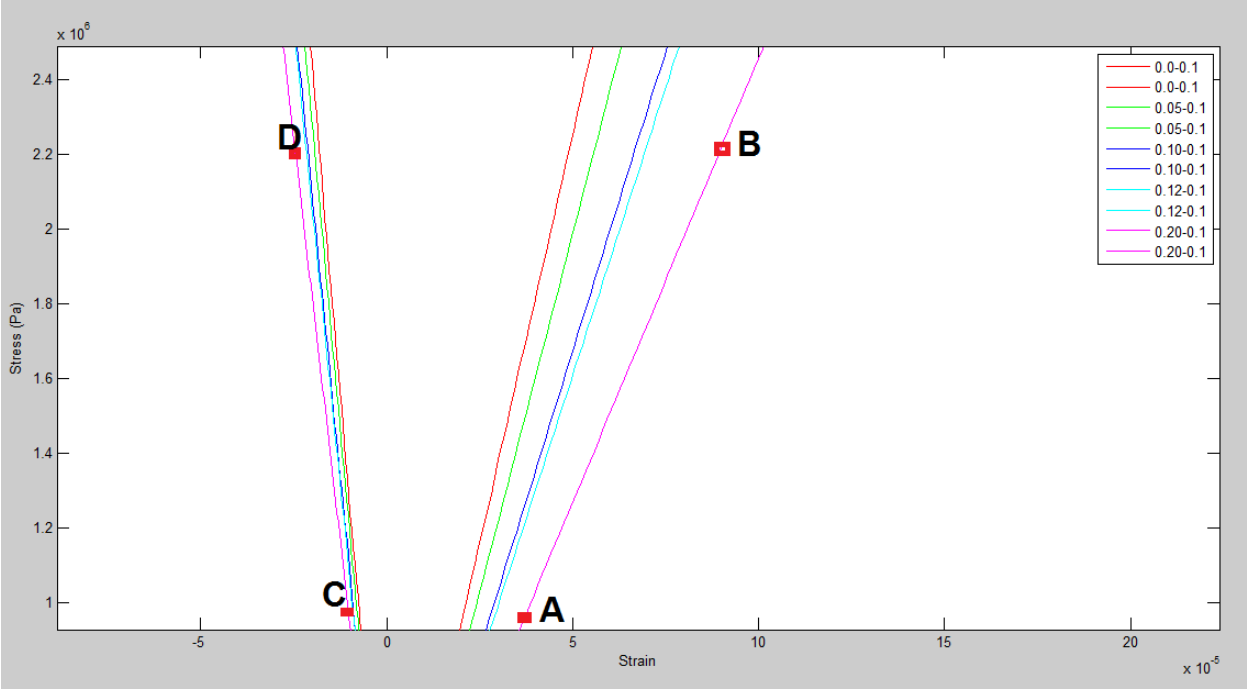

Figure A-3 Selecting the straight line section in the Matlab software

Appendix B Calculating the Friction Angle

Figure B.1 illustrates behaviour of an intact Marble Generated by the RocLab (developed by Rocscience Inc.) Software using the Hoek-Brown Criterion. The Hoek-Brown criterion is a criterion explaining rock failure with accuracy higher than the Mohr-Columbs Criterion; therefore it represents the drop in the friction angle with pressure. The procedure for calculating friction angle is as follows:

For each CCS test, an imaginary straight line was drawn to test at lower pressure, so that the straight line would be tangent to the both Mohr's circles. For example in Figure B-1, Line AB for CCS1 test and Line BC for CCS2 test. The slope of each line is calculated using Matlab software with basic geometrical methods and reported as friction angle at that pressure.

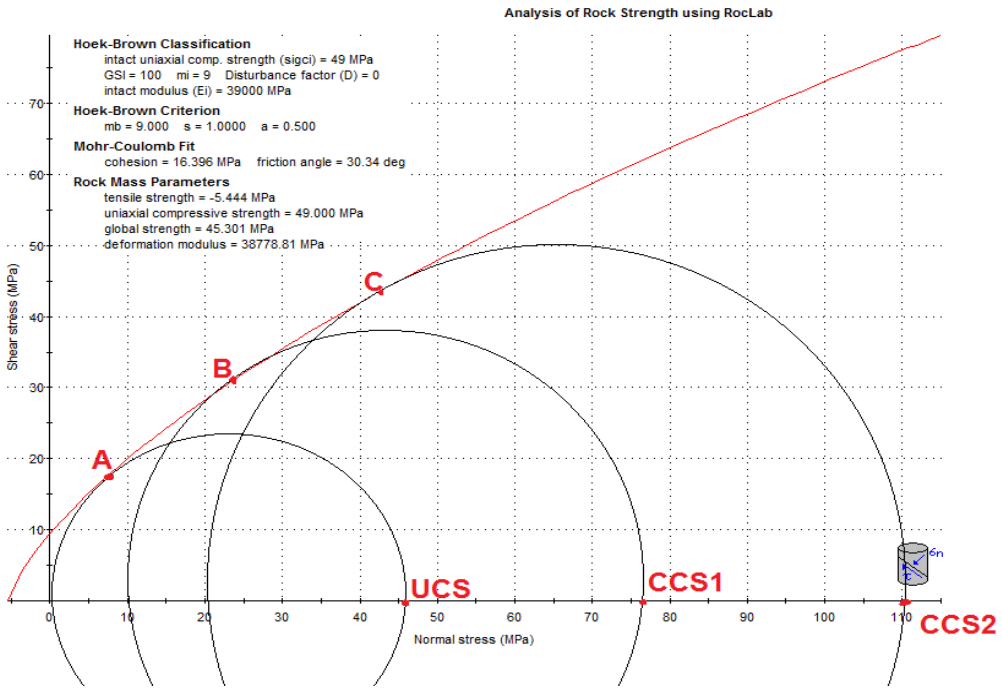

Figure B-1 Mohr's circles and failure envelope, Figure taken from the RocLab software

Appendix C Calculating ROP in two dimensions

Rate of Penetration (ROP) in drilling is the average axial velocity over the studied length at which the bit penetrates a rock. To measure this velocity in 2D the following steps are followed.

First the volume removed is calculated by integrating Y-position of the cutter over the cutting distance

The volume removed is divided by the Cutting Distance to obtain average depth of cut.

The average depth of cut is divided by simulation time to obtain ROP.

The procedure is illustrated in Figure C-1

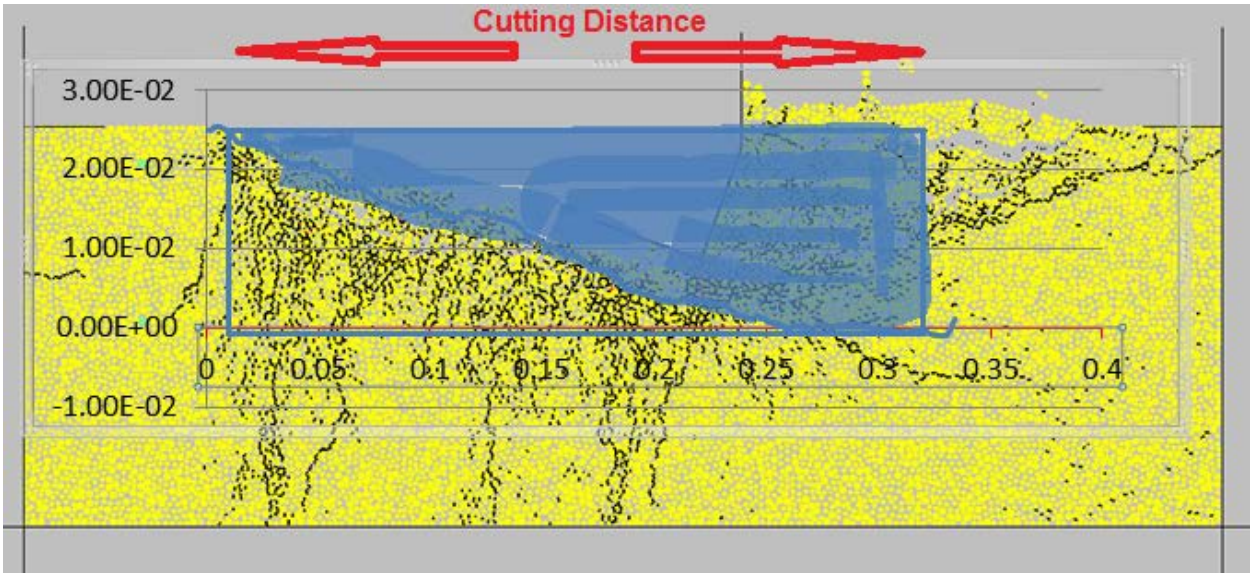

Figure C-1 Measuring the ROP. Blue area is the outline of the area the cutter has removed during its action. The Plot of Y-position of the cutter Vs. time is overlapped on the visual position of the cutter in the middle of the simulation.

Appendix D Drillability parameters

The parameters considered are in different categories to cover a wider range of properties for better explanation of the rock. They are physical, mechanical and micro-structural. The physical properties considered are porosity, density, compressional sonic wave (P-wave) velocity, and shear sonic wave (S-wave) velocity. The mechanical properties considered are UCS and Mohr's friction angle. The micro-structural properties considered are grain size and mineral type which causes hardness and abrasiveness in the rock. For simplicity, only quartz is considered. Quartz causes hardness in rock. Grain size also can be an indicator of the hardness as well. In the same mineralogy, smaller grain sizes result more contact area thus stronger rocks. The properties are usually measured from log data or direct physical testing. The physical properties are usually reported in the condition of absence of load or under low level of load.

Density

Density is a physical bulk property. It is measured as the mass per unit volume of the bulk. Density of the minerals are fixed and known; therefore, if the mineralogy of the rock is known, density can be used then for estimation of the porosity. Furthermore, using correlations between density and UCS, one can estimate UCS of the rock or using the Mohr friction the CCS can also be estimated. However, care should be taken. Considering Density alone can lead into error in estimations, as presence of cracks or formation fluid can create error in density measurements.

Porosity

Porosity is measured as the ratio of void or pore space in the rock by the total volume of the rock. It is one of the most usable parameters in different fields of the petroleum industry. It

represents the void space inside the rock which causes inhomogeneity in the rock with respect to failure process and pattern, elastic properties and wave propagation velocity.

Wave velocities

The two kinds of waves P-wave and S-wave are considered here. P-wave or primary waves are type of compressional waves that longitudinal in nature. They are the fastest waves in nature that travel through any material. However, their velocity is strongly dependent on the material and media. Stiffness of the material cracks, fractures and pore types are affecting the propagation speed and wave attenuation. Due to their speed, they are called Primary (P) waves because they are the first waves reaching the monitoring station. S-wave or secondary wave or shear sonic waves are transverse in nature, meaning they displace the medium perpendicular to the direction of their propagation, therefore are known to be the most corruptive. They are called Secondary (S) waves because they are slower that P-wave and arrive secondary to the monitoring stations. They are strongly affected by the Poisson's Ratio. Other properties like Young's Modulus, micro and macro structure and fluid saturations affect it as well.

Equations D.1 and D.2 [45, 46] represent the relationship of the wave velocities in a homogeneous media as a function of the elastic properties Young's Modulus and Poisson's Ratio:

$$v_p = \sqrt{\frac{K+\frac{4}{3}\mu}{\rho}} = \sqrt{\frac{\lambda+2\,\mu}{\rho}} \qquad \text{D.1}$$

$$\beta^2 = \frac{\mu}{\rho} \qquad \text{D.2}$$

Where:

K is the bulk modulus = $\frac{E}{3\,(1-2\nu)}$

μ is the shear modulus = $\frac{E}{2\,(1+\nu)}$

ρ is the density of the material

λ is the first Lamé parameter = $\frac{E\nu}{(1+\nu)(1-2\nu)}$

In the studies considering the wave velocities as a parameter, two very important points should be considered:

- Crack damage results in a decrease of elastic wave velocities and in the development of anisotropy. [47]

- The elastic properties, Young's Modulus and Poisson's Ratio, obtained from the wave velocities are dynamic properties and are different from the conventional elastic values result from normal stress-strain curves which are static values. [48]

Mineralogy

Mineralogy plays a significant role in wear and balling characteristics in drilling. For example, quartz, being the hardest minerals in common rock types, causes extensive wear. For simplicity, only quartz minerals are considered here as they are an indicator of hardness. [28]

Grain or Block Size

Grain size is one of most important features of the rocks which represent the rock's micro structure. It reflects its effect on other properties such as wave velocities, porosity, density and even rock strength. However, grain size is among one of the factors that has been least studied, mostly because of the difficulty in measuring it.

Unconfined Compressive Strength (UCS)

UCS is the maximum amount of the load carried by the rock during the standard Uniaxial Compression Strength test. During this test, the amount of the load carried by the rock increases to a maximum up to the point where the rock fails, then the load decrease significantly. Normally the failure occurs at about 2%-5% strain; therefore, the UCS could be used for estimating the slope of the line in stress-stress space (Young's Modulus of elasticity). Furthermore, using the Mohr friction angle, one could use the UCS to estimate the Confines Compressive Strength (CCS) of the rock.

Mohr Friction Angle

During the rock compression, shear failure inside the rock occurs along a plane where the shear forces are maximum (Figure D-1, the plane along τ). According to the Mohr's Hypothesis [49] criterion, the amount of the forces separating the two surfaces is a function of the normal forces (Equation D.3).

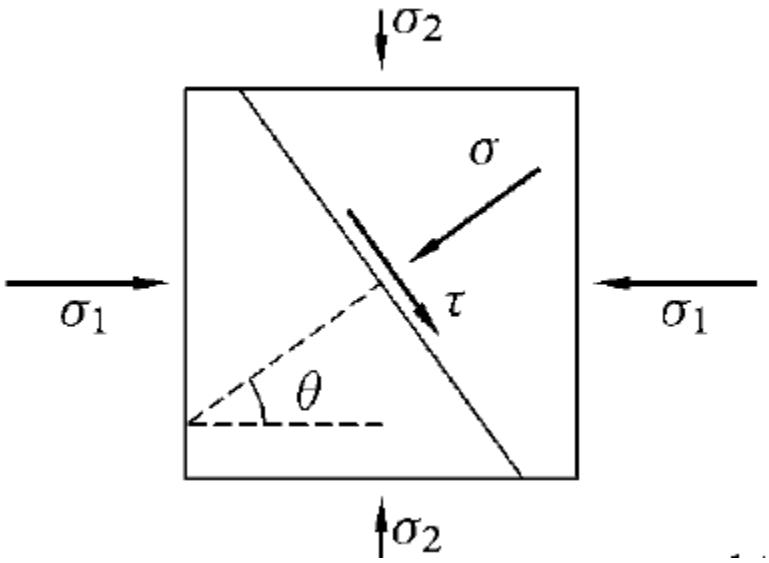

Figure D-1 Shear failure for a rock under compression [50]

$$\tau = f(\sigma') \qquad \text{D.3}$$

The relation between the normal stress and the shear stress is explained by the Mohr-Coulomb failure criterion as a linear relationship by:

$$\tau = S_0 + \mu\,\sigma' \qquad 9.4$$

Where S_0 is called cohesion and the μ is the coefficient of internal friction where $\tan(\varphi)=\mu$.

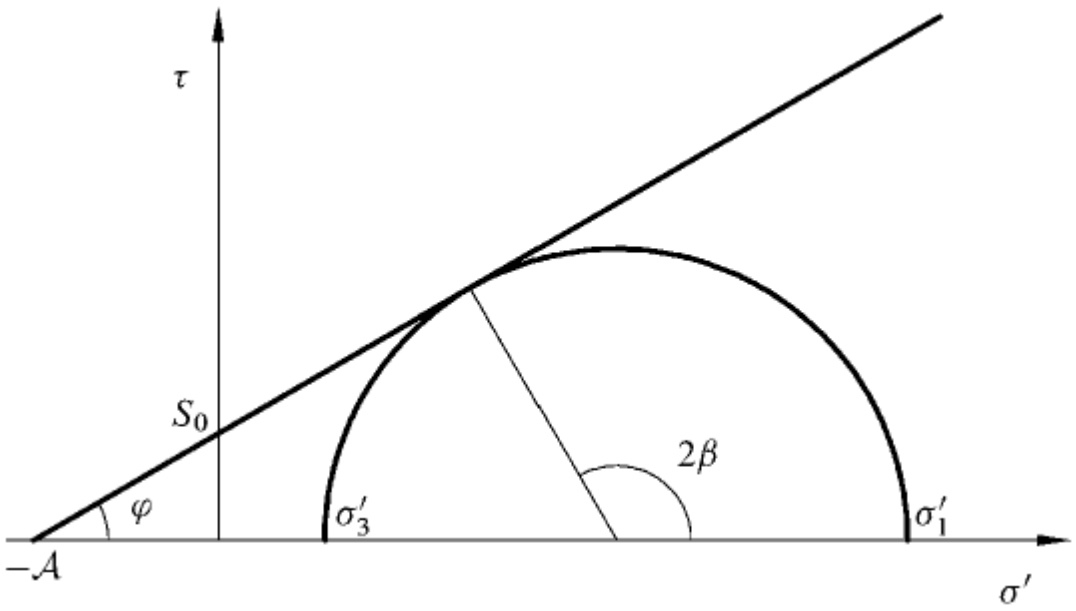

Figure D-2 Mohr-Coulomb failure criterion [51]

A Mohr-Colum criterion is a general criterion that estimates the relation between the normal stress and the shear stress by a straight line. This is a good assumption for the practical purpose in the borehole pressure where the Drillability is investigated [28]; however, as it will be shown in the future section and has seen by other researchers, the friction angle is not constant. The friction angle is highest in lowest confining pressures and decreases as the confining pressure increases [28, 52].

Appendix E Analyzing the Experimental Drillability data

This study is a follow-up work of another experimental study. The experimental data are part of research performed by Zhen Zhang for his M.Eng in Advanced Drilling Group at Memorial University of Newfoundland and currently (January 2014) is not published. Unfortunately, at the time of this work, the original experimental work had not been finalized and was at its last stages. Furthermore, a few issues with the output data of the experimental work were reported. The rest of this chapter will discuss the eight Drillability parameters one by one and will discuss the decisions made to select a set of target parameters to use as a reference for tuning the synthetic material. Table E-1 represents the experimental outputs available at for this study.

Table_ E-1 Raw Experimental Data, Empty cells are data that are not available yet

	UCS Value (MPa)	Porosity	Density (kg/m^3)	P-Wave Velocity (m/s)	S-Wave Velocity (m/s)	Mohr Friction Angle	Quartz content	Grain or Block Size
High Strength Concrete	-	-	-	-	-	-	-	-
Medium Strength Concrete	48.90	25.7%	2291.7	4527	3363	28.8°	-	-
Low Strength Concrete	21.59	32.5%	2013.9	4286	3103	24.3°	-	-

Table_ E-2 Target Properties, after Adjustments

	UCS (MPa)	density (kg/m3)	friction angle (degree)	E (GPa)	Poisson's Ratio	T (MPa)
Low Strength Concrete	21.59	2013.9	57	27.48	0.3	2.159
Medium Strength Concrete	48.9	2291.7	59	39.14	0.25	4.89
High Strength Concrete	90	2400	62	45	0.2	9

High Strength Material

As mentioned above, the experimental work was under progress and some of the required data were not available. The most important part of missing data was the measured properties of the strong material. To be able to perform this study and the future sensitivity analysis, it was

decided to estimate the properties of this strong material by extrapolating the properties of the other two materials, the medium and weak ones. These properties are tabulated after more discussions about the rest of the properties in table E-2.

Quartz Content and Grain or Block Size

It has been discussed earlier in [33, 29] that the produced assembly of the particles that create the synthetic material is a valid structure of its own and its micro-structure should not be confused with that of the actual rock. Therefore, the grain size of a synthetic DEM material should not be confused with the grain size of a real material. The grain size of a synthetic material should be calibrated so that the material represents a desired macroscopic behaviour. Furthermore, according to table 1 there is no experimental data available for the two parameters. Therefore, it has been decided not to consider these parameters for this simulation study.

Porosity

As stated earlier, the synthetic material is a valid structure of its own and its porosity as one of its micro-structure properties should not be confused with that of the actual rock. It also worth to mention that the reported values for the porosity is the porosity of a three dimensional specimen; while, the current simulation study is in two dimensions. Therefore it is arguable how to convert the three dimensional porosity into a two dimensional one. Besides, if the values are somehow converted, what is their meaning in two dimensions and how should they be compared with the original ones.

Assuming it has been decided to calibrate the porosity as well, based on the current material generation library, this property always ends up with the same value [33]. The libraries are designed to create a packed assembly of particles to simulate a desired elastic and mechanical

behaviour. Multiple methods were tested for the adjustment of the porosity, either by multiplying the radius of all particles by a constant number or by adjusting the porosity of initial packing. All of these methods either end up with creating an unstable rock or end up with the same constant number. It is possible to use more complicated schemes that require developing new codes; however, according to intellectual property agreement* the researcher is not permitted to develop new codes. Given these challenges, it has been decided not to include the porosity in the study as well.

Wave velocities and elastic properties

Wave velocities for weak and strong material are reported as in table E-1. The relations in appendix D can be used to calculate the dynamic Young's Modulus and Poisson's Ratio. However these relations will result in a Poisson's Ratio of less than zero. As stated in the beginning of the current chapter, an issues with the output data of the experimental work was reported which is caused by selecting an incorrect couplant in S-wave velocity test. Therefore these data are not useful anymore and a new method should be used for estimating elastic properties. Consulting this matter with the supervisors lead to selecting estimated values in the normal range of rocks for the Poisson's Ratio. Using these values and the relations in Appendix D, the dynamic Young's Modulus is calculated. However, the output values of the material testing process [33] are static values and can't be compared directly with dynamic values. Figure E-1 and Fjær [48] explain that at higher Young's Modulus the ratio of dynamic to static elastic properties fall close to one. Looking at table E-2, it can be concluded that medium and strong material fall in a safe category, but this is not a good assumption for the weak material. Therefore it is needed to develop a code to calculate wave velocities and use velocities for

calibration instead of elastic moduli. However, this cannot be performed because of the following reasons:

- The original values for calibration are estimated, therefore they are not accurate and they can be used for calibration process just as they are
- Due to intellectual property agreements, no code can be developed during this research phase

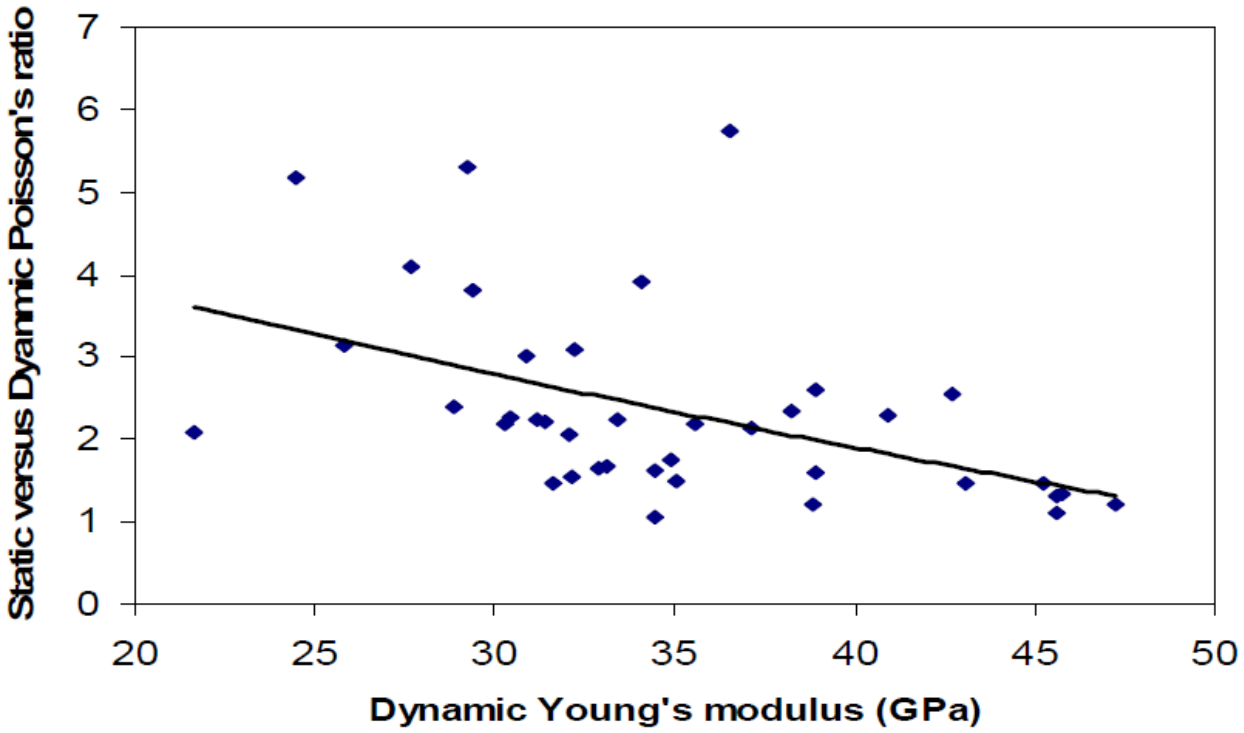

Figure E-1 Static/Dynamic Poisson's Ratio vs. dynamic Young Modulus [47]

Therefore it is decided to assume the estimated elastic values are valid static values for the calibration process. Appendix A explains different procedures for calculating Young's Modulus and Poisson's Ratio from the compression test results.

Mohr Friction Angle

The friction angle of the rock was reported as a single value. As many researchers stated [28, 52], this angle in reality is not constant and is highest at low confining pressures. Unfortunately, in the reported experimental data, it has not reported how the friction angle is calculated or measured and these values correspond to what confining pressure. Besides, the Flat-Joint contact model is a very realistic model in which it can predict this decreasing angle phenomenon as well. Figure E.2 and Table E.3 show the flat–joint model predictions of this phenomenon for the strongest material. Appendix B explains how these angles are calculated using UCS and CCS values at different confining pressures. Since the procedure and confining pressure for experimental angles reported are unknown, some arbitrary values were selected for the target of calibration at low pressure of 350 psi.

Table E-3, Friction angle at different pressures for strong sample with smallest min. particle size

	Confining Pressure (Psi)	Strength (MPa)	Friction Angle (degree)
	0	84.3	
1	350	119.5	60.65
2	850	141	46.36
3	1200	160	43.4
4	2000	188.5	42.5

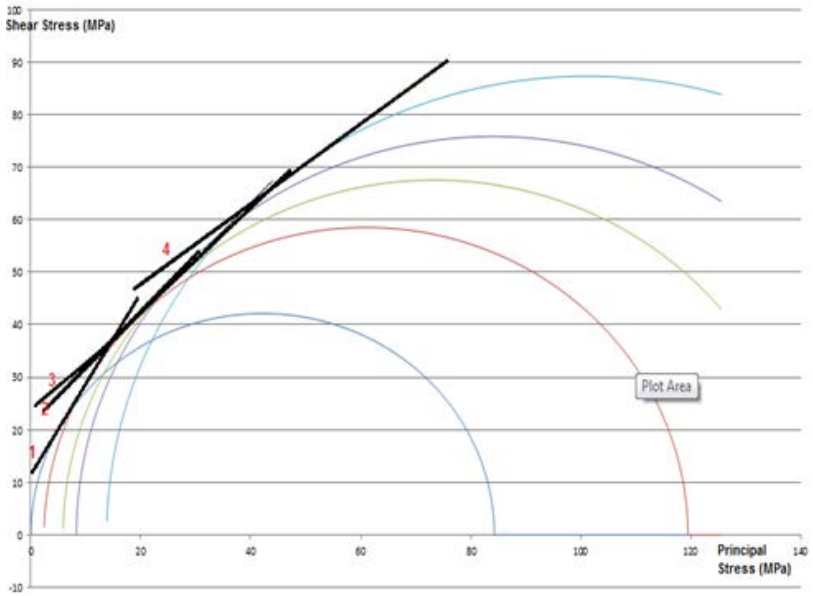

Figure E-2 Mohr Circles for compression test of the strongest material shows drop in friction angle with pressure

Tensile Strength

In the older contact model of linear parallel bond model, there was no method for calibrating tensile strength separately from UCS; therefore, one needed to sacrifice one for another. However, in the Flat-Joint model, this task can be performed easily and tensile strength can be calibrated almost separately from UCS. As described before, in a Flat-Joint model the contact plane is actually in the form of facets which can be fully bonded, partially bonded or unbounded. Also, because of existence of facets, the contacts can resist rotation even in an unbounded state and strength can occur with interlocking the faceted particles. Therefore there is way more control over behaviour of the sample than old of linear parallel bond model.

Unfortunately, the tensile strength of the specimen was not reported separately in the experimental work. However, since the contact model being used has the capability of

calibrating this strength as well it has been decided to include this property in the calibration process. The values of tensile strength were estimated based on the following general rule of thumb:

$$\text{Tensile Strength} = 0.1 * \text{UCS} \tag{E.1}$$

Appendix F Tuning Procedure summary

Table_ F-1, tests performed to tune the medium material according to the standard calibration procedure. Orange cells are the parameters specific to the Flat-Joint contact model which are used for the tuning process. The green cells are the target macro-properties that are being monitored. In each step, the input parameters that are varying are marked as darker orange.

order	Min. Part. Size (mm)	Ec (Gpa)	Krat	Bond sigma_b (Mpa)	Bond cohesion	bond f-a	Bonded Ratio	Gapped Ratio	Slit Ratio	E (Gpa)	Nu (%)	T (Mpa)	UCS (Mpa)	CCS (Mpa)	rock F-A
1	0.6	57	1.5	90	0	0	1	0	0	37	1.1				
2	0.6	60	2.5	90	0	0	1	0	0	36	18				
3	0.6	70	2.9	90	0	0	1	0	0	40	18				
4	0.6	75	3.1	90	0	0	1	0	0	41	21				
5	0.6	75	3.3	90	0	0	1	0	0	42	21				
6	0.6	70	3.3	90	0	0	1	0	0	39	21				
7	0.6	70	3.5	90	0	0	1	0	0	38.5	22				
8	0.6	68	3.7	90	0	0	1	0	0	37	22.5				
9	0.6	68	3.9	90	0	0	1	0	0	37	23				
10	0.6	60	2.5	10	0	0	1	0	0	37	23	4.33			
11	0.6	60	2.5	11	0	0	1	0	0	37	23	4.67			
12	0.6	75	3.3	11.5	70	0	1	0	0	36	38	4.36	54		
13	0.6	70	3.3	11.9	60	0	1	0	0	36	32	4.84	49		
14	0.6	68	3.9	12	55	0	1	0	0	33	36	4.9	43		
15	0.6	70	3.5	12	57	0	1	0	0	36	24	4.68	40		
16	0.6	70	3	12	57	0	1	0	0	39	24.3	4.15	49		
17	0.6	70	3	12	57	0	0.95	0.05	0	37.5	19	3.76	31		
18	0.6	70	3.2	15	59	0	0.95	0.05	0	35	21	5.63	38.7		
19	0.6	73	3.4	15	61	0	0.95	0.05	0	35	21.5	4.83	37		
20	0.6	82	3.7	14.5	65	23	0.95	0.05	0	39.4	22.5	4.8	33.5		
21	0.6	82	3.7	14.5	80	23	0.95	0.05	0	39	23	4.8	36		
22	0.6	82	3.9	14.5	80	23	0.95	0.05	0	37.5	28.5	5.06	40		
23	0.6	82	3.8	14.5	80	23	0.95	0.05	0	37.5	24.5	4.24	38		
24	0.6	82	3.9	14.5	80	23	0.95	0.05	0	37	25.5	5	35		
25	0.6	73	3.4	15	61	21	0.95	0.05	0	34.5	24	4.83	39	63	55
26	0.6	74	3.4	15.5	65	21	0.95	0.05	0	35	23	5.8	41	60.5	51
27	0.6	74	3.4	15.5	65	23	0.95	0.05	0	35	23	5.8	41	61	52
28	0.6	80	3.4	15	65	23	0.95	0.05	0	37	24	5.47	35	58.2	54
29	0.6	80	3.7	15	65	23	0.95	0.05	0	38.5	21	5.24	34.5	59.3	55
30	0.6	82	3.9	14.5	90	23	0.95	0.05	0	36	26.5	5	36.3	60	55
31	0.6	82	3.9	14.5	90	25	0.95	0.05	0	36	26.9	5	36.3	61	55
32	0.6	82	3.8	14.5	95	25	0.95	0.05	0	35	28	4.72	39	70.5	59
33	0.6	82	3.8	14.5	95	30	0.95	0.05	0	34.5	28.5	4.72	39.5	73	60
34	0.6	83	3.8	14.5	105	25	0.95	0.05	0	36	26.5	4.86	44	84	
35	0.6	83	3.8	14.5	105	23	0.95	0.05	0	36.5	26.5	4.86	45	87	63
36	0.6	83	3.8	14.5	105	21	0.95	0.05	0	36.6	26	4.86	45	82	61
37	0.6	83	3.8	14.5	105	19	0.95	0.05	0	36.7	25.9	4.86	44.7	81	61
38	0.6	83	3.8	14.5	105	16	0.95	0.05	0	36.7	25.9	4.86	44.5	81	61
39	0.6	83	3.8	14.5	105	13	0.95	0.05	0	36.7	25.8	4.86	44	79	61
40	0.6	83	3.8	14.5	105	10	0.95	0.05	0	36.8	25.7	4.86	43.5	80	61